

**IDENTIFICATION AND FUNCTIONAL ANALYSIS OF A
CIRCULAR RNA CIRCZNF800 INVOLVED IN REGULATING
COLORECTAL CANCER STEMNESS PROPERTIES**

By

VIMALAN A/L RENGGANATEN

A thesis submitted to the Department of Pre-clinical Sciences,
M. Kandiah Faculty of Medicine and Health Sciences,
Universiti Tunku Abdul Rahman,
in partial fulfilment of the requirements for the degree of
Doctor of Philosophy (Medical Science)

March 2023

ABSTRACT

IDENTIFICATION AND FUNCTIONAL ANALYSIS OF A CIRCULAR RNA CIRCZNF800 INVOLVED IN REGULATING COLORECTAL CANCER STEMNESS PROPERTIES

Vimalan A/L Rengganaten

Colorectal cancer (CRC) is one of the most diagnosed cancers. Effective therapeutic interventions remain challenging due to the existence of a rare population of chemo-resistant CRC cancer stem cells (CrCSC). In a spheroidal culture model, the CrCSC population is enriched with enhanced CSC-like properties. However, the molecular events governing CSC properties in the CrCSC population remains poorly understood. Circular RNAs (circRNAs) are long non-coding regulatory RNAs associated with various biological functions. The present study aimed to elucidate the biological role of circRNAs in maintaining CSC properties in CRC cells. CircRNA sequencing was performed using Illumina technology. qRT-PCR and RNA FISH were used to evaluate the expression levels of circRNA. *In vitro* transcription and CRISPR Cas13d RNA editing system were used to modulate the expression levels of the circRNA. Whole-transcriptome sequencing of RNA of CRC spheroidal cells revealed over 8,000 differentially expressed circRNAs. The top 8 differentially expressed circRNAs were identified and the interacting miRNAs and mRNA transcripts were predicted. KEGG analysis revealed the enrichment of various CSC-associated signalling pathways; the pluripotency regulating pathways were most significantly up-regulated. Two circRNAs,

hsa_circ_0066631 (circDCBLD2) and hsa_circ_0082096 (circZNF800), were predicted and experimentally validated to sponge five miRNAs, releasing post-transcriptional inhibition of six mRNA transcripts involved in the regulation of stemness. Literature analysis showed that the predicted miRNAs acted as tumour suppressors and the targeted transcripts regulated various CSC signalling pathways. As a candidate circRNA for further in-depth analysis, circZNF800 was shown to be significantly up-regulated in CRC tumour tissues. CircZNF800 overexpression promoted CSC phenotypes, including proliferation, expression of CSC and intestinal stem cell markers, and tumorigenicity, all of which were reversed by CRISPR Cas13d-mediated circZNF800 knockdown. CircZNF800 was shown to sponge miR-140-3p, miR-382 and miR-579 which, in turn, increased the levels of *ALK7*, *FZD3* and *WNT5A*, which are involved in the regulation of CSC properties. In conclusion, circZNF800, identified in CrCSC circRNA profiling, was shown to participate in regulating CSC properties in CRC.

ACKNOWLEDGEMENT

To Appa and Amma, this is for you.

The idea of getting a PhD was planted at the tender age of 14, when I first learned about the idea of the highest form of education. The 17 years journey has now come to its natural end. Along this odyssey, I have faced countless ups and downs, challenges, successes and most importantly, I have had *way too* many cups of coffee. Many people have left an impactful impression through their aspirations and motivations along the various phases of my PhD journey; To all of them, thank you.

But none of this would be possible without my mentor, Senior Professor Dr. Choo Kong Bung. I would like to thank Professor Choo for all the guidance, motivation, encouragement and advice he has shared with me throughout my postgraduate journey. I express my deepest gratitude to Professor Choo for everything he has done for me. I would like to also record my appreciation to Professor Dr Chiou Shih-Hwa for supporting my PhD project. I would like to also thank Associate Professor Dr. Ong Hooi Tin for her guidance and support. Special mention to Professor Dr. Huang, Chiu-Jung for her constant advice and mentorship on manuscript and thesis writing.

I am deeply indebted to my family for their constant understanding and moral support, especially after being apart from home during the pandemic. I am grateful for their sacrifices and patience throughout this journey. Needless to say, I have had some amazing friends who have been my moral support for the past 5 years. I also had the opportunity of working alongside very supportive lab mates at both Universiti Tunku Abdul Rahman and National Yang-Ming Chiao Tung University. From the bottom of my heart, I thank everyone who has helped me in any way. Thank you!

I would like to also express my gratitude to Universiti Tunku Abdul Rahman, National Yang-Ming Chiao Tung University and Taipei Veterans General Hospital, Taipei, Taiwan for providing the facilities and resources to conduct my experiment. This work was supported by UTAR Research Fund (UTARRF) 6200/O26.

APPROVAL SHEET

This thesis entitled “**IDENTIFICATION AND FUNCTIONAL ANALYSIS OF A CIRCULAR RNA CIRCZNF800 INVOLVED IN REGULATING COLORECTAL CANCER STEMNESS PROPERTIES**” was prepared by VIMALAN RENGGANATEN and submitted as partial fulfilment of the requirements for the degree of Doctor of Philosophy (Medical Science) at Universiti Tunku Abdul Rahman.

Approved by:



(Associate Prof. Dr. Ong Hooi Tin

Date: 14 March 2023

Supervisor

Department of Pre-Clinical Science

M. Kandiah Faculty of Medicine and Health Sciences

Universiti Tunku Abdul Rahman



(Prof. Dr. Choo Kong Bung)

Date: 14 March 2023

Co-supervisor

Department of Pre-Clinical Science

M. Kandiah Faculty of Medicine and Health Sciences

Universiti Tunku Abdul Rahman



(Prof. Dr. Chiou Shih-Hwa

Date: 14 March 2023

External co-supervisor

Institute of Pharmacology

National Yang-Ming Chiao Tung University

M. KANDIAH FACULTY OF MEDICINE AND HEALTH SCIENCES
UNIVERSITI TUNKU ABDUL RAHMAN

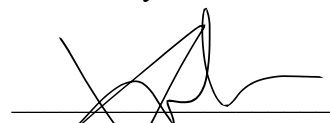
Date: 14 March 2023

SUBMISSION OF THESIS

It is hereby certified that VIMALAN A/L RENGGANATEN (ID No: 17UMD06744) has completed this thesis entitled “IDENTIFICATION AND FUNCTIONAL ANALYSIS OF A CIRCULAR RNA CIRCZNF800 INVOLVED IN REGULATING COLORECTAL CANCER STEMNESS PROPERTIES” under the supervision of Associate Professor Dr. Ong Hooi Tin (Supervisor) from the Department of Pre-Clinical Sciences, M. Kandiah Faculty of Medicine And Health Sciences, and Senior Professor Dr. Choo Kong Bung (Co-Supervisor) from the Department of Department of Pre-Clinical Sciences, M. Kandiah Faculty of Medicine And Health Sciences and Professor Dr. Chiou Shih-Hwa (External co-supervisor) from the Institute of Pharmacology, National Yang-Ming Chiao Tung University, Taiwan.

I understand that University will upload softcopy of my thesis in pdf format into UTAR Institutional Repository, which may be made accessible to UTAR community and public.

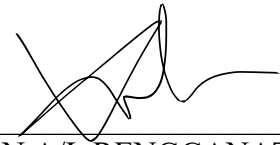
Yours truly,



Vimalan A/L Rengganaten

DECLARATION

I hereby declare that the dissertation is based on my original work except for quotations and citations which have been duly acknowledged. I also declare that it has not been previously or concurrently submitted for any other degree at UTAR or other institutions.



VIMALAN A/L RENGGANATEN

Date: 14 March 2023

TABLE OF CONTENTS

	Page
ABSTRACT	II
ACKNOWLEDGEMENT	IV
APPROVAL SHEET	VI
SUBMISSION OF THESIS	VII
DECLARATION	VIII
TABLE OF CONTENTS	IX
LIST OF TABLES	XV
LIST OF FIGURES	XVI
LIST OF ABBREVIATIONS	XX
CHAPTER	
1.0 INTRODUCTION	1
2.0 LITERATURE REVIEW	5
2.1 Colorectal cancer	5
2.1.1 Risk factors of CRC	7
2.1.2 Modifiable CRC risk factors	8
2.1.3 Non-modifiable CRC risk factors	9
2.2 Colorectal cancer stem cells	11
2.2.1 Regulation of colorectal cancer stem cells	12
2.2.2 Identification of colorectal cancer stem cell population	14
2.3 <i>In vitro</i> enrichment tools of colorectal cancer stem cells	16
2.3.1 Spheroidal culture	17
2.4 Non-coding regulatory RNAs	20
2.4.1 MicroRNAs	20
2.4.2 Circular RNAs	22
2.4.2.1 Biogenesis and properties of circRNA	23
2.4.3 Biological roles of circRNA	24
2.4.3.1 CircRNA as a transcriptional regulator	25

	2.4.3.2	CircRNA as post-transcriptional regulator	26
	2.4.4	Roles of circRNA in CRC	26
3.0		MATERIALS AND METHODS	28
3.1		Cell culture	28
	3.1.1	Colorectal cell lines	28
	3.1.2	Spheroidal culture	30
3.2		CRC clinical patient tissues	31
3.3		Genome-wide circular RNA profiling	32
	3.3.1	RNA extraction	32
	3.3.2	Library preparation	33
3.4		Bioinformatics analysis	34
	3.4.1	Selection of top differentially expressed circRNA	35
	3.4.2	Construction of circRNA-miRNA-mRNA axis	35
3.5		Quantitative analysis of RNA	36
	3.5.1	cDNA conversion	36
	3.5.2	Circular RNA quantitative real-time PCR	37
	3.5.3	mRNA quantitative real-time PCR	39
	3.5.4	MicroRNA quantitative real-time PCR	41
3.6		Characterisation of circular RNA properties	41
	3.6.1	Actinomycin D treatment	41
	3.6.2	RNase R treatment	43
	3.6.3	RNA Fluorescence In Situ Hybridisation (FISH) assay	44
	3.6.4	Dual immunofluorescent assay of RNA FISH and protein immunofluorescent	47
3.7		Circular RNA overexpression system	48
	3.7.1	Plasmid cloning	48
	3.7.2	<i>In vitro</i> transcription of circRNA	49

3.7.3	Agarose-formaldehyde gel electrophoresis	50
3.7.4	RNA transfection	51
3.7.5	Subcutaneous transplantation of CRC cells	51
3.8	CRISPR Cas13d knockdown	52
3.8.1	Plasmid cloning	52
3.8.2	Transient transfection of CRISPR Cas13d	53
3.8.3	Stable expression of CRISPR Cas13d CRC cells	53
3.8.3.1	Lentivirus generation of CRISPR Cas13d	53
3.8.3.2	Lentivirus transduction	54
3.8.3.3	Selection and expansion of stably transduced CRISPR Cas13d cells	55
3.8.4	Subcutaneous transplantation of stably expressed CRISPR Cas13d cells	55
3.9	Functional assays	56
3.9.1	Flowcytometry analysis	56
3.9.2	EdU assay	57
3.9.3	Colony-forming assay	58
3.9.4	RNA pulldown assay	59
3.10	Statistical analysis	60
4.0	RESULTS	61
	<u>Part 1: CircRNA expression profiling of CRC spheroidal cells</u>	61
4.1	Genome-wide sequencing of circRNA established a differentially expressed profile in CRC spheroidal cells	61
4.2	Identification of top differentially expressed circRNAs unveiled a core circRNA–microRNA–mRNA network that regulates stemness	63
4.2.1	Validation of expression of the top differentially expressed circRNAs in CRC spheroidal cells	66

4.2.2	Construction and mapping of core pluripotency-associated network	66
4.3	Validation of the predicted core network in CRC spheroidal cells	68
4.4	Construction of circRNA-miRNA-mRNA stemness regulatory network	74
<u>Part 2: Selection and characterisation of a candidate circular RNA hsa_circ_0082096/circZNF800</u>		81
4.5	Up-regulation of hsa_circ_0082096 expression was observed in a passage-dependent manner in spheroidal culture of CRC cell lines	81
4.6	Nomenclature and molecular characteristics of hsa_circ_0082096/ circZNF800	83
4.7	CircZNF800 exhibited common features of circular RNA	89
4.7.1	Sanger sequencing validated the circZNF800 backsplicing junction	89
4.7.2	CircZNF800 was RNase R resistant with longer half-life	89
4.8	CircZNF800 expression levels were significantly higher in CRC clinical tissues compared to the host transcript	92
4.8.1	Expression of circZNF800 coincided with high proliferative tumour cell population in CRC tissues and in intestinal stem cell population in normal tissues	94
<u>Part 3A: Phenotypic and genotypic modulations of circZNF800 overexpression in relation to stemness regulation</u>		98
4.9	Establishment of an ectopic overexpression system of circZNF800	98
4.9.1	Generation and validation of <i>in vitro</i> transcribed self-circularising circZNF800	100
4.9.2	Successful cellular uptake of circZNF800 in chemical transfection	102

4.10	Ectopic overexpression of circZNF800 enhanced CSC-like properties in WiDr cells	104
4.10.1	CircZNF800 increased cell proliferation	105
4.10.2	CircZNF800 up-regulated cancer and intestinal stem cell markers	107
4.10.3	CircZNF800 up-regulated expression of stemness markers in CRC cells	110
4.11	CircZNF800 enhanced tumourigenicity in mice	112
	<u>Part 3B: Functional molecular modulations of circZNF800 overexpression</u>	115
4.12	CircZNF800 down-regulated the expression of targeted miRNAs to positively regulate downstream genes of the predicted pluripotency pathways	115
4.12.1	CircZNF800 sponges the predicted tumour suppressive miRNAs hsa-miR-140-3p, -miR-382 and -miR-579	115
4.12.2	CircZNF800 up-regulated pluripotency-associated target transcripts of the miRNAs	118
	<u>Part 3C: Phenotypic and genotypic modulations of circZNF800 knockdown in relation to stemness regulation</u>	122
4.13	CircZNF800 knockdown via CRISPR Cas13d suppressed CSC-like properties	122
4.13.1	Construction and validation of CRISPR Cas13d-mediated knockdown of circZNF800	123
4.13.2	Knockdown of circZNF800 diminished stemness properties in CRC cells	125
4.13.3	Impaired tumour-forming abilities in a mice model transplanted with circZNF800 knockdown cells	130

<u>Part 3D: Functional molecular modulations of circZNF800</u>	135
<u>knockdown</u>	
4.14 Knockdown of circZNF800 up-regulated expression levels of tumour suppressive miRNAs and down-regulated transcripts of pluripotency-associated pathways	135
5.0 DISCUSSION	138
5.1 Use of spheroidal culture in the study of cancer stem cells	138
5.2 Integrative analysis of circRNA unveiled a complex post-transcriptional gene regulation network in cancer stem cells	139
5.3 CircRNA-mediated regulation is involved in activities of the pluripotency pathways	141
5.4 CircZNF800 mediates CSC-like properties in CRC cells	144
5.5 Targeted knockdown of circZNF800 may be a potential therapeutic approach in CRC treatment	148
6.0 Conclusions	151
6.1 Conclusions	151
6.2 Limitations of the study	154
6.2 Future investigations	155
REFERENCES	157
APPENDICES	181

LIST OF TABLES

Table	Title	Page
3.1	List of circular RNA primers	38
3.2	List of mRNA primers	40
3.3	List of microRNA primers	42
3.4	Probe sequences	45
4.1	Top eight differential expressed circRNAs in the spheroidal CRC	65
4.2	Predicted miRNAs and affected CSC-associated functions based on literature review	77
4.3	Involvement of the target mRNAs in CSC-associated properties and the implicated signalling pathways	78
4.4	Molecular characteristics of circZNF800 and circDCBLD2	85
4.5	Interactions of the circZNF800 with the predicted core miRNAs	116
4.6	Predicted circZNF800 and miRNAs binding activity	117

LIST OF FIGURES

Figure	Title	Page
4.1	Genome-wide circRNA profiling of CRC spheroidal cells	62
4.2	Identification of the top four differentially expressed circRNAs in CRC spheroidal cells	64
4.3	Validation of the predicted top differentially expressed circRNAs	69
4.4	Identification of interacting miRNAs and mRNAs with the top four differentially expressed circRNAs	70
4.5	Bioinformatics analysis of mRNA transcripts of the circRNA-miRNA-mRNA axis of CRC spheroidal cells	71
4.6	Predicted circRNA-miRNA-mRNA network of pluripotency signalling pathways targeted by hsa_circ_0066631 and hsa_circ_0082096	72
4.7	Validation of the expression levels of the predicted miRNA in CRC spheroid cells	73
4.8	Validation of the expression levels of the predicted mRNA transcripts	75
4.9	Mapping of predicted circRNA-miRNA-mRNA axis in regulation of stemness in CRC cells	80
4.10	Expression of candidate circular RNAs on different passages of CRC spheroidal cells	82
4.11	Expression of hsa_circ_0082096 in spheroidal cells derived from various CRC lines	84

4.12	Full-length sequence of circZNF800	88
4.13	Experimental validation of circZNF800 backsplice junction	90
4.14	Characterisation of hsa_circ_0082096 for distinct circular RNA properties	91
4.15	Expression of <i>ZNF800</i> and circZNF800 in CRC patient samples	93
4.16	RNA FISH analysis of circZNF800 expression in CRC patient tissues	95
4.17	Co-localisation analysis of circZNF800 with intestinal cells and proliferative markers	97
4.18	Illustration of circZNF800 overexpression generation system	99
4.19	Generation of <i>in vitro</i> transcribed circZNF800 RNA	101
4.20	Evaluation of the transfection efficiency of <i>in vitro</i> transcribed circZNF800	103
4.21	Effects of circZNF800 overexpression on CRC cell proliferation	106
4.22	Effects of circZNF800 overexpression on CSC markers expression levels	108
4.23	Effects of circZNF800 overexpression on expression levels of intestinal stem cell markers	109
4.24	Effects of circZNF800 overexpression on expression levels of pluripotency markers	111
4.25	Schematic illustration of the mouse model used to study the effects of circZNF800 overexpression on tumorigenicity	113

4.26	Effects of circZNF800 overexpression on tumorigenicity in mice	114
4.27	CircZNF800 RNA pulldown analysis of predicted miRNAs	119
4.28	Effects of circZNF800 overexpression on the expression levels of the predicted miRNAs	120
4.29	Expression analysis of predicted pluripotency-associated pathways upon circZNF800 RNA overexpression	121
4.30	Establishment and validation of circZNF800 knockdown system	124
4.31	Effects on CRC cell proliferation upon circZNF800 knockdown	126
4.32	Effects on CSC markers expression levels upon circZNF800 knockdown	127
4.33	Effects on intestinal stem cells markers expression levels upon circZNF800 knockdown	128
4.34	Evaluation of core pluripotency markers upon circZNF800 knockdown	129
4.35	Evaluation of sphere-forming abilities on circZNF800 knockdown cells	131
4.36	Effects of circZNF800 knockdown on colony-forming abilities	132
4.37	Schematic illustration of mouse model used to study the effects of circZNF800 knockdown on tumorigenicity	133
4.38	Effects on tumorigenicity on circZNF800 knockdown in mice	134
4.39	Validation of the expression levels of miRNAs upon circZNF800 knockdown	136

4.40	Expression analysis of predicted pluripotency-associated pathways upon circZNF800 knockdown	137
6.1	Overview of the biological findings of the present work	153

LIST OF ABBREVIATIONS

2D	Two-dimensional
3D	Three-dimensional
AAV	Adeno-associated virus
ALDH1	Aldehyde dehydrogenase isoform 1
APC	Adenomatous polyposis coli
CeRNAs	Competing endogenous RNAs
CircRNA	Circular RNA
CRC	Colorectal cancer
CrCSC	Colorectal cancer stem cells
CRISPR	Clustered Regularly Interspaced Short Palindromic Repeats
CrRNA	Crispr RNA
CSC	Cancer stem cells
Cy3	Cyanine-3
Cy7	Cyanine-7
DAPI	4',6-diamidino-2-phenylindole
DCBLD2	CUB and LCCL domain containing 2
DMSO	Dimethyl sulfoxide
EMT	Epithelial-mesenchymal transition
FBS	Foetal bovine serum
FISH	Fluorescent <i>in situ</i> hybridisation
GAPDH	Glyceraldehyde 3-phosphate dehydrogenase
GFP	Green fluorescent protein
GO	Gene ontology

GTP	Guanosine-5'-triphosphate
ISC	Intestinal stem cell
KEGG	Kyoto Encyclopaedia of Genes and Genomes
LincRNA	Long intervening non-coding RNA
LncRNA	Long non-coding RNA
MEM	Minimum Essential Medium
MgCl ₂	Magnesium chloride
MiRNA	MicroRNA
MMR	Mismatch repair
PBS	Phosphate-buffered saline
PES	Polyether sulfone
PiRNA	Piwi-interacting RNA
polyHEMA	Polyhydroxyethylmethacrylate
qRT-PCR	Quantitative real-time PCR
RBP	RNA-binding protein
RNAi	RNA interference
SFM	Serum-free medium
SiRNA	Short interfering RNA
SSC	Saline-sodium citrate
UTR	Untranslated region
ZNF800	Zinc-finger protein 800

CHAPTER 1

INTRODUCTION

Globally, the incidence rate of colorectal cancer (CRC) remains high (Taborda, Ramírez and Bernal, 2017). In Malaysia and Taiwan, CRC remains a common top malignancy (Kuo *et al.*, 2020; Schliemann *et al.*, 2020). Colorectal cancer stem cell (CrCSC) population have been linked with the chemo- and radio-resistant population (Das, Islam and Lam, 2020). The current chemo-and radio-therapeutic regimes are believed to be less efficient against the CrCSC population, and have been postulated to result in a high recurrence rate amongst advanced CRC patients (Frank *et al.*, 2021).

CrCSC is made up of population that possess enhanced stemness and oncogenicity (Puglisi *et al.*, 2013; Iyer, Sin and Ng, 2019). Residing intestinal stem cells in the crypts of intestines have been hypothesised to frequently acquire multiple gain-of-function oncogenic mutations (Huels and Sansom, 2015). The resulting enhanced stem cell properties with unlimited proliferation in the CrCSC population have become a clinical challenge for therapeutic interventions (Agliano, Calvo and Box, 2017).

As CrCSC populations are relatively scarce in tissue samples and cancer cell lines, isolating and enriching this population for further investigations has been a hurdle (Matsui, 2016). In our previous investigations, a simple robust system via spheroidal culture was developed to enrich stemness in CRC cells. Spheroidal

culture is an anchorage-independent culture that positively selects cells that resist anoikis, programmed cell death that is induced upon loss of extracellular matrix (Fang *et al.*, 2005; He *et al.*, 2014; Fekir *et al.*, 2019). Cells resistant to anoikis have been shown to exhibit CSC-like properties in various cancers (Adeshakin *et al.*, 2021).

The previous data indicated spheroidal culture was able to enrich CRC population with enhanced CSC-like properties in a passage-dependent manner (Rengganaten, 2016). The enhanced expression levels of Yamanaka factors, *OCT4*, *SOX2*, *KLF4*, *CMYC* and *NANOG* in the established CRC spheroidal cells are indicative of stemness properties (Aponte and Caicedo, 2017). Furthermore, the CRC spheroidal cells exhibited enhanced colony-forming, migration and invasion properties. The CRC spheroidal cells also showed resistance toward common chemotherapeutic drugs, 5-fluorouracil and oxaliplatin (Blondy *et al.*, 2020). These previous data on the molecular characteristics of the established CRC spheroidal cells are consistent with CrCSC population enrichment in spheroidal culture. However, to date, the molecular mechanisms governing the CSC properties in CrCSC populations remain unclear.

Circular RNAs (circRNAs) are novel group of RNAs, which are categorised under competing endogenous RNAs (ceRNAs). CircRNAs are formed by backsplicing of exons and/or introns into three variants: exonic circRNAs (80% of all circRNAs), intronic RNAs and combined exon and intron circRNAs (Dong *et al.*, 2017). CircRNAs are widely involved in vast processes including microRNA (miRNA) sponges, modulating transcriptional machinery by regulating RNA-

binding proteins, or by directly translating to short peptides (Dong *et al.*, 2017; Wang *et al.*, 2017). Acting as miRNA sponges, circRNAs compete with targeted mRNA for miRNA binding sites, which in return regulate specific miRNAs and expression of the downstream target (Dou *et al.*, 2016; Xie *et al.*, 2016). CircRNAs are involved cancer development (reviewed by Dong *et al.*, 2017). The regulation of circRNAs in CrCSC remains to be investigated.

The involvement of circRNAs in various oncogenic hallmarks has warranted a more systematic circRNA-targeting tool to investigate the knockdown effects of specific circRNA (Verduci *et al.*, 2021). The recent discovery of CRISPR Cas13d system that enables RNA targeting has been highlighted as a potent tool for circRNA expression modulation (Wang, Zhang and Gao, 2020). Using an anti-sense RNA to target a specific RNA transcript, the ribozyme complex within the CRISPR Cas13d cleaves and degrades the targeted RNA transcript (Zhang *et al.*, 2021b). In context of circRNA investigations, the specificity of RNA targeting is essential to ensure a systematic knockdown of candidate circRNAs without significant effects on the linear host transcript. Selective knockdown of circRNA by the CRISPR Cas13d system has, indeed been reported (Li *et al.*, 2021b).

Using the previously established CRC spheroidal culture in our laboratory, the primary goal of the study was to understand the involvement of circRNA in regulating CSC properties in CrCSC cells and to identify potential candidate circRNA that could be used for therapeutic intervention. The goal was achieved by accomplishing the following objectives:

1. To establish the circular RNA profile of colorectal cancer stem cell-like population derived from spheroidal culture by whole-transcriptome RNA sequencing.
2. To identify candidate circular RNAs involved in stemness regulation via a circular RNA-microRNA-mRNA axis by bioinformatics analysis.
3. To elucidate the cellular and functional roles of a candidate circular RNA in mediating stemness properties of colorectal cancer cells by various molecular and biochemical methodologies.

CHAPTER 2

LITERATURE REVIEW

2.1 Colorectal cancer

Colorectal cancer (CRC) remains one of the most commonly diagnosed cancers (Bray *et al.*, 2018). CRC is the second life-threatening form of cancer with the third highest prevalence globally (Siegel *et al.*, 2020). In 2020, 10% of total cancer incidences and cancer-related mortalities are associated with CRC (Xie, Chen and Fang, 2020). On initial presentation, 20% of newly diagnosed CRC patients appear to be metastatic, while 25% are initially diagnosed with localised tumours before progressing to advanced stages. Less than 20% of patients diagnosed with advanced stages survive beyond 5 years from initial diagnosis (Biller and Schrag, 2021).

CRC follows a classical cancer progression model, which begins with the accumulation of mutations in key driver genes including tumour suppressors and oncogenes (Qiu, Zhang and Chen, 2020). Epigenetic dysregulations are also associated with the initiation of CRC, which collectively with the genetic mutations could transform normal epithelial intestinal cells into precancerous lesions (Grady and Markowitz, 2015). Without therapeutic interventions, the lesions could further develop into advanced adenocarcinoma and metastasise to different organs.

The common genomic alterations in CRC can be divided into two categories, chromosomal instability and microsatellite instability (Kasi *et al.*, 2020). Chromosomal instabilities are found in 85% of total CRC patients (Grady and Carethers, 2008). The general phenotypes of chromosomal instabilities include aneuploidy and polyploidy, which affect chromosomal structure and integrity (Grady and Markowitz, 2015). Alterations in the chromosomes are known to affect various tumour suppressors and oncogenes in CRC.

The most commonly implicated chromosomal instability is the mutation of *APC* (adenomatous polyposis coli), a tumour suppressor. (Kasi *et al.*, 2020). *APC* negatively regulates Wnt signalling pathways that are involved in the differentiation of intestinal stem cell population (Zoratto *et al.*, 2014). *APC* mutation dysregulates which results in hyperactivation of proliferation in the intestinal cells. *APC* mutations have also been reported to occur during the CRC precancerous development (Zhang and Shay, 2017). Other common mutations associated with CRC development include *KRAS* and *TP53* (Xie, Chen and Fang, 2020).

Microsatellite instability refers to the inability of the cells to repair alterations in genomic repeats, contributed by the gene inactivation in the DNA mismatch repair (MMR) mechanism (Kasi *et al.*, 2020). The most commonly affected pathways resulting from microsatellite instability are TGF- β and epidermal growth factor pathways, which often result in the activation of cell proliferation (Itatani, Kawada and Sakai, 2019). Other than genomic alternations, CRC developments are also associated with changes at epigenetic levels. DNA methylation at tumour suppressor promoters, which leads to the silencing of tumour

suppressive properties, is reported to occur in 40% of CRC patients (Kim and Kang, 2014).

Furthermore, other epigenetic factors are also reported to be involved in CRC development (Zoratto *et al.*, 2014). Epigenetic instabilities associated with chromatin modifications and microRNAs could either activate oncogenic pathways or inactivate tumour suppressive genes, leading to the dysregulation in cellular proliferation of intestinal cells (Baylin and Jones, 2016). Chromatin modifications could potentially inactivate tumour suppressive properties of various proteins (Qin *et al.*, 2020). The involvement of microRNA in CRC development is covered in Subsection 2.5.1 below.

2.1.1 Risk factors of CRC

CRC tumorigenesis is a multifactorial process involving a range of risk factors. The risk factors of CRC can be divided into two categories; modifiable and non-modifiable factors. The modifiable risks include obesity, diet, smoking, alcohol and other medical conditions such as diabetes. The non-modifiable factors focus on age, race, gender, hereditary mutations and family history (Kanth and Inadomi, 2021).

2.1.2 Modifiable CRC risk factors

Given the increasing trend of CRC incidence in emerging markets, evidence of changes in lifestyle attributed to modifiable risks could explain the increased number of CRC cases (Rawla, Sunkara and Barsouk, 2019). Thus, identifying these factors could avert the risk of developing CRC. Obesity, which is often associated with a lack of physical training and sedentary lifestyles, has been shown to increase the risk of developing CRC by 50% (Sawicki *et al.*, 2021). Medical intervention via health campaigns against obesity has shown success in CRC prevention (Arnold *et al.*, 2017).

Diet has also been contributed as a risk factor in the development of CRC. Consumption of high red meat and low fibre diet has been linked with higher risk of CRC (Lewandowska *et al.*, 2022). CRC risk increases by 17% with the consumption of every 100 g of processed red meat (Casella *et al.*, 2018) due to the high fats and inflammatory substances generated during the high-heat cooking process (Kim, Coelho and Blachier, 2013). A high fruits and vegetable diet has a protective effect against CRC and reduces the risk of CRC by 50% (Amersi, Agustin and Ko, 2005). High-fibre diet reduces the transient time of the stool in the intestine and increases the water content in the stool, thus reducing inflammation and contact time of potential dietary carcinogens in the intestine (Sawicki *et al.*, 2021).

Smoking and high alcohol consumption have been associated with various cancer developments. Smoking rises the risk of CRC by three folds while more than

three daily drinks of alcohol can heighten the risk of CRC by 40% (Rawla, Sunkara and Barsouk, 2019). The increased risks of CRC in smoking and high alcohol intake have been well understood: elevation of the levels of carcinogens and reactive oxygen species leads to increased chances of DNA mutations in the intestinal cells (Rossi *et al.*, 2018).

Other non-genetic inheritance diseases such as diabetes type 2 have also been associated with higher CRC risk. Diabetic patients are at 1.3-fold risk of developing CRC compared to the non-diabetic group (Peeters *et al.*, 2015). Diabetes, which is often a result of a sedentary lifestyles, could lead to increased insulin levels due to insulin resistance. The high levels of insulin can, in turn, induce hyperproliferation in the colonic cell population, constituting a precursor event in CRC development (Sawicki *et al.*, 2021).

2.1.3 Non-modifiable CRC risk factors

Age, gender and race have been individually identified as potential risk factors for CRC. Almost 90% of diagnosed CRC patients are above 50 years old, with CRC 30 times more prone to develop in individuals above 65 years old compared to the younger population (Rawla, Sunkara and Barsouk, 2019). The statistical data indicates while CRC is an age-related disease, growing incidence rate amongst younger-age groups again highlights the impacts of sedentary lifestyles and the need for preventive intervention of CRC (Edwards *et al.*, 2010).

Males are at higher risk of developing CRC than females, with males facing a poorer prognosis (Keum and Giovannucci, 2019). The disparity between genders remains poorly understood; however, sex hormones have been associated to influence CRC development. Race and ethnicity have also been listed as CRC risk factors (Xi and Xu, 2021). African-Americans are at higher risk of developing CRC in American society, with recorded higher mortalities. Globally, Europeans are reported to have the highest prevalence and mortality associated with CRC (Wong *et al.*, 2019).

Specific genetic mutations have been associated with an increased risk of developing CRC, which accounts for up to 10% of total CRC cases. Individuals with a family history of CRC have a significantly higher risk of developing CRC, correlating with the degree of consanguinity (Henrikson *et al.*, 2015). Hereditary conditions, such as Lynch syndrome and familial adenomatous polyposis coli, could eventually lead to the development of CRC (Kolligs, 2016). Other than that, inflammatory bowel disease, also known as Crohn's disease, which is a result of genetic and environmental factors, is at least six-fold higher risk of developing CRC (Hnatyszyn *et al.*, 2019).

2.2 Colorectal cancer stem cells

In a solid tumour mass, the vast majority of the cells lack the ability to self-renew with limited tumorigenicity (Gupta *et al.*, 2019). The existence of a small population of cells within a tumour mass that exhibits enhanced self-renewal and tumorigenicity abilities is known as cancer stem cells (CSC) (Munro *et al.*, 2018). CSC population has been linked to various cellular processes associated with increased tumour aggressiveness. CSC hypothesis evolves around two possibilities: (i) oncogenic mutation(s) in the stem cell population residing in certain organs; or (ii) de-differentiation mutation(s) that allow terminally differentiated cells to acquire stem-cell like properties (Alhulais and Ralph, 2019). The resulting CSC population have shown enhanced oncogenic properties and self-renewal, and inherited unlimited cell division capacities (Munro *et al.*, 2018).

The CSC population that is found in CRC is known as colorectal cancer stem cell (CrCSC) population. CrCSC is believed to arise from the acquisition of oncogenic mutations in the intestinal stem cell (ISC) population (van der Heijden and Vermeulen, 2019). The long-lived ISC population in the intestine is a good candidate for acquiring various genetic mutations to initiate CRC development (Munro *et al.*, 2018). The hypothesis followed a bottom-up theory, which dictates that the initiation of CRC begins in the bottom of intestinal crypt where the ISC population is residing (Alhulais and Ralph, 2019). The hypothesis acquires further support when reports show that introducing adenomatous polyposis coli (*APC*) mutation gives rise to the formation of adenoma only in LGR5⁺ population, which resembles ISC, but not in LGR5⁻ population (Barker *et al.*, 2009).

2.2.1 Regulation of colorectal cancer stem cells

The CrCSC population makes up from 0.1% to 10% of the entire tumour mass. The small fraction of the CrCSC population has been associated with enhanced tumorigenicity, recurrence and chemoresistance in CRC (Pashirzad *et al.*, 2022). The association of CrCSC population with increased oncogenicity is attributed to the higher plasticity observed in the CrCSC population (van der Heijden and Vermeulen, 2019). Furthermore, CrCSC population has been shown to constantly activate various stemness-associated pathways, including Wnt/ β -catenin and Notch signalling pathways (Conciatori *et al.*, 2019).

The activations of specific signalling pathways are important in the regulation of various CrCSC properties. The constant up-regulation of Wnt/ β -catenin signalling pathway has been shown to increase the differentiation potential and chemoresistance in CrCSC population (Zhou *et al.*, 2018). In normal homeostasis, Wnt/ β -catenin signalling controls the cell fate of ISC population. The signalling pathway is highly activated from the bottom of the intestinal crypt, where ISC population is primarily residing (Angius *et al.*, 2021). Wnt/ β -catenin signalling activation is gradually suppressed upon moving upstream of the crypt. This event allows a systematic differentiation of the colonic crypts, producing progenitor cells with limited self-renewal capacity (Gupta *et al.*, 2019). However, as APC mutations are common in CRC, the mutations often result in hyperactivation of the Wnt/ β -catenin signalling pathway (van der Heijden and Vermeulen, 2019) and uncontrolled proliferation of ISC-like population in CRC, yielding highly metastatic and therapy-resistant cells (Angius *et al.*, 2021).

Besides Wnt/ β -catenin, activation of the Notch signalling pathway has also been implicated in regulating CrCSC properties. Notch pathway is important in the

embryogenesis, differentiation and epithelial-mesenchymal transition (EMT) processes (Munro *et al.*, 2018). Notch pathway inhibits apoptosis by repressing cell cycle regulators (Gupta *et al.*, 2019). In CrCSC population, the activation of the Notch signalling pathway enhances the self-renewal abilities, migratory properties of CrCSC, and anti-apoptotic mechanism to resist therapeutic interventions, including radio- and chemo-therapy (Angius *et al.*, 2021).

Similarly, dysregulation of the Hedgehog signalling pathways, which maintain the stemness properties in ISC population could result in the hyperplasia of ISC population and acts as a precursor for CRC development (Wu *et al.*, 2017). The Hedgehog activation in CRC cells results in enhanced CrCSC properties, including tumourigenicity, metastasis and recurrence (Varnat *et al.*, 2009). Interestingly, the crosstalk between the Wnt and Hedgehog signalling pathways enhances the CrCSC phenotype resulting in increased CRC metastatic abilities (Song *et al.*, 2015).

2.2.2 Identification of colorectal cancer stem cell population

CRC is composed of a heterogeneous cell population. CRC consists of cells of different self-renewal potentials, forming a hierarchy based on cellular potency (van der Heijden and Vermeulen, 2019). CrCSC population forms the top of the hierarchy, which are transformed intestinal cells with enhanced stemness and oncogenic properties (Angius *et al.*, 2021). Phenotypic markers to discriminate the intestinal stem cell population and non-CrCSC cancer population remain a challenge (van der Heijden and Vermeulen, 2019).

CD133⁺ cell population has been well documented to exhibit CSC-like properties in various solid tumours. CD133 is a glycoprotein localised in the transmembrane, and is involved in cellular differentiation and epithelial-mesenchymal transition (EMT) (Angius *et al.*, 2021). CD133⁺ cells isolated from CRC populations mimic functional properties of CrCSC, including enhanced self-renewal, higher cellular proliferation, migratory abilities and resistant to radio- and chemotherapy (Todaro *et al.*, 2007; Zhi *et al.*, 2015; Gisina *et al.*, 2019).

CD44 is another common CrCSC marker. CD44 is involved in cell adhesion and migration under normal physiological conditions (Gupta *et al.*, 2019). CD44⁺ population exhibits enhanced tumorigenicity and cell proliferation in CRC, compared to CD44⁻ population (Marhaba *et al.*, 2008). Knockdown of CD44 in CRC cells reduces self-renewal abilities and tumorigenicity in a mouse model (Du *et al.*, 2008). In the same study, limiting-dilution transplantation assays of CD44⁺

and CD44⁻ CRC cells show that a mere 100 cells of CD44⁺ population were sufficient to initiate tumour growth (Du *et al.*, 2008).

ALDH1 (Aldehyde dehydrogenase isoform 1) is a metabolic enzyme responsible for aldehyde conversion. Different isoforms of ALDH1 have been identified as CSC markers for different cancer types (Kozovska *et al.*, 2018). The high expression levels of ALDH1 correlate inversely to different degrees of CRC differentiation (Rassouli, Matin and Saeinasab, 2016). Furthermore, due to the metabolic involvement of ALDH1, CRC cells expressing high levels of ALDH1 often exhibit chemoresistance properties (Deng *et al.*, 2014).

Besides phenotypic markers, molecular markers have been associated in identifying CrCSC population. Since the discovery of the Yamanaka reprogramming transcriptional factors, Oct4, Sox2, Klf4, cMyc and Nanog, which are implicated in the maintenance of cellular potency in stem cells, various studies have focused on investigating the expression levels of these transcriptional factors in CSC populations (Bradshaw *et al.*, 2016). Each of the transcriptional factors has been correlated with enhancing the CSC properties, either individually or in different combinations (Munro *et al.*, 2019).

Oct4 has been associated with cancer recurrence, metastasis and increased levels of undifferentiated CRC population (Dai *et al.*, 2013; Amini *et al.*, 2014). Sox2 maintains the cellular potency and increased the metastatic potential of CRC population (Neumann *et al.*, 2011). Nanog, expressed downstream of Oct4 and Sox2, has been shown to correlate with a poor prognosis of CRC (Hadjimichael *et*

al., 2015). Klf4 controls chemoresistance properties in regard to CSC population while cMyc is a proto-oncogene involved in CRC development (Munro *et al.*, 2018). However, since these transcriptional factors are not exclusively expressed in CrCSC population, they are not good candidates for CrCSC identification purposes.

2.3 *In vitro* enrichment tools of colorectal cancer stem cells

Colorectal cancer stem cells (CrCSC) population makes up a small fraction of the entire tumour mass, hence, there is a need for *in vitro* culturing approaches (Pashirzad *et al.*, 2022). The culturing of CrCSC should take into account enrichment of the CRC population and maintaining the stemness properties by preventing cell differentiation. Furthermore, long-term propagation of the CrCSC population while preserving the typical properties CSC, such as self-renewal abilities, should also be considered (De Angelis *et al.*, 2021).

Isolation based on phenotypic CrCSC surface markers using flowcytometry has been reported. CD133, CD44 and ALDH1 have been used to isolate potential CrCSC population using flowcytometry (Wahab *et al.*, 2017). While the fluorescence-activated cell sorting approach has shown promising results on CrCSC enrichment, maintaining the CrCSC population in long-term cultures has been challenging. Due to the asymmetrical cell division, the sorted population continues to be heterogenous with a mixture of different stages of differentiated CRC cells upon propagation (De Angelis *et al.*, 2021).

Another approach to enrich CrCSC population is by using serial transplantation of xenograft tumours in mice. Patient-derived tissues or cell lines can be used to generate xenograft tumours (De Angelis *et al.*, 2021). Using the limiting dilution process, the tumour-initiating cells can be enriched to enable tumour growth during each serial transplantation (Dieter *et al.*, 2011). Thus, constant pure CrCSC cells are cultured throughout. However, this approach is time-consuming, expensive and laborious (Ibarrola-Villava, Cervantes and Bardelli, 2018).

2.3.1 Spheroidal culture

Conventional cell culture method uses the two-dimensional (2D) approach in which cells are grown as monolayer culture on a solid surface. The 2D method does not represent the physiological condition nor provides the *in vivo* microenvironment for the growth of the cells (Hoarau-Vechot *et al.*, 2018). Furthermore, the 2D culture changes the cellular architecture by creating a flattened cell morphology and altering cell-to-cell communication (Colombo and Cattaneo, 2021). The artificial effects of the 2D culture are often associated with the lack of consistency of the *in vitro* data and the inability to reproduce similar data in animal models (Zhang *et al.*, 2020a).

In contrast, three-dimensional (3D) cultures that promote cell-to-cell and cell-to-matrix interactions have been widely accepted as an effective method to culture CSC populations. By mimicking the complex microenvironment exhibited in the tumour microenvironment, anchorage-independent 3D culture allows a natural physiological and structural architecture for cellular growth.

3D culture, also known as spheroidal culture, is a commonly used method in enriching cancer cells with CSC-like properties (Zhang *et al.*, 2020a). By culturing the cancer cells in an anchorage-independent condition, cells with higher cellular potency survive the culture conditions and form floating spheres (Colombo and Cattaneo, 2021). The anchorage-independent culture allows cells to be resistant to anoikis, a programmed cell-death process that occurs when terminally differentiated cells lose cell-to-matrix interaction (Zhang *et al.*, 2020a; Velletri *et al.*, 2022). Moreover, CSC populations are known to resist anoikis and proliferation without any matrix. The resulting spheroids can be propagated under similar conditions for many passages to enrich the cancer cells with higher CSC-like properties (De Angelis *et al.*, 2021).

Furthermore, spheroidal culture is able to recapitulate the architecture of *in vivo* tumour structure. Nutrient and oxygen gradients are formed due to the geometry of the spheroids to simulate the hypoxia conditions in tumour mass, allowing for cellular heterogeneity (Holle, Young and Spatz, 2016). Other than that, the maintenance of the cell-to-matrix interaction controls conditions more similar to *in vivo* environment, including pH and oxygen levels (Herrmann *et al.*, 2014; Zhang *et al.*, 2020a).

Cells generated from spheroidal culture have shown close resemblance to CSC population, including cells from CRC. CRC cell lines, HT29 and Caco-2 were subjected to spheroid culture and the resulting spheres exhibited classical properties of CrCSC, including up-regulation of CrCSC markers and stemness transcriptional factors and EMT markers (Gheytauchi *et al.*, 2021). Similarly, spheres generated from CRC patient-derived tissues expressed higher levels of CrCSC markers, CD133, CD44 and ALDH1. Furthermore, the spheres also exhibited resistance to cetuximab and recapitulated the original tumour pathology when transplanted into mice (Lee *et al.*, 2015). These reports highlight the reliability of spheroidal culture as an *in vitro* means for CrCSC enrichment using CRC tissue and cell lines.

In our previous work, we developed a CrCSC spheroidal cell model, using HCT-15 and WiDr (CRC cell lines) to enrich CRC cells with the derived cell population shown to resemble CrCSC. The spheroidal culture was subjected to serial passaging of the spheres, aimed to enrich the CSC population in the CRC cells. Characterisation of the resulting CRC spheroids showed increased levels of CSC markers, chemoresistance, migration and invasion properties (Rengganaten, 2016). The CrCSC spheroidal model thus established was used in the present study for further investigation.

2.4 Non-coding regulatory RNAs

Non-coding RNAs refer to single-stranded RNA transcripts that are not translated into proteins. However, non-coding RNAs can regulate gene expression at the post-transcriptional level (Shirmohamadi *et al.*, 2020), regulating various important biological processes; dysregulation of the non-coding RNAs has been commonly reported as oncogenic factors (Slack and Chinnaiyan, 2019). Non-coding RNAs are classified based on the size of the RNA; short non-coding RNAs and long non-coding RNAs. Short non-coding RNAs include short interfering RNA (siRNA), microRNA (miRNA) and piwi-interacting RNA (piRNA) (French and Pauklin, 2021). Long non-coding RNAs (lncRNAs) are non-coding RNAs longer than 200 nucleotides, which include sense, antisense, intergenic and intronic lncRNAs. More recently, a group of novel lncRNA, known as circular RNA (circRNA), was discovered (Slack and Chinnaiyan, 2019).

2.4.1 MicroRNAs

MicroRNA (miRNA) is a non-coding RNA between 18 – 25 nucleotides in length. MiRNAs act at the post-transcriptional levels by complementarily binding with the 3'-untranslated region (UTR) of target transcripts, leading to degradation and inhibition of translation. The degradation of the target mRNA is facilitated by an RNA-induced silencing complex. Despite being relatively short, miRNAs exert a wide range of regulatory control, given the fact that a miRNA has multiple mRNA targets and an mRNA can be targeted by multiple miRNAs. As such, miRNAs are

often denoted as master post-transcriptional regulators, having control over major biological processes. Thus, dysregulation of miRNAs could lead to the development of various diseases including cancer.

MiRNA dysregulation in cancer occurs when the levels of the miRNAs are abnormal, leading to negative modulation of tumour suppressive genes, or activation of oncogenic factors via suppressed expression of oncogene suppressors. Besides being involved in oncogenicity, miRNAs are also important in maintaining stemness in stem cells. MiR-21, a well-studied oncogenic miRNA, is up-regulated in various cancer types (Fulci *et al.*, 2007; Feng *et al.*, 2011; Feng and Tsao, 2016).

MiRNAs have been associated with the properties of CrCSC. MiR-137 is known to repress tumour growth in various cancers, including CRC, by down-regulating oncogenes such as MS11 (Balaguer *et al.*, 2010; Liu *et al.*, 2011). Furthermore, miR-137 also is involved in the stemness regulation in stem cell populations (Jiang, Ren and Nair, 2013). In CrCSC, the expression levels of miR-137 are down-regulated, contributing to the maintenance of stemness in CRC population (Sakaguchi *et al.*, 2016).

Similarly, miR-451 has been shown to be down-regulated in CrCSC population (Bitarte *et al.*, 2011), to control self-renewal, tumorigenicity and chemoresistance in CrCSC cells. Mechanistically, miR-451 indirectly down-regulates the Wnt signalling pathway, which is essential for CrCSC stemness maintenance. Modulation of miR-21, an oncogene, promotes CSC properties in CRC population (De Robertis *et al.*, 2018). Overexpression of miR-21 increases the

self-renewal properties of the CRC cells, while miR-21 knockdown significantly induces cellular differentiation in the CRC spheroidal cells. MiR-21 was shown to target TGF- β signalling pathway to exhibit the CSC properties in CRC cells (Yu *et al.*, 2012).

2.4.2 Circular RNAs

Circular RNA (circRNA) is a long non-coding RNA with the 3' and 5' ends covalently joined to form a circle. Discovered during the mid-1970s, circRNAs were initially thought to be a by-product of RNA splicing (Sanger *et al.*, 1976). Circularised RNAs were first identified in plant viroid and δ hepatitis virus. The first association of circRNA in human biology was made during the discovery of circularised isoforms of RNA transcripts from the *DCC* gene in the CRC (Nigro *et al.*, 1991). However, advancements in RNA sequencing have rapidly unlocked the potential roles of circRNAs. CircRNAs have now been associated with a wide range of biological processes in normal homeostasis and abnormal conditions (Harper, McDonnell and Whitehouse, 2019).

2.4.2.1 Biogenesis and properties of circRNA

Precursor mRNAs generated via RNA polymerase II are canonically spliced to generate linear mRNA transcripts (Tang *et al.*, 2021). However, in the case of circRNAs, the precursor mRNAs undergo a backsplicing process, a novel RNA splicing that remains poorly understood. A few reports have suggested that RNA circularisation through backsplicing is facilitated by inverted complementary sequences flanking the introns. The intron-pairing recruits RNA-binding proteins and spliceosome to facilitate the joining of the 3' and 5' ends. However, further investigation is needed to fully understand the formation of circRNA (Harper, McDonnell and Whitehouse, 2019; Shao, Pan and Xiong, 2021; Tang *et al.*, 2021).

CircRNAs can be categorized into three types based on the region of the mRNA transcripts retained in the circRNA; exonic circRNA, exonic-intronic circRNA and intronic circRNA (Shao, Pan and Xiong, 2021). Exonic circRNAs that are derived entirely from exonic regions of the precursor mRNA transcripts make up the most common type of circRNA. Exonic-intronic circRNAs refer to circRNAs composed of exons and introns of the precursor transcripts, while intronic circRNA is made up of introns only, also known as a lariat in conventional pre-mRNA splicing (Harper, McDonnell and Whitehouse, 2019). The functional difference between the different types remains to be elucidated.

CircRNAs have properties that are distinct from other types of RNAs. As circRNAs lack 5' cap and 3' poly(A) tail, circRNAs are more stable and resistant to RNase endonuclease degradation compared to linear mRNA transcripts (Harper, McDonnell and Whitehouse, 2019; Verduci *et al.*, 2021; Shao, Pan and Xiong, 2021). Some reports suggest that circRNAs could be tissue- and species-specific (Tang *et al.*, 2021; Lu *et al.*, 2022). Furthermore, circRNAs have been investigated as potential biomarkers for various diseased conditions due to the presence of circRNA in bodily fluids such as saliva, blood and urine (Jacky Lam and Dennis Lo, 2019; Verduci *et al.*, 2021).

2.4.3 Biological roles of circRNA

Most of the known biological roles of circRNAs involve regulating gene expression at post-transcriptional. CircRNAs could interact with RNA-binding proteins (RBPs) to regulate gene transcription activities while post-transcriptionally, circRNAs act as miRNA sponges, annulling translation suppression mediated by miRNAs. More recently, despite being categorised as non-coding RNAs, a few circRNAs have been shown to be translated to generate novel proteins. However, studies on the functionality of the circRNA-translated proteins are just beginning.

2.4.3.1 CircRNA as a transcriptional regulator

CircRNAs regulate the transcriptional activity by either suppressing or enhancing transcriptional levels of target mRNAs (Harper, McDonnell and Whitehouse, 2019; Shao, Pan and Xiong, 2021). CircRNAs could act as protein decoys by baiting selected proteins and inhibiting protein activities. Circ-Foxo3 was reported to bind with cell cycle regulator proteins to block downstream regulation in relation to breast cancer cell proliferation (Du *et al.*, 2016). Circ-Ago2 binds with the HuR protein to increase the export of the HuR protein into the cytoplasm. HuR then competitively binds with the 3' UTR region of target mRNAs to prevent degradation induced by miRNAs (Chen *et al.*, 2019).

CircRNAs are also known to regulate the alternative splicing mechanism by controlling the host gene expression levels. CircRNAs have been reported to form a complex with small nuclear ribonucleoprotein, which interacts with RNA polymerase II (Li *et al.*, 2015). The interaction with RNA polymerase II enhances the transcriptional activities of host gene. Circ-UBR5 binds with RNA-binding proteins QKI and Nova-1, which modulate the backsplicing mechanism of circRNA (Qin, Wei and Sun, 2018).

2.4.3.2 CircRNA as a post-transcriptional regulator

One of the most important biological roles of circRNA is to act as a miRNA sponge. By sponging miRNAs, and therefore removing miRNAs from the scene, circRNA plays a dominant role in post-transcriptional regulation, by controlling the miRNA availability and the downstream mRNA targets of the miRNA (Verduci *et al.*, 2021). Individual circRNAs might have multiple binding sites for the same or different miRNAs. CiRS-7 is one of the most well-known circRNAs that has been investigated for the role as a miRNA sponge (Harper, McDonnell and Whitehouse, 2019) of the tumour suppressor miRNA, miR-7. By containing up to 70 potential binding sites for miR-7, ciRS-7 effectively inhibits the tumour suppressive activity of miR-7 and induces increased cellular proliferation in various cancer types (Chen *et al.*, 2021).

2.4.4 Roles of circRNA in CRC

A few circRNAs have been shown to play a role in different aspects of CRC tumorigenesis. Circ-VAPA was shown to be up-regulated in CRC and by sponging miR-125a, circ-VAPA increases proliferation and EMT properties (Li *et al.*, 2019). CiRS-7 and circ-HIPK3 are also reported to be involved in CRC (Tang *et al.*, 2017; Zeng *et al.*, 2018). CiRS-7 promotes CRC progression by sponging miR-7 and the knockdown of CiRS-7 reduces the viability and colony-forming abilities of CRC cells. Similarly, by sponging miR-7, circ-HIPK3 and CiRS-7 have been proposed as potential targets for clinical intervention (Li *et al.*, 2021a).

Besides acting as oncogenic factors in CRC, circRNAs could also act as tumour suppressors. Circ-ITGA7 was found to be down-regulated in CRC tissue samples; however, Circ-ITGA7 overexpression in CRC inhibits cancer growth and metastasis by affecting Ras signalling pathways (Li *et al.*, 2018c). Overexpression of circ-FBXW7 suppresses proliferation, migration and tumour growth (Lu *et al.*, 2019). Despite the increasing list of circRNAs involved in CRC progression, no circRNA have been subjected to clinical trials.

On the other hand, circRNAs have also been associated with the maintenance of stemness in stem cell population. Circ-BIRBC6 was shown to maintain pluripotent state in human embryonic stem cells and to suppress cellular differentiation by sponging miR-34a and miR-145 (Yu *et al.*, 2017a). Circ-NOTCH was shown to facilitate the maintenance of stemness properties in gastric CSC population by sponging miR-449c-5p (Zhao *et al.*, 2020a).

However, circRNA involvement in CrCSC population remains unknown. Identification of a candidate circRNA involved in the maintenance of stemness in CrCSC population could be a first step in eradicating CRC. Being multipotent, stem cell differentiation therapy has been gaining attention as an approach to deplete CSC population in solid tumours (Arima, Nobusue and Saya, 2020). Understanding the role of circRNAs in CrCSC population could be advantageous in designing a potent differentiation therapy protocol for CRC.

CHAPTER 3

MATERIALS AND METHODS

3.1 Cell culture

Cell culture was performed in Class II Biosafety Cabinet (ESCO, Singapore). Aseptic techniques were observed during cell culture to prevent contaminations. All cells were maintained in a humidified incubator (ESCO, Singapore) with 5% CO₂ at 37 °C.

3.1.1 Colorectal cell lines

Human colorectal cancer (CRC) cell lines used in the study includes HCT-15, WiDr, HT-29, HCT-116, SW-480 and SW-620. HCT-15 was maintained in DMEM (Dulbecco's Modified Eagle Medium) high glucose (Gibco, Thermo Fisher Scientific, Massachusetts, USA), while WiDr was cultured in MEM (Minimum Essential Medium, Gibco, Thermo Fisher Scientific, USA). HT-29, HCT-116, SW-480 and SW-620 were all maintained in DMEM-F12 (Gibco, Thermo Fisher Scientific, USA). WiDr, HT-29 and HCT-116 are derivatives of colon adenocarcinoma of unspecified pathological grade based on the information from ATCC. HCT-15 was derived from a high-grade CRC tumour. SW-480 and SW-620 CRC cell lines were derived from the same patient, where SW-480 was derived from tissues of early colon adenocarcinoma and SW-620 developed from metastatic

colon cancer tissue of the same patient. HCT-15 and WiDr were used for the RNA sequencing and downstream analysis as the cell lines represent early and late-stage CRC disease, respectively.

The basal mediums were prepared based on the manufacturer's instructions and sterilized with 0.22 μm polyether sulfone (PES) filter (Biofill, China). All mediums were supplemented with 10% foetal bovine serum (FBS, Gibco, Thermo Fisher Scientific, USA) and 1% penicillin-streptomycin (Gibco, Thermo Fisher Scientific, USA). The mediums were stored at 4 °C until further use.

The cells were expanded from the cryopreserved cells. Frozen cryovials were thawed in 37 °C water bath and added into a prewarmed serum-supplemented medium. The medium containing the cells was centrifuged at 1,000 rpm for 3 min and the supernatant was discarded. The cell pellet was resuspended with the serum-supplemented medium and transferred into a culture dish (SPL, Korea). The cells were left in the humidified incubator overnight. The medium was replenished with fresh serum-containing medium, every two to three days. Upon reaching > 70% cell confluency, the cells were rinsed with phosphate-buffered saline (PBS, Amresco, Pennsylvania, USA) to remove residual FBS. The cells were incubated with 0.25% trypsin-EDTA (Gibco, Thermo Fisher Scientific, USA) to allow enzymatic dissociation until complete single-cell suspension was generated. Serum-containing medium was added to stop the enzymatic digestion and the cell suspension was centrifuged at 1,000 rpm for 3 min. The supernatant was discarded and the cell pellet was resuspended with fresh medium and seeded into a new culture dish, based on the seeding ratio between 1:5 to 1:10.

For cryopreservation, the dissociated single cell suspension was resuspended with PBS and centrifuged at 1,000 rpm for 3 min. The cell pellet was suspended with a mixture of 9 parts of FBS and 1-part dimethyl sulfoxide (DMSO, Sigma-Aldrich, Merck, Germany). The cell suspension was aliquoted into individual sterile cryovials (SPL, Korea) and placed in -80 °C in CoolCell freezing containers (Corning, New York, USA). For long-term storage, the vials were stored in liquid nitrogen.

3.1.2 Spheroidal culture

The spheroidal culture was performed based on the method used in our previous study (Rengganaten, 2016). Briefly, CRC cells were dissociated from the aforementioned method. The cells were stained and counted using 0.4% (v/v) trypan blue solution (Gibco, Thermo Fisher Scientific, USA) and seeded at 5×10^4 cells/ml for the spheroidal culture. The cells were resuspended in serum-free medium (SFM). SFM was prepared using DMEM-F12 (Gibco, Thermo Fisher Scientific, USA) supplemented with 0.24% (v/v) methylcellulose (Sigma-Aldrich, Merck, Germany), 20 ng/ μ L epidermal growth factor (Miltenyi Biotech, Germany), 10 ng/ μ L basic fibroblast growth factor (Miltenyi Biotech, Germany), $1 \times$ B27 supplement (Invitrogen, Thermo Fisher Scientific, USA), 0.4% bovine serum albumin (Sigma-Aldrich, Merck, Germany) and 1 mg/mL of insulin (Gibco, Thermo Fisher Scientific, USA). The cells were cultured in polyHEMA-coated culture flasks, (polyhydroxyethylmethacrylate, Sigma-Aldrich, Merck, Germany).

The cells were supplemented with additional fresh SFM on day 7 and continued to be grown to form spheroids for up to 14 days. On day 14, the spheroids were collected by centrifugation at 1,000 rpm for 3 min. The spheroids were either harvested for subsequent analysis or dissociated using StemPro™ Accutase™ Cell Dissociation Reagent (Gibco, Thermo Fisher Scientific, USA) for further passaging. The spheroid pellets were incubated with Accutase for up to 5 min before subjecting the spheroids to mechanical dissociation using pipettors. The cells were centrifuged and resuspended in PBS before seeding in the same condition for further cultivation.

3.2 CRC clinical patient tissues

Primary CRC and adjacent normal patient tissues were obtained from patients who undergo colectomy in Taipei Veterans General Hospital, Taiwan. The collection of CRC patient tissues was in accordance with the International Ethical Guidelines for Biomedical Research Involving Human Subjects and was approved by the Medical Ethical Committee of Taipei Veterans General Hospital, Taiwan (V110C-129). Written consents from the patients were obtained before tissue collection.

Paired adjacent normal and CRC tissues from 20 CRC patients were collected from different stages, ages and gender groups. The tissue samples were chopped into smaller pieces and stored in -80 °C in RNAlater (Invitrogen, Thermo Fisher Scientific, USA) for RNA extraction. Paraffin-embedding tissue slides, the tissues were fixed in 4% paraformaldehyde (Sigma-Aldrich, Merck, Germany)

overnight at 4 °C. The paraformaldehyde was rinsed off with PBS and subjected to tissue sectioning (Bio-Check Laboratories, Taiwan).

3.3 Genome-wide circular RNA profiling

The expression profile of circular RNA (circRNA) was established using RNA sequencing approach. HCT-15 and WiDr cells and the corresponding spheroidal cells were subjected to circRNA profiling as described below.

3.3.1 RNA extraction

CRC cells were collected through cell scrapping or centrifugation. The cell pellets were washed twice with PBS and collected with centrifugation at 4 °C. The supernatants were discarded and the pellets were homogenised with TRIzol reagent (Invitrogen, Thermo Fisher Scientific, USA). The cells were incubated for 10 min at room temperature. One part of 1-bromo-3-chloropropane (Molecular Research Center, Ohio, USA) was added to the homogenate and pulse-vortexed for a minute before incubating for 15 min at room temperature. The homogenates were centrifuged at 15,000 rpm for 15 min at 4 °C. The transparent clear phase of the mixture which contains RNA was transferred into a new tube. Equal parts of isopropanol (Sigma-Aldrich, Merck, Germany) were mixed and incubated at room temperature for 10 min. The solution was centrifuged at 10,000 rpm for 10 min at 4 °C. The supernatant was discarded and the RNA pellet was washed with 75%

ethanol (Sigma-Aldrich, Merck, Germany) twice by centrifugation at 10,000 rpm for 10 min at 4 °C. The supernatant was discarded and the RNA pellet was allowed to be air-dried. The RNA pellet was resuspended with RNase-free water and quantified using a UV spectrophotometer (Thermo Fisher Scientific, USA). RNAs with an $A_{260}:A_{280}$ ratio between 1.8 to 2.0 were used for subsequent experiments and stored at -80 °C for storage.

3.3.2 Library preparation

The extracted RNA was accessed for integrity and quality using Agilent Bioanalyzer 2100 (Santa Clara, California, USA). RNA samples with integrity numbers higher than 9 were used for circRNA profiling. Ribosomal RNA was depleted using Illumina Stranded Total RNA Prep with Ribo-Zero Plus (Illumina, California, USA), according to the manufacturer's instructions. The remaining RNAs were subjected to RNase R (Epicenter, Wisconsin, USA) treatment to remove linear RNA and enrich circRNA following the manufacturer's instructions (described further in Section 3.6.2). The RNA was fragmented using divalent cations under elevated temperatures. The library preparation was carried out using TruSeq Stranded Total RNA Library Prep Gold (Illumina, California, USA). Sequencing of the library was performed on the Illumina HiSeq™ 2500 system based on the manufacturer's protocol.

3.4 Bioinformatics analysis

Based on the RNA sequencing data, the circRNAs were identified using the find_circ database (Memczak *et al.*, 2013). The identified circRNAs were then analysed for the differential expression between the CRC parental and spheroidal cells. Using the DEGseq algorithm the differentially expressed circRNA profile was established. The *p*-values of differentially expressed circRNAs were adjusted using the Benjamini–Hochberg approach. The differentially expressed circRNAs were visualized using data mining tool Orange Data Visualising software (Demšar *et al.*, 2013).

MicroRNA (miRNA) interactions were predicted based on the putative binding sites in circRNAs. The predictions were performed using CircInteractome (Dudekula *et al.*, 2016). The prediction of mRNA targets of selected miRNAs was performed using the miRWalk database. For visualising, Cytoscape software was used to construct the circRNA-miRNA-mRNA network (Smoot *et al.*, 2011). Functional annotations of the mRNA transcripts identified in the circRNA-miRNA-mRNA network were performed using publicly available bioinformatics resources. Host genes of selected circRNAs and the predicted mRNAs were analysed using gene ontology (GO) and Kyoto Encyclopaedia of Genes and Genomes (KEGG) pathway using DAVID (version 6.8).

3.4.1 Selection of top differentially expressed circRNA

The top differentially expressed circRNAs were identified based on the unique circRNA junction reads from the RNA sequencing data. A combined of over 15,000 unique circRNAs were identified from the sequencing data of HCT-15 and WiDr cells. Orange Data Visualising software was used in identifying the consistently top up- and down-regulated circRNAs in CRC spheroidal cells based on both HCT-15 and WiDr circRNA profiles. The identification was done by gradually increasing the fold change difference between the CRC parental and spheroidal cells of HCT-15 and WiDr. The \log_2 fold change was uniformly increased starting from value 1 until the list was shortened to only contain four circRNA candidates that were up-regulated in both HCT-15 and WiDr spheroidal cells. For the down-regulated circRNAs, the values were gradually reduced until four candidates remained.

3.4.2 Construction of circRNA-miRNA-mRNA axis

Using the top four differentially expressed circRNAs, the interacting miRNAs were predicted using CircInteractome database. CircRNA-miRNA binding prediction with a context score percentile higher than 90 was selected. The identified circRNA-miRNA interactions were visualised using Cytoscape platform. To narrow the list of miRNAs, a stringent criterion was applied; each miRNA should have at least four or more interactions with the top four differentially expressed circRNAs. The narrowed list of miRNAs was used to identify the

downstream mRNA target transcripts using miRWalk and the interaction was visualized using Cytoscape. Similar to the miRNA's stringent criterion, the mRNAs list was narrowed by identifying mRNAs that had five or more interactions to miRNAs. The interaction between circRNAs, miRNAs and mRNAs that were identified based on the stringent criteria were constructed using Cytoscape. The narrowed list of mRNAs identified was then subjected to GO and KEGG analysis.

3.5 Quantitative analysis of RNA

The expression levels of circRNAs, miRNAs and mRNAs were evaluated using quantitative real-time PCR (qRT-PCR). The methods used in each quantification are described in this subsection.

3.5.1 cDNA conversion

Total RNA extracted as described in Section 3.3.1 was subjected to cDNA conversion for circRNA and mRNA qRT-PCR analysis. Reverse transcription of the RNA to cDNA was performed using SuperScript III Reverse Transcriptase (Invitrogen, Thermo Fisher Scientific, USA). Firstly, the RNA (5 μ g) was mixed with 50 ng of random hexamers and 0.5 mM dNTP Mix. The mixture was incubated at 65 °C for 5 min and placed on ice for 1 minute. Next, 1 \times RT buffer, 0.05 M DTT and 200 U of SuperScript® III RT enzyme were added to the RNA mixture to a final volume of 20 μ L. The RNA mixture was then incubated at 25 °C for 10 min,

50 °C for 50 min and 85 °C for 5 min and hold at 4 °C. The cDNA was either immediately used or stored at -20 °C for future use.

3.5.2 Circular RNA quantitative real-time PCR

CircRNA expression levels were analysed using quantitative real-time PCR (qRT-PCR) based on specific primers spanning the unique backsplice junction of circRNAs. The primers were designed using NCBI primer blast tool. Based on the backsplice junction obtained from CircInteractome, divergent primers were designed to ensure selective amplification of the circRNA. The list of primers used in circRNA identification is shown in Table 3.1. The cDNA was assessed using qRT-PCR assay using SYBR Select Master Mix (Applied Biosystems, Thermo Fisher Scientific, USA). The qRT-PCR assay was performed based on the manufacturer's instructions. cDNA (50 ng) was mixed with forward and reverse primers (0.2 µM), and 5 µL of SYBR Select Master Mix (2×) to a final volume of 20 µL per well. The mixture was incubated in QuantStudio™ 3 Real-Time PCR System (Applied Biosystems, Thermo Fisher Scientific, USA). The mixture was first incubated at 50 °C for 2 min, 95 °C for 2 min, followed by 40 cycles of 95 °C for 3 sec and 60 °C for 30 sec. The assay was performed in triplicates and the housekeeping gene, GAPDH (Glyceraldehyde 3-phosphate dehydrogenase) was used as an internal control. Relative circRNA expression levels were calculated using the comparative C_T ($\Delta\Delta C_T$) method.

Table 3.1 List of circular RNA primers

Circular RNA (hsa)	Forward primer (5' – 3')	Reverse primer (5' – 3')
circ_0066631	AACAAGGTGATGGATGTGGA	TGCGAACTCTCTCTCCCATC
circ_0082096	GGCTCTTGTCTGGAACATAAC	TCTGAAGAGACTGCGGCATA
circ_0002970	GCCGGTGATGTAGACGAAAG	CTATCTCCTCCCCGATGTGC
circ_0008599	AATGACTGGTCTACGTGGGG	GGACCAGAAACCTGCAGTGT
circ_0000400	TTCGCCTCCTAATCCCTAGC	CCGTGTTCCAGGCAGTAGA
circ_0005174	GGACTTCCGGGGTAATGACA	TCTTGATGGGACCGTTTTATC
circ_0005507	AGAATTGAAGCTGCGGGGTA	GGCACTCCTTCCCTACTGT
circ_0040238	ACTTGGGTACATCTGGGGAC	GCAGACTTCCACGTTGTTCA

3.5.3 mRNA quantitative real-time PCR

mRNA transcript expression levels were analysed qRT-PCR based on primers designed using NCBI primer blast tool. Exon-exon junction spanning primers were designed to amplify mature mRNA sequences. The list of primers used in mRNA expression analysis is shown in Table 3.2. The cDNA was assessed using qRT-PCR assay using SYBR Select Master Mix (Applied Biosystems, Thermo Fisher Scientific, USA). The qRT-PCR assay was performed based on the manufacturer's instructions. cDNA (50 ng) was mixed with forward and reverse primers (0.2 μ M), and 5 μ L of SYBR Select Master Mix (2 \times) to a final volume of 20 μ L per well. The mixture was incubated in QuantStudio™ 3 Real-Time PCR System (Applied Biosystems, Thermo Fisher Scientific, USA). The mixture was first incubated at 50 °C for 2 min, 95 °C for 2 min, followed by 40 cycles of 95 °C for 3 sec and 60 °C for 30 sec. The assay was performed in triplicates and the housekeeping gene, GAPDH (Glyceraldehyde 3-phosphate dehydrogenase) was used as an internal control. Relative circRNA expression levels were calculated using the comparative C_T ($\Delta\Delta$ C_T) method.

Table 3.2 List of mRNA primers

mRNA	Forward primer (5' – 3')	Reverse primer (5' – 3')
FZD3	AAAGCTCGCTGTCGCTGG	GAAATGCTATCCTCAGACCCC
IL6ST	ACAGAACAGCATCCAGTGTC	TCTGGAGGCAAGCCTGAAATTA
SKIL	TATGCAGGACAGTTGGCAGAA	TTGCTTCCCGTTCCTGTCTG
SMAD2	TGTTTTTCAGTTCCGCCTCCA	GCCTCTTGTATCGAACCTGC
ACVR1C	CCAACAGCATCACCAAATGCC	CAGCATCGCAGCTATGGACA
WNT5A	ACTATGGCTACCGCTTTGCC	GGTTGTACACCGTCCTGCG
OCT4	AACCTGGAGTTTGTGCCAGGGTTT	TGAACTTCACCTTCCCTCCAACCA
SOX2	AGAAGAGGAGAGAGAAAGAAAGGGAGAGA	GAGAGAGGCAAACCTGGAATCAGGATCAAA
KLF4	CATCTCAAGGCACACCTGCGAA	TCGGTCGCATTTTTGGCACTGG
CMYC	CCTGGTGCTCCATGAGGAGAC	CAGACTCTGACCTTTTGCCAGG
NANOG	TTTGTGGGCCTGAAGAAAAC	AGGGCTGTCCTGAATAAGCAG
GAPDH	CTCAACTACATGGTTTACATGTTC	TGGAAGATGGTGATGGGATT
U6	GCTTCGGCAGCACATATACTAAAAT	CGCTTCACGAATTTGCGTGTCAT

3.5.4 MicroRNA quantitative real-time PCR

Stem-loop qRT-PCR was performed to evaluate the expression levels of miRNAs (Kramer, 2011). Stem-loop, forward and universal reverse primers are listed in Table 3.3. Following RNA extraction, 1 µg RNA was reverse transcribed with SuperScript III Reverse Transcriptase (Invitrogen, Thermo Fisher Scientific, USA) with stem-loop primers. The resulting cDNA was subjected to quantitative real-time RT-PCR using SYBR® Select Master Mix (Thermo Fisher Scientific, USA) in QuantStudio™ 3 Real-Time PCR System (Applied Biosystems, Thermo Fisher Scientific, USA). U6 was used as the housekeeping control. Relative circRNA expression levels were calculated using the comparative C_T ($\Delta\Delta C_T$) method.

3.6 Characterisation of circular RNA properties

3.6.1 Actinomycin D treatment

Actinomycin D was used to access the half-life of candidate circRNA and corresponding host gene (Vo *et al.*, 2019). CRC cells were seeded at 5×10^5 cells/well in 6-well plate and incubated overnight. After treatment with 2.5 µg/mL of actinomycin D (Sigma-Aldrich, Merck, Germany), the cells were harvested for RNA extraction at different time points: 0h (as control), 1h, 2h, 4h, 8h and 24h.

Table 3.3 List of microRNA primers

MicroRNA	Stem-loop RT primer (5' – 3')	Forward primer (5' – 3')
miR-140-3p	GTCGTATCCAGTGCAGGGTCCGAGGTATTCGCACTGGATACGACGGCACCA	AATACGCGTACCACAGGGTAG
miR-224	GTCGTATCCAGTGCAGGGTCCGAGGTATTCGCACTGGATACGACCTAAACG	AAGCCGCGTCAAGTCACTAGT
miR-548c-3p	GTCGTATCCAGTGCAGGGTCCGAGGTATTCGCACTGGATACGACGCAAAG	CGCGGCCCAAAAATCTCAAT
miR-579	GTCGTATCCAGTGCAGGGTCCGAGGTATTCGCACTGGATACGACAATCGCG	ATGCGCGCTTCATTTGGTATAA
miR-382	GTCGTATCCAGTGCAGGGTCCGAGGTATTCGCACTGGATACGACCGAATCC	AAGCCGCAGAAGTTGTTTCGTG
miR-548m	GTCGTATCCAGTGCAGGGTCCGAGGTATTCGCACTGGATACGACCAAAAAC	CCGCCGCA CAAAGGTATTTGT
miR-616	GTCGTATCCAGTGCAGGGTCCGAGGTATTCGCACTGGATACGACAAGTCAC	CTGCGCGAACTCAAAACCCTT
miR-548m	GTCGTATCCAGTGCAGGGTCCGAGGTATTCGCACTGGATACGACCAAAAAC	CCGCCGCA CAAAGGTATTTGT
miR-616	GTCGTATCCAGTGCAGGGTCCGAGGTATTCGCACTGGATACGACAAGTCAC	CTGCGCGAACTCAAAACCCTT
U6 RT primer	TGACACGCAAATTCGTGAAGC	
Universal reverse	GTCGTATCCAGTGCAGGGTCC	

3.6.2 RNase R treatment

CircRNAs are known to exhibit resistance to RNase R treatment due to the closed loop structure and lack of polyA tail (Pandey *et al.*, 2019). RNA extracted from CRC cells were subjected to RNase R (Lucigen, Thermo Fisher Scientific, USA) treatment based on the manufacturer's instructions. Ten μg of RNA was treated with 2 μL of RNase R (20 U/ μL), 1 \times RNase Buffer and brought to a final volume of 20 μL using RNase-free water. A control group of RNA was prepared without the addition of RNase R enzyme. The mixture was incubated for 30 min at 37 °C. The resulting RNAs were recovered using lithium chloride precipitation approach. Upon treatment, the final volume of the RNAs was adjusted to 50 μL using RNase-free water. Lithium chloride (8M, Sigma-Aldrich, Merck, Germany) was added at 1:2 parts and mixed well. The mixture was incubated at -20 °C for 2 h and centrifuged at 15,000 rpm for 15 min at 4 °C. The supernatant was discarded and the RNA pellet was washed with cold 75% ethanol twice. The pellet was collected through the same centrifugation steps and the pellet was airdried. The RNA pellet was resuspended with RNase-free water and subjected to cDNA conversion for qRT-PCR analysis.

3.6.3 RNA Fluorescence In Situ Hybridisation (FISH) assay

RNA FISH assay was used to visualize and validate the expression levels of the candidate circRNA. An anti-sense RNA, conjugated with fluorescence probe, cyanine-5 was synthesised (MDBio Inc, Taiwan). The sequence used was based on the unique backsplice junction of the candidate RNA which allows discrimination between the host transcript and the circRNA. The probe sequence used in the RNA FISH assay is listed in Table 3.4. Paraffin-embedded CRC patient tissues sliced 5 μm thick were used in the RNA FISH assay.

The protocol was modified from previous works (Dunagin *et al.*, 2015; Meng, Zhao and Lao, 2018). The slides were washed with PBS twice for 5 min each. For antigen retrieval, antigen unmasking buffer (saline-sodium citrate, SSC, 20 \times) was prepared by mixing 3 M sodium chloride and 0.3M sodium citrate in nuclease-free water at pH 7. The slides were rinsed with 1 \times SSC buffer before placing the slides in a Coplin jar filled with 1 \times SSC buffer and autoclaved at 100 $^{\circ}\text{C}$ for 5 min before leaving the slides to cool down to room temperature. The tissue slides were then incubated with 100% xylene (Sigma-Aldrich, Merck, Germany) for 10 min and replaced with fresh 100% xylene for 5 min. The slides were then incubated with 95% ethanol (Supelco, Merck, Germany) for 10 min and 70% ethanol for 1 h. The slides were left to air-dry for 10 min.

Table 3.4 Probe sequences

Probe	Sequence (5 – 3')
RNA FISH probe	(Cy5)CATCTTTTAATAAAAATATGCTTAAGT TGTTTAGTTCCAGACAAGAGCCTTAGATCT TGT
CRISPR Cas13d crRNA1	AGTTGTTTAGTTCCAGACAAGAGCC
CRISPR Cas13d crRNA2	AGTTCCAGACAAGAGCCTTAGATCT
RNA pulldown scramble	CTACCTTAAGTAAAGGAGAAGAAGCTTTTC ACTGGAGTTGTCCAATTCTTGTTGAATTA GATGGTGATGTTAATGGGCACAAATTTTC TGTCAGTGGAGAGGGTGAAGGTGATGCAA CATACGGAAAACCTTACCCTTAAATTTATTT GCACTACTGGAAAACCTGTTCCATGG CCAACACTTGTCACTACTTTCTCTTATGGT GTTCAATGCTTTTCAAGATACCCAGATCAT ATGAAGCGGCACGACTTCTTCAAGAGCGC CATGCCTGAGGGATACGTGCAGGAGAGGA CCATCTTCTTCAAGGACGACGGGAACTAC AAGACACGTGCTGAAGTCAAGTTTGAGGG AGACACCCTCGTCAACAGGATCGAGCTGA AAGGAATCGATTTCAAGGAGGACGGAAA CATCCTCGGCCACAAGTTGGAATACAACCT ACAACCTCCACAACGTATACATCATGGCC GACAAGCAAAAAGAACGGCATCAAAGCCA ACTTCAAGACCCGCCACAACATCGAAGAC GGCGGCGTGCAACTCGCTGATCATTATCA ACAAAATACTCCAATTGGCGATGGCCCTG TCCTTTTACCAGACAACCATTACCTGTCCA CACAATCTGCCCTTTCGAAAGATCCCTTTC GAAAGATCCCAACGAAAAGAGAGACCAC ATGGTCCTTCTTGAGTTTGTAACAGCTGCT GGGATTACACATGGCATGGATGAACTATA CAAATAAGAGCTCGAGGTCTGCACAAGGA GAAACAAGATGGCTAGCTCTAACGTGACT TACAAAGCAAAAAGCGATCTCAGGT

Pre-hybridisation buffer was prepared by dissolving 3% of bovine serum albumin (Sigma-Aldrich, Merck, Germany) with 4× SSC buffer and warmed to 45 °C. Hybridisation buffer was prepared by mixing 10% dextran sulphate (Sigma-Aldrich, Merck, Germany) and 10% deionised formamide (Sigma-Aldrich, Merck, Germany) in a 4× SSC buffer. The slides were incubated with the prewarmed pre-hybridisation buffer for 20 min at 45 °C in a humid chamber. The anti-sense circRNA sequence conjugated with Cyanine-5 fluorescent probe was mixed with the hybridisation buffer at a final concentration of 200 nM. The probe was denatured at 65 °C for 10 min and left on the ice to cool down. The pre-hybridisation buffer was removed from the tissue slides and the hybridisation buffer containing the circRNA probe was added to the tissue slides. A clean coverslip was placed above the tissue slide. The slides were incubated in a humid chamber at 45 °C overnight, protected from light.

On the next day, the tissue slides were washed with 4×, 2× and 1× SSC buffer, at 37 °C, 5 min each. The slides were stained with 4',6-diamidino-2-phenylindole (DAPI, Invitrogen, Thermo Fisher Scientific, USA) at 1: 10,000 dilutions in PBS for 10 min. The slides were washed thrice with PBS, 5 min each. The slides were airdried before mounting (DAKO, Agilent, California, USA) with coverslip and sealed. The RNA was visualised using at 650 nm excitation and 670 nm emission and were captured using FV3000 Confocal Laser Scanning Microscope (Olympus, Japan).

3.6.4 Dual immunofluorescent assay of RNA FISH and protein immunofluorescent

Dual RNA FISH and protein immunofluorescence assay was used to visualise the co-localisation of candidate circRNA with intestinal stem cell markers, Lgr5, Sox9, and proliferation markers, Ki-67. The procedure for this assay is similar to RNA FISH as described in Section 3.6.3 with slight modification. Upon overnight incubation with the circRNA probe, rinsing with different concentrations of SCC buffer, the tissue slides were incubated with primary antibodies of protein markers; Lgr5 (ab219107, Abcam, United Kingdom), Sox9 (14-9765-82, eBioscience, Thermo Fisher Scientific, USA) and Ki-67 (#9129, Cell Signalling Technology, Massachusetts, USA). Primary antibodies were diluted at 1:100 in 10% foetal bovine serum, 0.5% Triton X-100 (Supelco, Merck, Germany) and 5% BSA. The slides were incubated for 1 h at room temperature at dark. The slides were rinsed thrice with PBS, 5 min each at room temperature. Goat anti-mouse IgG secondary antibody conjugated with Alexa Fluor 546 (Invitrogen, Thermo Fisher Scientific, USA) and goat anti-rabbit IgG secondary antibody conjugated with Alexa Fluor 488 (Invitrogen, Thermo Fisher Scientific, USA) were used. Secondary antibodies were diluted in the same buffer as the primary antibody. The slides were incubated with the secondary antibodies for 1 h at room temperature at dark. The slides were rinsed thrice with PBS, 5 min each at room temperature. The slides were stained with DAPI at 1: 10,000 dilutions in PBS for 10 min. The slides were washed thrice with PBS, 5 min each. The slides were airdried before mounting (DAKO, Agilent, California, USA) with coverslip and sealed. The RNA was visualised at 650 nm excitation and 670 nm emission. The protein markers were visualised based

on specific secondary antibodies used according to the manufacturer's protocol. The fluorescent images were captured using FV3000 Confocal Laser Scanning Microscope (Olympus, Japan).

3.7 Circular RNA overexpression system

3.7.1 Plasmid cloning

Overexpression of candidate circRNA was done using permutated group I self-catalytic of *td* gene intron plasmid, driven by T7 RNA polymerase. The plasmid was a gift from Professor Dr. Manuel Ares (University of California, Santa Cruz, refer Appendix A). Full-length sequence of circRNA was obtained from CircInteractome and cloned in between the 3' and 5' splice site of the plasmid. Restriction enzymes, AflII and MfeI (New England Biolabs, NEB, United Kingdom) were used to cleave the plasmid and T4 DNA ligase (NEB, UK) was used to ligate the mature candidate circRNA sequence into the plasmid, based on the manufacturer's instructions. The ligated plasmids were transformed using DH5 α competent cells (YB Biotech, Taiwan). The competent cells were plated on Lysogeny broth agar (Sigma-Aldrich, Merck, Germany) supplemented with ampicillin (Sigma-Aldrich, Merck, Germany). Single bacterial colonies were selected and Sanger sequencing was performed to verify the cloning.

3.7.2 *In vitro* transcription of circRNA

The *in vitro* transcription was performed using (HiScribe™ T7 Quick High Yield RNA Synthesis Kit, NEB, UK) to generate linear transcripts of circRNA based on the manufacturer's instructions. Briefly, in a 20 µL volume reaction, 1 µg of linearised DNA plasmid was mixed with NTP buffer mix, T7 RNA polymerase mix and topped up with nuclease-free water. The reaction was incubated at 37 °C for 2 h. The template DNA was removed by the addition of DNase I (Invitrogen, Thermo Fisher Scientific, USA) and incubated at 37 °C for 30 min. The resulting RNA was purified using the abovementioned lithium chloride precipitation. For modified RNA, Cy3-UTP was added at a 1:4 ratio.

Circularisation of the RNA was induced by first heating the RNA to 65 °C for 3 min and placed on the ice for 10 min. The RNA was mixed with GTP (NEB, UK) and MgCl₂ (Thermo Fisher Scientific, USA) at a final concentration of 10 mM in 1× PNK buffer (NEB, UK). The mixture was heated at 55 °C for 35 min. The RNA was purified using lithium chloride precipitation and resuspended in nuclease-free water. The RNA was stored at -80 °C for further use.

3.7.3 Agarose-formaldehyde gel electrophoresis

The *in vitro* transcribed circRNA was assessed and visualised in agarose-formaldehyde gel electrophoresis. Agarose-formaldehyde gel was prepared by dissolving by heating 2 g of molecular biology grade agarose (Thermo Fisher Scientific, USA) in 72 mL of nuclease-free water. The agarose was left to cool down to 55 °C before adding 10 mL of 10× MOPS (Thermo Fisher Scientific, USA) and 18 mL of deionised formaldehyde (Sigma-Aldrich, Merck, Germany). The agarose was mixed well before adding 1× SYBR™ Gold Nucleic Acid Gel Stain (Invitrogen, Thermo Fisher Scientific, USA). The agarose was poured into a gel tray and left to solidify.

The solidified agarose gel was submerged into a 1× MOPS buffer. The agarose gel was loaded with 500 ng of RNA mixed with 1× RNA loading dye (Thermo Fisher Scientific, USA). Single-strand 1-kb RNA ladder (Thermo Fisher Scientific, USA) was used as a reference. The agarose gel was run at 60 V for 2 h. The agarose gel was visualised under the exposure of UV light using UVP BioSpectrum Imaging System (Thermo Fisher Scientific, USA).

3.7.4 RNA transfection

CRC cells were seeded at 5×10^5 cells per well in 6-well plate for overnight incubation. The medium was replenished before the RNA transfection. The RNA transfection was performed using Lipofectamine 2000 (Invitrogen, Thermo Fisher Scientific, USA) based on the manufacturer's instructions. For each well, 2.5 μg of RNA was diluted in 125 μL of OptiMEM medium (Gibco, Thermo Fisher Scientific, USA). In a separate tube, 7.5 μL of Lipofectamine 200 was diluted in 125 μL of OptiMEM medium. The diluted RNA and diluted Lipofectamine 2000 was mixed and incubated at room temperature for 5 min. The mixture was added dropwise into each well. The 6-well plate was briefly centrifuged at 2,300 rpm for 10 min. The plate was left to be incubated for 48 h for subsequent analysis.

3.7.5 Subcutaneous transplantation of CRC cells

The animal work was performed based on the Guidelines for Laboratory Animal Welfare in the Taipei Veterans General Hospital, Taiwan. Ethical approval for the work has been obtained from the Department of Medical Research of Taipei Veterans General Hospital. BALB/c nude mice were bought from National Laboratory Animal Center, Taipei, Taiwan. WiDr cells were prepared at a cell density of 2.5×10^6 cells per flank. The cells were injected subcutaneously into each dorsal flank of the nude mice. The tumours were left to grow $\sim 500 \text{ mm}^3$. The pre-treatment dimensions of the tumours were recorded.

In vivo RNA transfection was performed using TransIT®-QR Delivery Solution (Mirus Bio, Wisconsin, USA). For each flank, 10 µg of RNA or 10 µL of saline was diluted in 90 µL of TransIT®-QR Delivery Solution to a final volume of 100 µL. The mixture was injected intratumorally within 15 min of preparation. The treatment was performed 4 times, every two to three days. The tumours were left to grow for 20 days and tumour sizes were measured using a calliper. The mice were sacrificed based on the Guidelines for Laboratory Animal Welfare and the tumours were harvested for imaging.

3.8 CRISPR Cas13d knockdown

3.8.1 Plasmid cloning

CRISPR Cas13d plasmid was purchased from Addgene (#138148, Massachusetts, USA, refer Appendix B for full map). Two crRNA (crRNA) sequences were designed and synthesised based on the backsplice junction of candidate circRNA to induce knockdown, as listed in Table 3.4. A scramble sequence was generated as a negative control. The plasmid was digested with BsmBI (NEB, UK), based on the manufacturer's instructions. The digested plasmid was ligated with the crRNA or scramble sequence and single transformed bacterial colonies were selected as described in Section 3.7.1. Sanger sequencing was performed to verify the sequence of the recombinant plasmids.

3.8.2 Transient transfection of CRISPR Cas13d

Transient knockdown of candidate circRNA using CRISPR Cas13d was achieved using Lipofectamine 3000 (Invitrogen, Thermo Fisher Scientific, USA), based on the manufacturer's instructions. Briefly, CRC cells were seeded at 5×10^5 cells per well in 6-well plate for overnight incubation. The medium was replenished before transfection. For each well, 125 μ L of OptiMEM medium was diluted with 7.5 μ L of Lipofectamine 3000. In a separate tube, 125 μ L of OptiMEM medium was diluted with 2.5 μ g of CRISPR Cas13d plasmid DNA and 5 μ L of P3000 reagent. The solutions from both tubes were mixed by gentle vortex and left to incubate for 15 min at room temperature. The mixture was then added dropwise into the well and left to incubate for 48 h for further analysis.

3.8.3 Stable expression of CRISPR Cas13d CRC cells

3.8.3.1 Lentivirus generation of CRISPR Cas13d

Lentivirus vector carrying CRISPR Cas13d to knockdown candidate circRNA was generated. To generate the lentivirus, 293T cells were seeded to reach 90% cell confluence in 24 h in a 10 cm dish using DMEM F-12 medium supplemented with 10% FBS. The medium was replenished fresh medium 24 h post-seeding. The 293T cells were transfected with 10 μ g of CRISPR Cas13d DNA plasmid and lentivirus packing plasmids, 5 μ g pMD2.G and 5 μ g psPAX2.

Lipofectamine 3000 was used as transfection reagent as described in Section 3.8.2, based on the manufacturer's instructions. Lipofectamine 3000 (41 μ L) was diluted in OptiMEM medium (1.5 mL). In a separate tube, 1.5 mL of OptiMEM medium was mixed with the CRISPR Cas13d plasmid DNA, lentivirus packaging plasmids and P3000 reagent (35 μ L). The mixtures in each tube were mixed well. The OptiMEM medium containing Lipofectamine 3000 was added into the tube containing the plasmid DNAs and mixed well, before incubating for 15 min at room temperature. The mixture was added dropwise onto the 293T cells and incubated overnight. On the next day, the medium was replenished and the cells were incubated for 48 h to produce lentiviruses. The medium containing the lentivirus was collected into a tube and centrifuged at 1,000 rpm for 3 min to sediment cells and debris. The medium was filtered using a 0.45 μ m pore-size filter (Biofill, China) and stored at -80 °C for future use.

3.8.3.2 Lentivirus transduction

CRC cells were seeded at 5×10^5 cells per well in 6-well plate for overnight incubation. On the day of transduction, the cells were rinsed with PBS. Into each well, 2 mL of the lentivirus supernatant was added. The supernatant was supplemented with 8 μ g/mL of polybrene (Sigma-Aldrich, Merck, Germany). The 6-well plate was centrifuged at 2,300 rpm for 1 h at room temperature. The cells were incubated for 48 h. The cells were replenished with fresh medium and left to incubate for 24 h.

3.8.3.3 Selection and expansion of stably transduced CRISPR Cas13d cells

The CRISPR Cas13d transduced CRC cells were selected using puromycin (InvivoGen, California, USA). Upon transduction, the cells were supplemented with 10 µg/mL of puromycin. The medium was replenished with fresh medium supplemented with 5 µg/mL of puromycin, every day for three days. On day four, the puromycin concentration was reduced to 2 µg/mL and the medium was replenished every two to three days. The cells were passaged upon reaching 70% confluency while maintaining the cells under puromycin selection. The cells were cultured in a puromycin-free medium before performing any functional assays, for at least two passages.

3.8.4 Subcutaneous transplantation of stably expressing CRISPR Cas13d cells

Stably transduced CRISPR Cas13d WiDr cells, either carrying CrSC as control or CrRNA targeting circRNA were prepared at a cell density of 2.5×10^6 cells per flank in PBS. The cells were injected subcutaneously in each dorsal flank of the nude mice. The tumours were allowed to form for a week. The tumour volume was measured every two to three days using callipers. The tumours were grown up to 30 days before the mice were sacrificed. The tumours were harvested for imaging.

3.9 Functional assays

3.9.1 Flowcytometry analysis

CRC cells were harvested using Accutase (Gibco, Thermo Fisher Scientific, USA). CRC cells were washed twice with PBS and an adequate amount of Accutase reagent was added, as per the manufacturer's instructions. The cells were incubated for 5 min. The cells were mechanically detached using vigorous pipetting. PBS was added to the cells and the cell suspension was centrifuged at 1,000 rpm for 3 min at room temperature. The cells were resuspended in 1 mL of PBS and 5×10^5 cells were transferred aliquoted for each flowcytometry marker. For phenotypic surface markers such as CD44 (#3570, Cell Signalling Technology, USA), CD133 (#5860, Cell Signalling Technology, USA) and Lgr5, the cells were blocked with 5% bovine serum albumin in PBS, 15 min at room temperature. For intracellular staining for SOX9, before blocking, the cells were fixed with 4% paraformaldehyde for 10 min at room temperature. The cells were collected through centrifugation and blocked with 5% bovine serum albumin in PBS with 1% Triton X-100 for 15 min at room temperature. The cells were washed twice with PBS and collected through centrifugation at 1,000 rpm for 5 min at 4 °C.

The cells were resuspended in 5% bovine serum albumin in PBS with 1:100 dilution of the primary antibody. The cells were incubated for 30 min at room temperature. The cells are washed twice with PBS and collected through centrifugation. Secondary antibodies, anti-mouse Alexa Fluor 594 (#A11005,

Invitrogen, Thermo Fisher Scientific, USA) and anti-rabbit Alexa Fluor 488 (A-11008) were added at 1:100 dilution in 5% bovine serum albumin in PBS, incubated for 30 min at room temperature, protected from light. The cells were washed twice with PBS and collected by centrifugation. The cells were resuspended in 300 μ L of PBS and left on ice at dark for acquisition. FACS Canto-II analyser (BD Biosciences, USA) was used to acquire the flow cytometry data.

3.9.2 EdU assay

The proliferation rate was accessed using EdU Staining Proliferation Kit (iFluor 488) (Abcam, UK) based on the manufacturer's instructions. Upon 48h of either DNA or RNA transfection, CRC cells were harvested at a cell density of 5×10^5 cells/mL in foetal bovine serum-supplemented medium. Into the 1 mL cell suspension, 20 μ M of EdU stock solution was added and the cells were incubated for 4h at 37 $^{\circ}$ C in a 5% CO₂ humidified incubator. The cells were collected through centrifugation at 300 \times g for 5 min at 4 $^{\circ}$ C. The cell pellet was washed twice with Wash Buffer and collected through centrifugation. The supernatant was removed and the cells were resuspended in 100 μ L of Fixation Solution. The cells were incubated for 20 min at room temperature at dark. The cells were centrifuged and the fixation solution was removed. The cells were washed twice in Wash Buffer and collected through centrifugation. The cell pellet was resuspended in 100 μ L of 1 \times Permeabilisation Buffer and incubated for 15 min at room temperature. The reaction mix was prepared by mixing 1 \times Tris-buffered saline, 100 μ M copper sulphate, 500 μ M iFlour 488 azide and 1 \times Additive solution to a final volume of

500 μ L. The mixture was added to the cells and incubated for 30 min at room temperature, at dark. The cells were collected through centrifugation and washed twice with 1 \times Permeabilisation Buffer. The cell pellet was resuspended in 300 μ L PBS and data acquisition was performed using FACS Canto-II analyser (BD Biosciences, USA).

3.9.3 Colony-forming assay

The colony-forming assay was used to assess the self-renewal abilities of the cells. Upon 48h of DNA transfection, CRC cells were harvested and seeded at 2,500 cells per well in a 6-well plate. The cells were incubated for 10 to 14 days. The medium was replenished every three to four days. Crystal violet staining was used to visualise the colonies formed. Crystal violet staining solution was prepared by dissolving 0.5 g of crystal violet powder (Sigma-Aldrich, Merck, Germany) in 80 mL distilled water. After completely dissolving the crystal violet powder, 20 mL of methanol (Sigma-Aldrich, Merck, Germany) was added to the solution. Upon colony formation, the medium was discarded and 2 mL of crystal violet solution was added to each well. The colonies were stained for 20 min at room temperature. Using running water, the excess staining was removed the stained colonies were left to dry for imaging.

3.9.4 RNA pulldown assay

Interacting miRNAs with candidate circRNA was identified using RNA pulldown assay. CRC cells were grown to reach 80% confluency and the cells were scrapped for harvesting. The cell pellet was collected through centrifugation at 1,000 rpm for 5 min at 4 °C. The cell pellet was resuspended in 1× RIPA buffer (Abcam, UK) supplemented with RNase inhibitor (Invitrogen, Thermo Fisher Scientific, USA) and vortexed gently. The cell suspension was left to incubate on ice for 30 min. The mixture was centrifuged at 15,000 rpm for 15 min at 4 °C. The supernatant containing the cell lysate was transferred into a new tube. Bradford assay (Bio-Rad, California, USA) was used in determining the protein concentration of the cell lysate based on the instructions of the manufacturer.

An amount of 200 µg cell lysate was subjected to RNA extraction using TRIzol as described in Section 3.3.1. For the RNA pulldown assay, 2000 µg of cell lysate for each group of RNA was aliquoted. Using *in vitro* transcription, modified UTP with biotin (Jena Bioscience, Germany) was used in generating full-length circRNA as described in Section 3.7.2. A scramble RNA was generated in a similar approach as control. The cell lysate was incubated with 500 ng of RNA of either scramble RNA or candidate circRNA. The mixture was gently agitated at 4 °C for 4h. Meanwhile, 100 µL of Streptavidin Mag Sepharose beads (Cytiva, Massachusetts, USA) for each RNA group was aliquoted into a new tube. Using a magnetic rack, the streptavidin magnetic beads are collected at the side of the tube and the supernatant was discarded.

The magnetic beads were washed three times using bead wash buffer containing 500 mM sodium chloride, 20 mM Tris (pH 8.0), 2 mM EDTA and 1% Triton X-100. All chemicals used were purchased from Sigma-Aldrich (Merck, Germany). The washed beads were transferred into the RNA-cell lysate mixture and left to agitated overnight at 4 °C. The next morning, the mixture was placed on the magnetic stand and the supernatant was discarded. The beads were washed three times using the bead washing buffer supplemented with RNase inhibitor. The beads were resuspended in TRIzol and RNA extraction was performed. Stem-loop qRT-PCR was performed to quantitate the levels of miRNA enrichment.

3.10 Statistical analysis

All experiments were performed in triplicates. The triplicated data were evaluated for statistical significance using the standard paired Student's *t*-test. Comparisons were made between the control group and the treated group, unless specified otherwise. The Prism GraphPad software was used to evaluate the significance levels and graph construction.

CHAPTER 4

RESULTS

Part 1: CircRNA expression profiling of CRC spheroidal cells

4.1 Genome-wide sequencing of circRNA established a differentially expressed profile in CRC spheroidal cells

Based on our previous work, we have established an *in vitro* 3D spheroidal culture model as an effective method of enriching stemness properties in CRC cells to mimic CrCSC-like population (as described in Chapter 1). CRC cell lines, HCT-15 and WiDr were used to generate spheroidal cells (Rengganaten, 2016). The spheroidal cells exhibited common characteristics of CSC. Using the established model, the circular RNA expression profiles of the CRC spheroidal cells were first established. Using RNA-sequencing pipeline, RNAs from the parental CRC cells, HCT-15 and WiDr, and the counterpart spheroid cells were subjected to RNA sequencing.

The sequencing data identified over 15,000 circRNAs, with differential expression in the parental and spheroid cells (Figure 4.1A). Differential expression analysis illustrated 1,503 circRNAs that were uniquely expressed in the HCT-15- and WiDr-derived spheroid cells. Collectively in HCT-15 and WiDr, 636 circRNAs were identified to be only expressed in the parental cells. Host transcript analysis

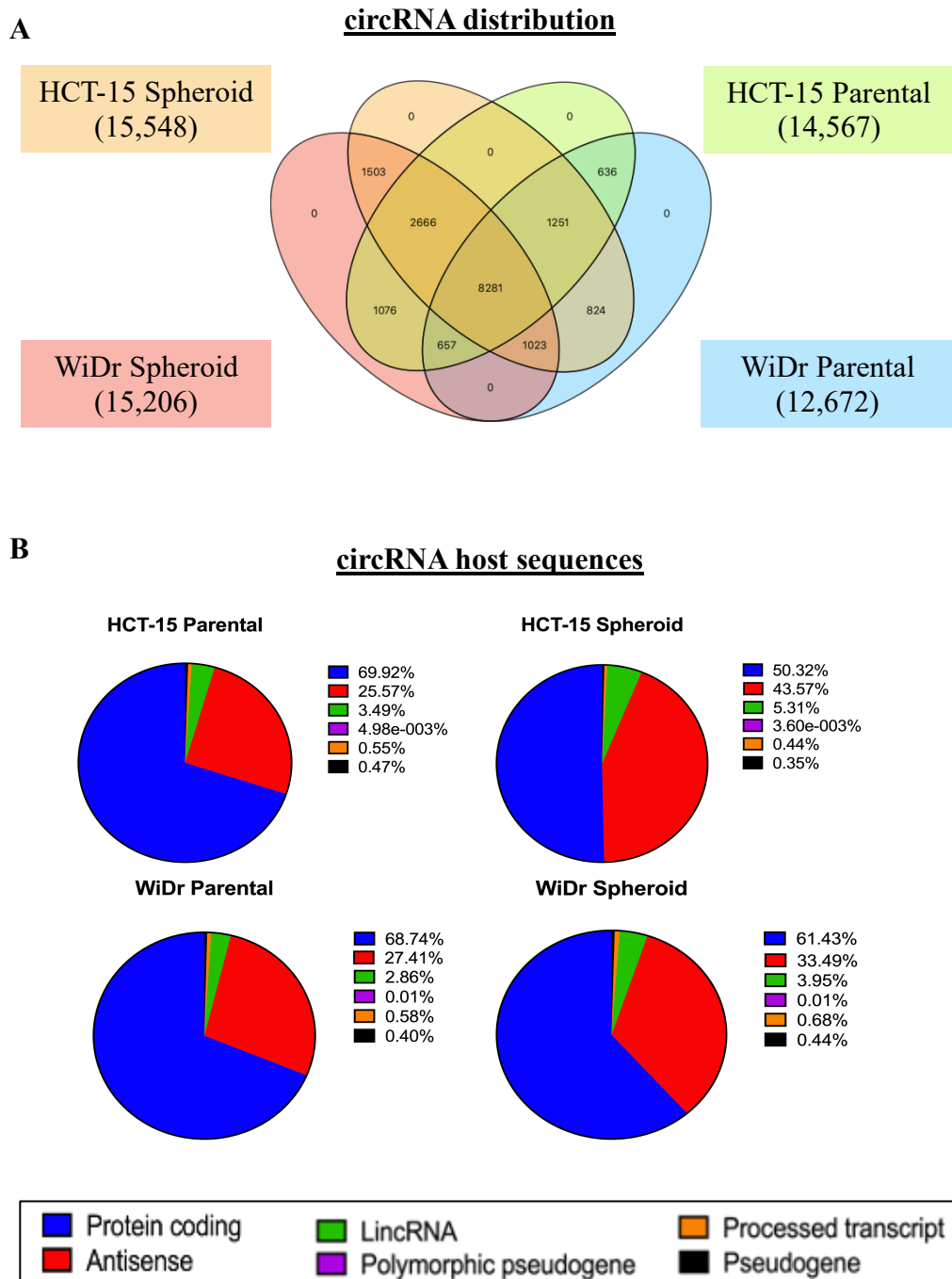


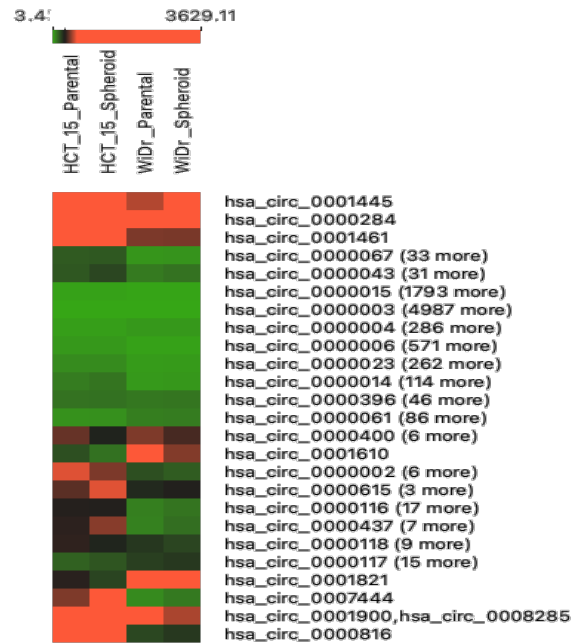
Figure 4.1 Genome-wide circRNA profiling of CRC spheroidal cells. (A) CircRNA distribution in CRC parental and spheroidal cells. **(B)** Host transcript analysis of the differentially expressed circRNAs.

indicated that the differentially expressed circRNAs in CRC spheroidal cells were primarily derived from protein-coding RNAs (Figure 4.1B). However, the results showed a general shift of circRNA derived from protein-coding RNA to antisense and long intervening non-coding RNA (lincRNA) during the spheroid formation. The biological implication of these observations remains to be investigated.

4.2 Identification of top differentially expressed circRNAs unveiled a core circRNA–microRNA–mRNA network that regulates stemness

A total of 8,281 circRNAs were differentially expressed in the spheroid cells. A heatmap of the circRNA distribution was generated to illustrate the expression patterns of the differentially expressed circRNAs in the parental and spheroidal cells (Figure 4.2A). Bioinformatics analysis was performed using the differentially expressed circRNA profile to identify the top four up- and down-regulated circRNAs. Hsa_circ_0002970, circ_0008599, circ_0066631 and circ_0082096 were identified to be up-regulated in CRC spheroidal cells (Figure 4.2B) The down-regulated circRNAs in CRC spheroidal cells include while hsa_circ_0000400, circ_0005174, circ_0005507 and circ_0040238 (Figure 4.2C). Table 4.1 lists the dataset of the differentially expressed circRNAs.

A Differentially expressed circRNAs (n=8281)



B

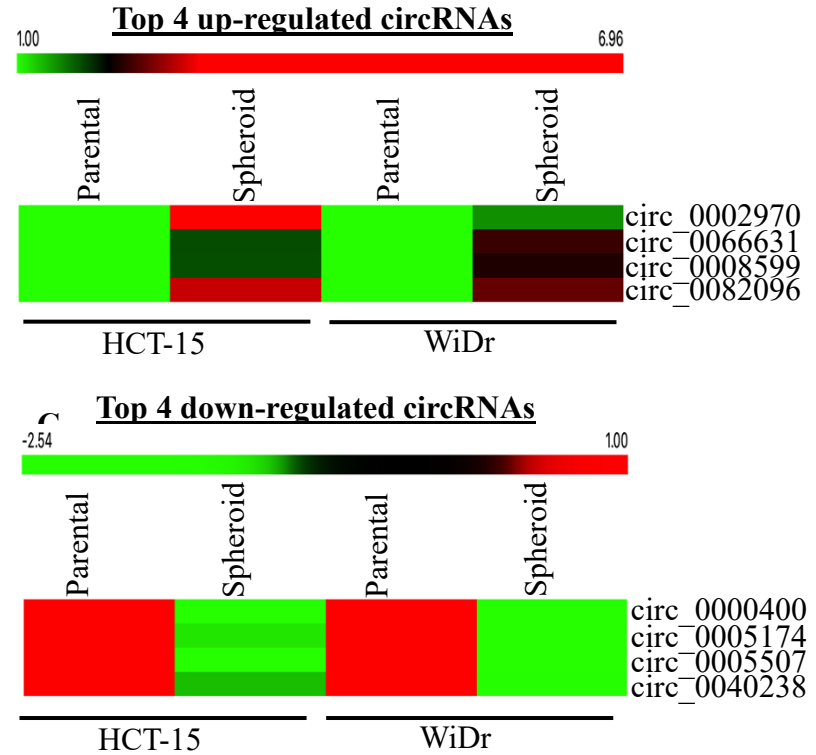


Figure 4.2 Identification of the top four differentially expressed circRNAs in CRC spheroidal cells. (A) Hierarchical clustering of differentially expressed circRNAs in CRC spheroidal cells. Numbers in brackets plus one indicate the total circRNA in the heatmap. Hierarchical clustering of top four up- (B) and down-regulated (C) circRNAs in the CRC spheroidal cells.

Table 4.1 Top eight differential expressed circRNAs in the spheroidal CRC

CircRNA ID (hsa_)	HCT-15		Fold change (log ₂)	P-value	WiDr		Fold change (log ₂)	P-value
	Parental	Spheroid			Parental	Spheroid		
<u>Upregulated circRNA</u>								
circ_0002970 (circKIAA1199)	0	70.041	6.96	7.34E-06	31.892	84.479	1.39	0.0440
circ_0008599 (circMIR31HG)	43.960	139.655	1.63	0.0017	15.380	67.332	2.10	0.0030
circ_0066631 (circ DCBLD2)	37.906	117.341	1.62	0.000066	21.074	83.910	2.00	0.0011
circ_0082096 (circZNF800)	5.878	38.815	2.60	0.0030	9.682	47.797	2.26	0.0130
<u>Downregulated circRNA</u>								
circ_0000400 (circTUBA1B)	445.113	121.834	-1.83	0.0085	488.659	149.084	-1.70	2.21E-08
circ_0005174 (circSNHG12)	19.487	8.0366	-1.20	0.6087	11.391	1.455	-2.54	0.6759
circ_0005507 (circCRIM1)	107.582	29.003	-1.87	7.57E-06	17.089	3.568	-2.08	0.5388
circ_0040238 (circCOG4)	138.420	65.182	-1.08	0.0051	37.588	11.649	-1.59	0.7378

4.2.1 Validation of expression of the top differentially expressed circRNAs in CRC spheroidal cells

The expression of the top differentially expressed circRNAs were validated using qRT-PCR assay. Divergent primers were designed based on the backsplice junction of each circRNAs. The qRT-PCR analysis concurred with the expression patterns observed in the bioinformatics analysis (Figure 4.3). The expression levels of all the top four up-regulated circRNAs were significantly higher in the CRC spheroidal cells compared to the parental cells (Figure 4.3A). Similarly, the down-regulated circRNAs were generally lower in expression levels in the spheroidal cells (Figure 4.3B). The only exception is circ_0005174, which was found to be up-regulated in the WiDr spheroids, as opposed to down-regulation observed in the bioinformatics analysis; however, the change in the expression level was not significant. The discrepancies between the RNA sequencing data and qRT-PCR analysis is within the acceptable false-positive rate of Next-Generations sequencing (Kim *et al.*, 2019).

4.2.2 Construction and mapping of core pluripotency-associated network

MicroRNAs (miRNAs) are sponged by circRNAs to indirectly regulate the expression of downstream transcripts (Panda, 2018; Zhang *et al.*, 2019). A circRNA-miRNA regulatory network was mapped by identifying the predictive miRNAs targeted by the top eight differentially expressed circRNAs. Using the CircInteractome online database, the predictive interacting miRNAs were first

identified (as described in Section 3.4). By imposing a stringent criterion of each predicted miRNAs should have at least four interacting circRNAs, 15 miRNAs were further identified (Figure 4.4A). The target-transcripts were predicted using miRWalk algorithm by using a stringent selection criterion of at least five interactions of the target-transcripts with the predicted miRNAs. A resulting 121 mRNA transcripts were predicted to be collectively targeted by the 15 miRNAs (Figure 4.4B), thus establishing a circRNA-miRNA-mRNA regulatory network. To further understand the biological implications of the identified network, Gene Ontology (GO) and Kyoto Encyclopaedia of Genes and Genomes (KEGG) analyses were performed. The GO analysis of the mRNA transcripts predicted the involvement of these transcripts in primarily DNA binding activities, regulation of transcription, protein phosphorylation and Wnt signalling pathways (Figure 4.5A). The KEGG analysis indicated that signalling pathways involved in regulating pluripotency of stem cells were most enriched (Figure 4.5B). Furthermore, other implicated pathways include Wnt and ErbB signalling pathways, which are also closely associated with CSC properties (Clark *et al.*, 2012; de Sousa and Vermeulen, 2016). The predicted KEGG pathways are indicative of a regulatory network driven by the circRNA-miRNA-mRNA axis reported here in enriching CSC-like properties in CRC spheroidal cells.

To further establish the possible regulation of stemness properties in colorectal cancer stem cells, subsequent analysis focused on the pluripotency signalling pathways identified from the KEGG analysis. Core mRNAs, *ACVR1C/ALK7*, *FZD3*, *IL6ST/GP130*, *SKIL/SNON*, *SMAD2* and *WNT5A* were identified to be involved in the predicted pluripotency signalling pathways

mediated by circRNA-miRNA-mRNA axis based on the KEGG analysis. The six mRNA transcripts were collectively targeted by five miRNAs, hsa-miR-140-3p, -miR-224, -miR-382, -miR-548c-3p and -miR-579m, which in turn were under the control of two of the top up-regulated circRNAs, hsa_circ_0066631 and hsa_circ_0082096 (Figure 4.6).

4.3 Validation of the predicted core network in CRC spheroidal cells

To obtain experimental evidence to support the predicted circRNA-miRNA-mRNA regulatory axis, the expression levels of the five miRNAs and six mRNAs were validated using stem loop qRT-PCR and qRT-PCR, respectively. The expression levels of circRNAs identified in this network were already validated to be up-regulated in CRC spheroidal cells (Figure 4.2A).

All five miRNAs were significantly down-regulated in CRC spheroidal cells (Figure 4.7A), correlating with the up-regulated expression of hsa_circ_0066631 and hsa_circ_0082096 via miRNA sponging. Upon serum-induced differentiation of the CRC spheroidal cells, the expression levels of the miRNAs reverted to the parental levels (Figure 4.7A), supporting the possible involvement of the miRNAs in regulating stemness in CRC cells.

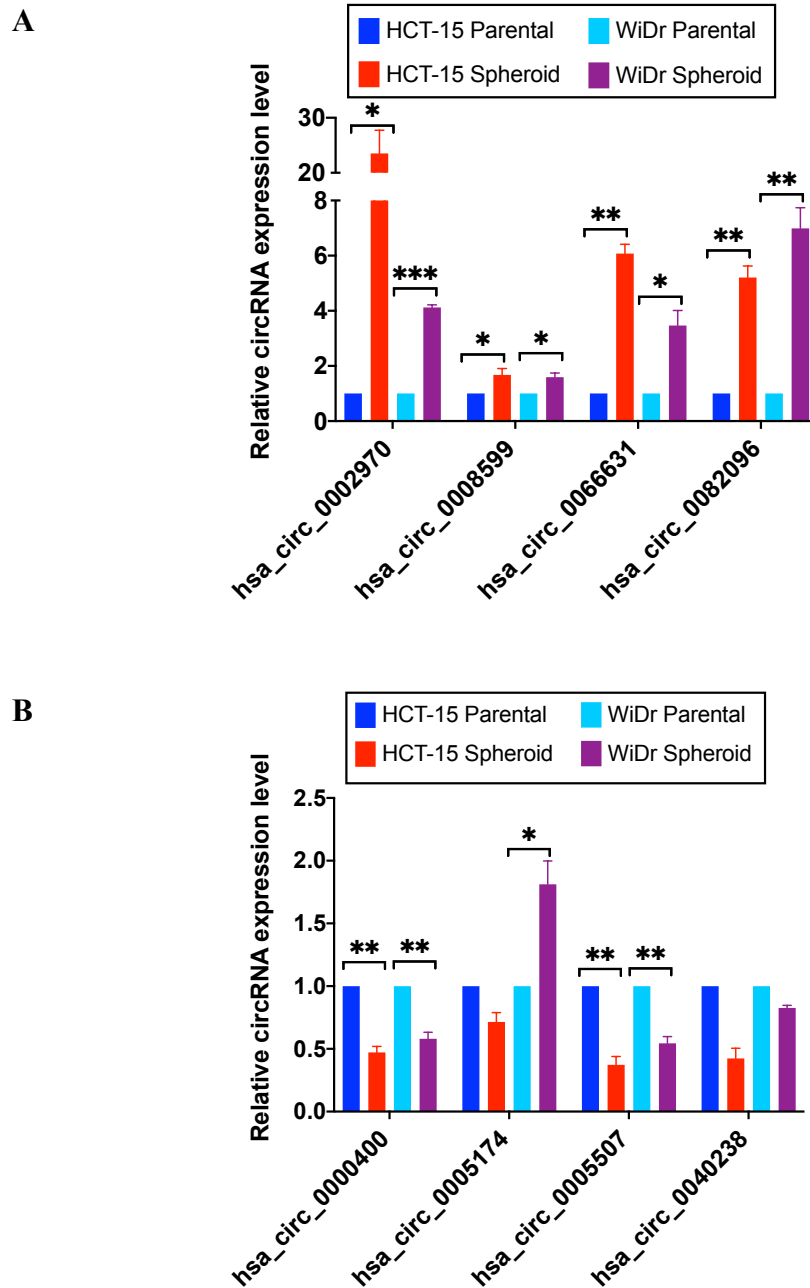
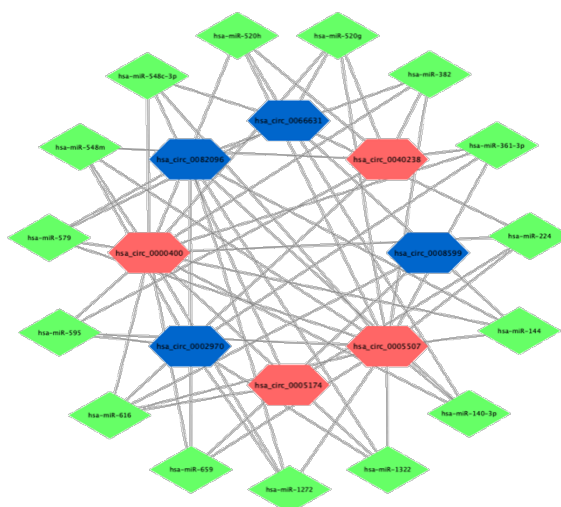


Figure 4.3 Validation of the predicted top differentially expressed circRNAs.

qRT-PCR analysis of the top four up- (A) and down-regulated (B) circRNAs relative to the CRC parental cells. * $p < 0.05$, ** $p < 0.01$ and *** $p < 0.001$ were values relative to the parental cells.

A

Predicted interacting miRNAs



B

Predicted interacting miRNA-mRNA network

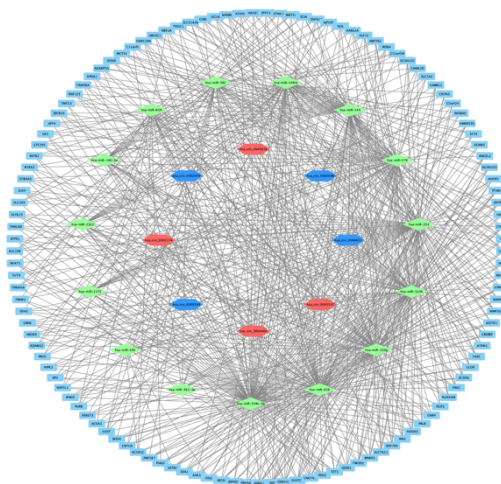
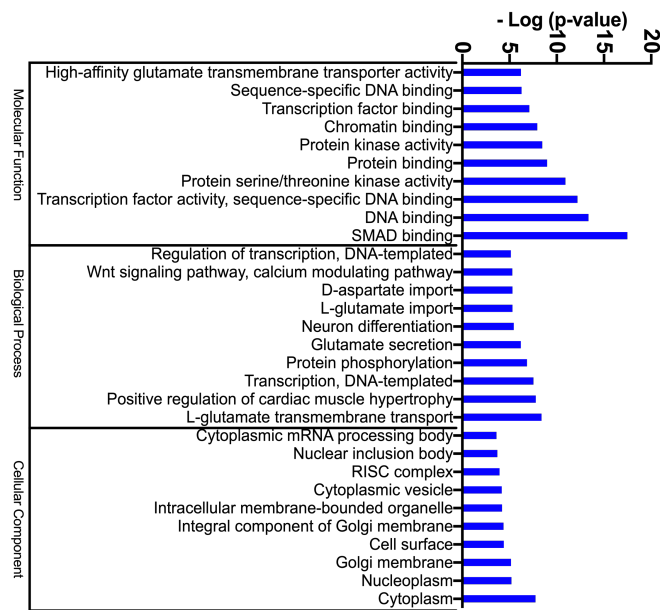


Figure 4.4 Identification of interacting miRNAs and mRNAs with the top four differentially expressed circRNAs. (A) The predicted miRNA-circRNA interaction map. Blue and red hexagons indicate up- or down-regulated circRNAs, respectively; green diamonds represent predicted miRNAs. The miRNAs were selected by a criterion of at least four interactions with the top differentially circRNAs. (B) Predicted mRNA transcripts in a miRNA-circRNA-mRNA interaction map; the mRNAs (light blue boxes on the outside rim) were selected based on at five interactions with the predicted miRNAs. Hexagons and diamonds are as in (A).

A

Gene ontology (GO) analysis



B

KEGG analysis

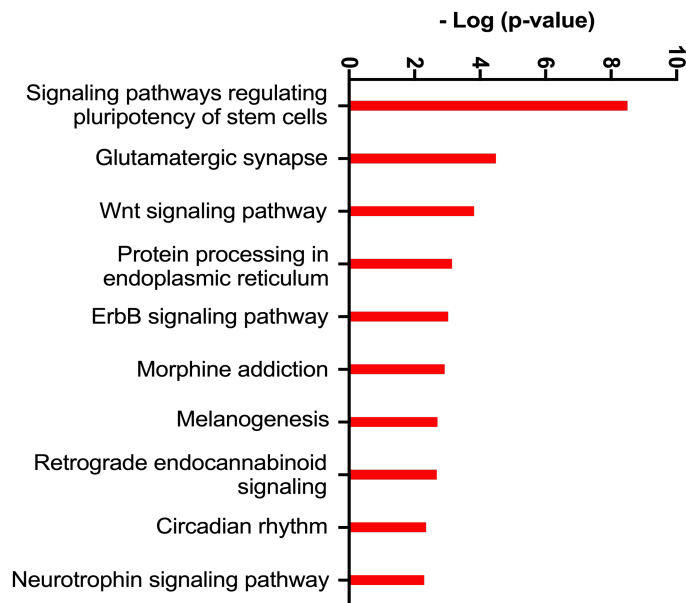


Figure 4.5 Bioinformatics analysis of mRNA transcripts of the circRNA-miRNA-mRNA axis of CRC spheroidal cells. (A) Gene ontology (GO) and (B) Kyoto Encyclopaedia of Genes and Genomes (KEGG) analysis of the identified mRNA transcripts from Figure 4.4B.

Predicted regulatory network

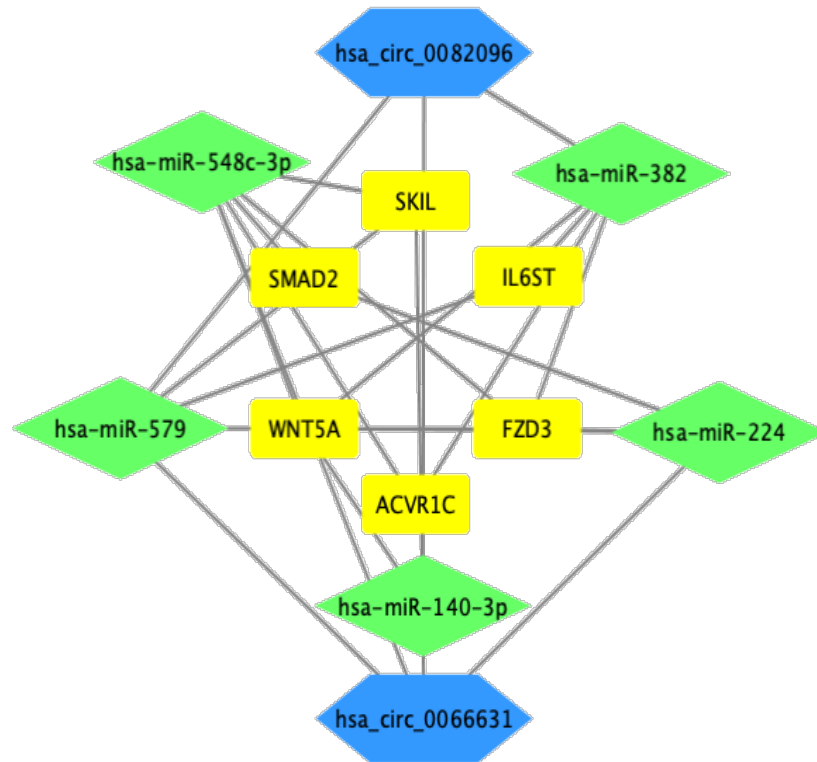
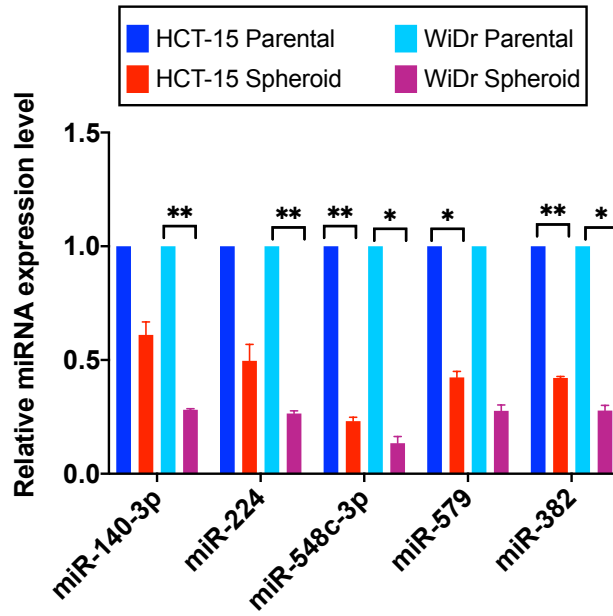


Figure 4.6 Predicted circRNA-miRNA-mRNA network of pluripotency signalling pathways targeted by hsa_circ_0066631 and hsa_circ_0082096. The up-regulated circRNAs (in blue hexagon), miRNA (in green diamond) and mRNA (in yellow box) are predicted to regulate stemness in CRC spheroidal cells.

A



B

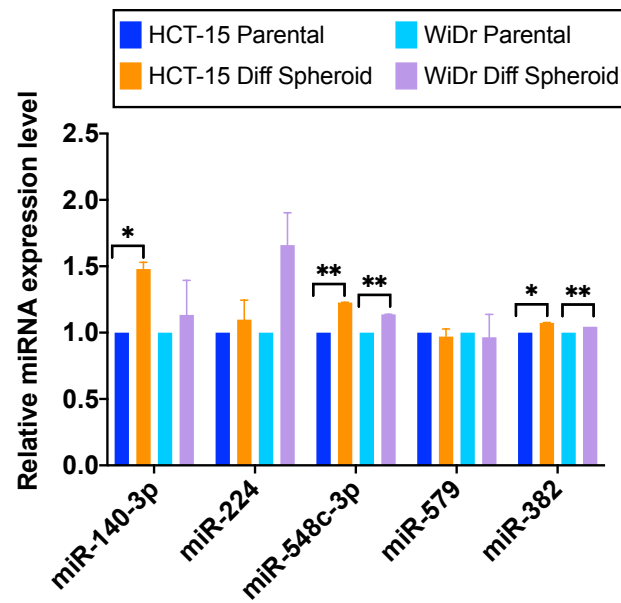


Figure 4.7 Validation of the expression levels of the predicted miRNA in CRC spheroid cells. Relative expression levels of the predicted miRNAs in the (A) spheroid cells and (B) serum-induced differentiated cells. MiRNA analysis was performed by stem loop qRT-PCR using small nucleolar RNA U6 as the normalisation control. * $p < 0.05$ and ** $p < 0.01$ were relative to the parental CRC cells.

Likewise, the expression levels of the mRNA transcripts in the predicted regulatory network tallies with our prediction, where all six predicted mRNAs were up-regulated in CRC spheroidal cells (Figure 4.8A), and expression was down-regulated on serum-induced differentiation (Figure 4.8B). The results are in line with miRNA suppression prevents degradation of the downstream mRNA transcripts. In short, RNA sequencing established the differential expression profile of circular RNA, and, coupled with bioinformatics analysis, revealed an epigenetic regulatory network driven by a circRNA-miRNA-mRNA axis in regulating stemness properties in CRC spheroidal cells.

4.4 Construction of circRNA-miRNA-mRNA stemness regulatory network

To put the predicted circRNA-miRNA-mRNA regulatory network in the context of other known biochemical pathways in the cell, an extensive literature review was performed. The five miRNAs which were down-regulated in the CRC spheroidal cells were reported to be tumour suppressive (Yu *et al.*, 2016; Kalhori *et al.*, 2019; Yao *et al.*, 2019; Wang *et al.*, 2020). By targeting various downstream transcripts, these miRNAs have been associated to inhibit CSC-related properties, including cell proliferation, chemoresistance, migration and invasion. The full list of references for the CSC-related properties is shown in Table 4.2.

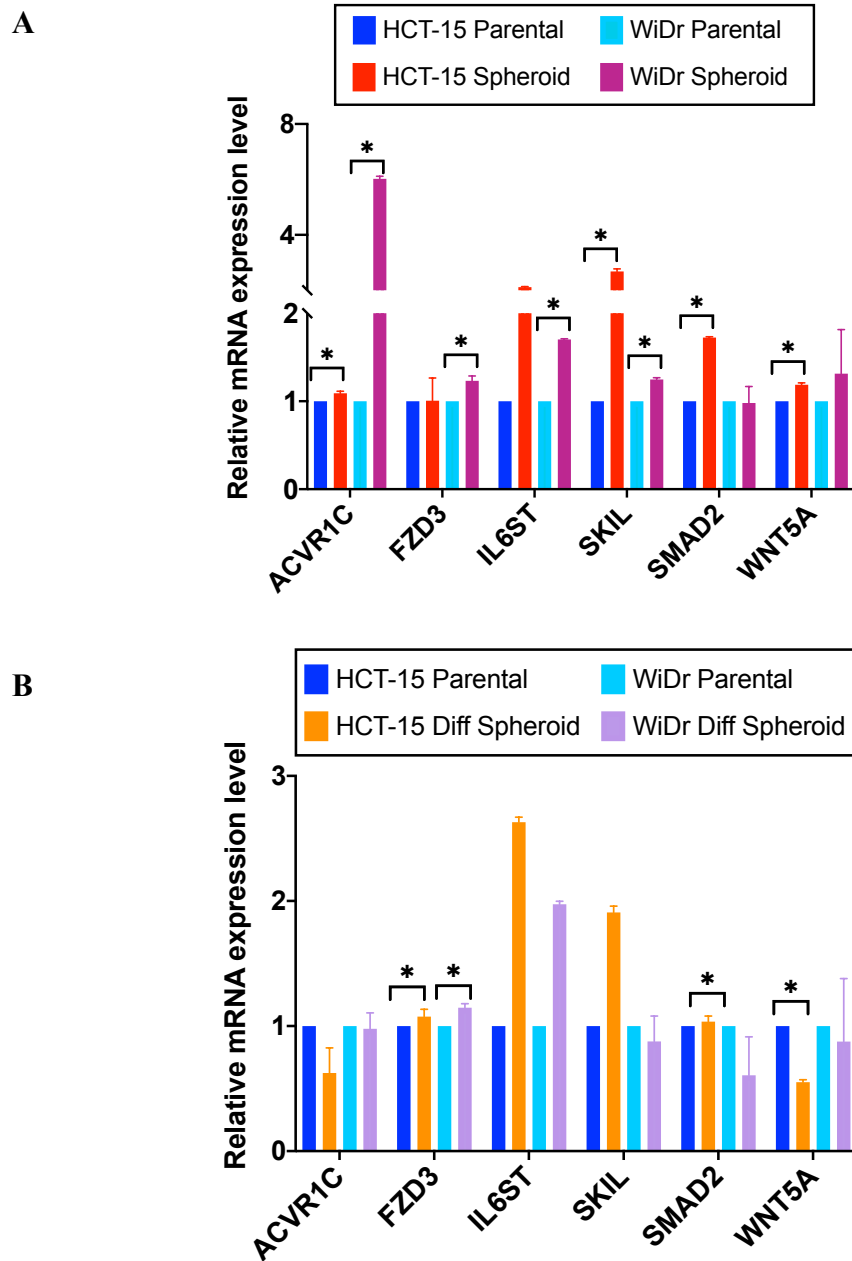


Figure 4.8 Validation of the expression levels of the predicted mRNA transcripts. Relative expression levels of the predicted mRNA transcripts in the (A) spheroid cells and (B) serum-induced differentiated cells using qRT-PCR. GAPDH was used as the normalisation control. * $p < 0.05$ and ** $p < 0.01$ were relative to the parental CRC cells.

The KEGG analysis of the transcripts targeted by the circRNA-miRNA axis identified six mRNAs that were involved in the regulation of pluripotency pathways. Literature analysis concurred that the six KEGG-predicted mRNAs were involved in regulating various CSC-like properties, including the associations with pluripotency properties (see Table 4.3 for full references).

Furthermore, the six mRNAs are linked with four major signalling pathways. IL6ST/GP130 is an integral part of the GP130/STAT signalling pathway, interacting with STAT3 to induce naïve pluripotency and self-renewal (Yu *et al.*, 2017b; Bourillot *et al.*, 2020). SKIL/SNON and ACVR1C/ALK7, acting via the Activin/Nodal and TGF- β signalling pathways, are involved in the phosphorylation and association of SMAD2/3 with SMAD4 to enter the nucleus to exert transcriptional activation functions on the target genes (Tsuneyoshi *et al.*, 2012; Bertero *et al.*, 2018). FZD3 and WNT5a regulate β -catenin in Wnt/ β -catenin signalling to contribute to self-renewal, EMT-associated biological processes and differentiation (Keller *et al.*, 2016; Xia *et al.*, 2018). A scheme based on the bioinformatics data and the literature review is compiled in Figure 4.9.

Table 4.2 Predicted miRNAs and affected CSC-associated functions based on literature review

miRNA	Affected functions ^a	Cancer	References
miR-548c-3p	Tumour suppressor Enhances the migration and invasion Inhibits proliferation and promote apoptosis	Lung Oesophageal Breast	(Wang <i>et al.</i> , 2020) (Ni <i>et al.</i> , 2018) (Shi <i>et al.</i> , 2015)
miR-579-3p	Tumour suppressor STAT3-mediated chemoresistance Controls cancer progression and drug resistance	Glioblastoma Melanoma Melanoma	(Kalhori <i>et al.</i> , 2019) (Wang <i>et al.</i> , 2018) (Fattore <i>et al.</i> , 2016)
miR-382	Inhibits cell growth and invasion Inhibits cell proliferation and invasion Inhibits cell growth and migration Inhibited cell proliferation, migration, invasion	Colorectal Retinoblastoma Colorectal Colorectal	(Zhou <i>et al.</i> , 2016) (Song <i>et al.</i> , 2017) (Ren, Zhang and Jiang, 2018) (Yao <i>et al.</i> , 2019)
miR-140-3p	Tumour suppressor Inhibits cell growth and invasion Inhibits cancer stem cell survival and invasive potential Suppresses cell growth; induces apoptosis	Lung Lung Colorectal Colorectal	(Huang <i>et al.</i> , 2019) (Dong <i>et al.</i> , 2016) (Yu <i>et al.</i> , 2016) (Jiang <i>et al.</i> , 2019)
miR-224	Associated with metastasis Tumour progression Cancer progression and chemoresistance	Colorectal Colorectal Colorectal	(Wang <i>et al.</i> , 2017) (Li <i>et al.</i> , 2016) (Amankwatia <i>et al.</i> , 2015)

^aCSC-associated functions are shown in thick letters.

Table 4.3 Involvement of the target mRNAs in CSC-associated properties and the implicated signalling pathways

mRNA (Alias)	Signalling pathway	CSC-related properties	References
ACVR1C (ALK7)	TGF- β /Activin/ Nodal/Smad2	Proliferation and invasion	(Principe <i>et al.</i> , 2018a)
FZD3 (Fz-3)	Wnt/ β -catenin	Proliferation	(Xia <i>et al.</i> , 2018)
IL6ST (Gp-130)	Stat3 signalling	Tumorigenesis initiation	(Ahmad <i>et al.</i> , 2017)
	Stat3/Wnt/ β -catenin	Tumorigenesis initiation	(Hill <i>et al.</i> , 2018)
	Jak/Stat3	Chemoresistance	(Li <i>et al.</i> , 2018b)
	Stat3	Naïve pluripotency	(Bourillot <i>et al.</i> , 2020)
	Jak/Stat3	Self-renewal	(Burdon <i>et al.</i> , 1999)

Table 4.3 (Cont'd)

mRNA (Alias)	Signalling pathway	CSC-related properties	References
SKIL (SnoN)	TGF- β	Chemoresistance	(Sengupta <i>et al.</i> , 2013)
	TGF- β	Tumorigenesis	(Massagué and Xi, 2012)
	PI3K/AKT	Cancer cell proliferation	(Zhong <i>et al.</i> , 2019)
	Activin/Nodal	Pluripotency maintenance	(Tsuneyoshi <i>et al.</i> , 2012)
	TGF- β	Epithelial-mesenchymal transition	(Cai <i>et al.</i> , 2019)
SMAD2	TGF- β	Pluripotency maintenance	(Dahle and Kuehn, 2016)
	TGF- β /Akt	Stemness maintenance	(Scheel <i>et al.</i> , 2011)
	TGF- β /Smad/Snail	Epithelial-mesenchymal transition	(Bojkova <i>et al.</i> , 2020)
	Nodal/Activin	Pluripotency maintenance	(Kaufman-Francis <i>et al.</i> , 2014)
Wnt5A	TGF- β	Migration and invasion	(Suwannakul <i>et al.</i> , 2020)
	TGF- β	Migration and self-renewal	(Longati <i>et al.</i> , 2013)

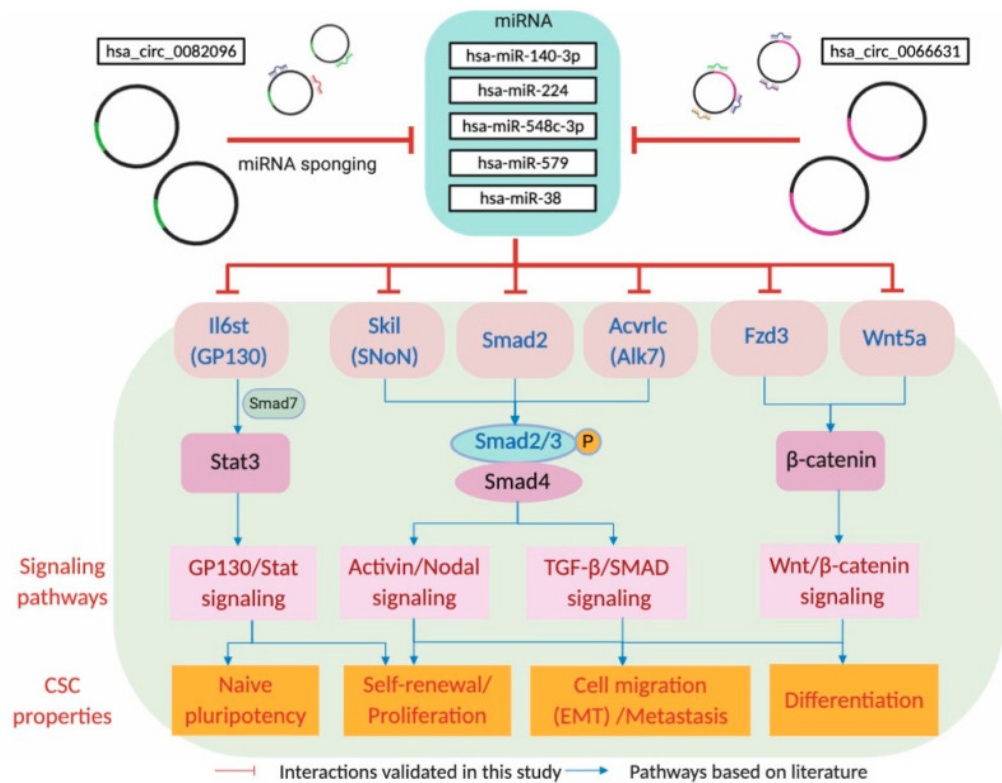


Figure 4.9 Mapping of predicted circRNA-miRNA-mRNA axis in regulation of stemness in CRC cells. The regulatory network was constructed based on bioinformatics and literature analyses as described in the text (Section 3.3). In the top part of the scheme, the two circRNAs are shown to sponge the five predicted miRNAs, which, in turn, modulate the respective signalling pathways (shown in pink boxes) via the gene products of the predicted miRNA-targeted transcripts (shown in red letters), subsequently in the modulation of known CSC properties (orange boxes).

Part 2: Selection and characterisation of a candidate circular RNA hsa_circ_0082096/circZNF800

4.5 Up-regulation of hsa_circ_0082096 expression was observed in a passage-dependent manner in spheroidal culture of CRC cell lines

The bioinformatics analysis revealed that two up-regulated circRNAs, viz hsa_circ_0066631 and hsa_circ_0082096, in CRC spheroidal cells could govern pluripotency signalling pathways (Figure 4.9). Further analysis showed that relative to the parental cells, hsa_circ_0066631 showed inconsistent expression levels on increasing passages of the CRC spheroidal cells from P0, P3 to P5, and the circRNA was up-regulation upon the serum-induced differentiation in both HCT-15 and WiDr cells (Figure 4.10A).

In contrast, hsa_circ_0082096 expression levels were consistently up-regulated on increasing passages of both HCT-15- and WiDr-derived spheroidal cells (Figure 4.10B). Furthermore, upon serum-induced differentiation of the CRC spheroidal cells, hsa_circ_0082096 expression was down-regulated, reverting to the levels of the parental cells. The up-regulation of hsa_circ_0082096 in the CRC spheroidal cells and down-regulation upon serum-induced differentiation suggest that hsa_circ_0082096 plays a functional role in the maintenance of stemness in CRC cells.

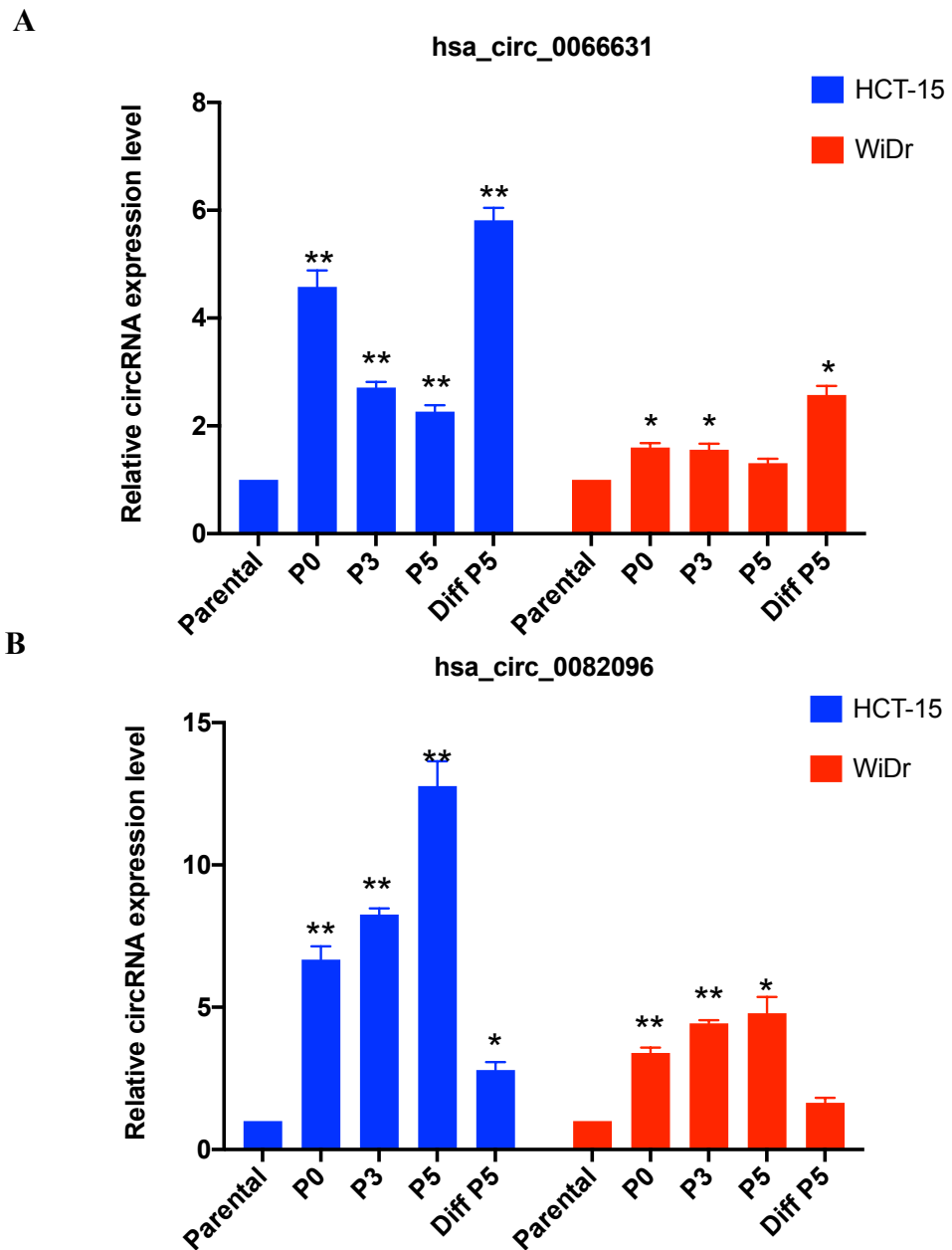


Figure 4.10 Expression of candidate circular RNAs on different passages of CRC spheroidal cells. The expression levels of circular RNA (A) hsa_circ_0066631 and (B) hsa_circ_0082096 were analysed using qRT-PCR on different passages of the spheroidal culture (P0, P3 and P5) and on the serum induced differentiation (Diff P5). “P” is abbreviated for passage. * $p < 0.05$ and ** $p < 0.01$ were values relative to the parental cells.

Further analysis was performed to investigate the expression of hsa_circ_0082096 in other CRC spheroidal cells. CRC cell lines, HCT-116, HT-29, SW-480 and SW-620, were used to generate spheroidal cells. The morphological images of the generated CRC spheroidal cells are displayed in Figure 4.11A. Compared to the parental cells, all CRC spheroidal cells exhibited higher expression levels of hsa_circ_0082096 (Figure 4.11B), corroborating the potential involvement of the circRNA in CRC stemness maintenance. Therefore, hsa_circ_0082096 was selected as a potential candidate for downstream analysis.

4.6 Nomenclature and molecular characteristics of hsa_circ_0082096/ circZNF800

Based on information in the CircBase and CircInteractome databases, hsa_circ_0082096 is a circular RNA derived from the transcript of the human *circZNF800* gene. The *ZNF800* gene (NM_176814) is composed of six exons and has been predicted to generate a total of eight circRNAs, including hsa_circ_0082096 (Table 4.4). The hsa_circ_0082096 isoform is derived from backsplicing of exons four and five of the transcript and is 1,837 nucleotides in length. Details on hsa_circ_0066631 and host gene, *DCBLD2* are available in Table 4.4.

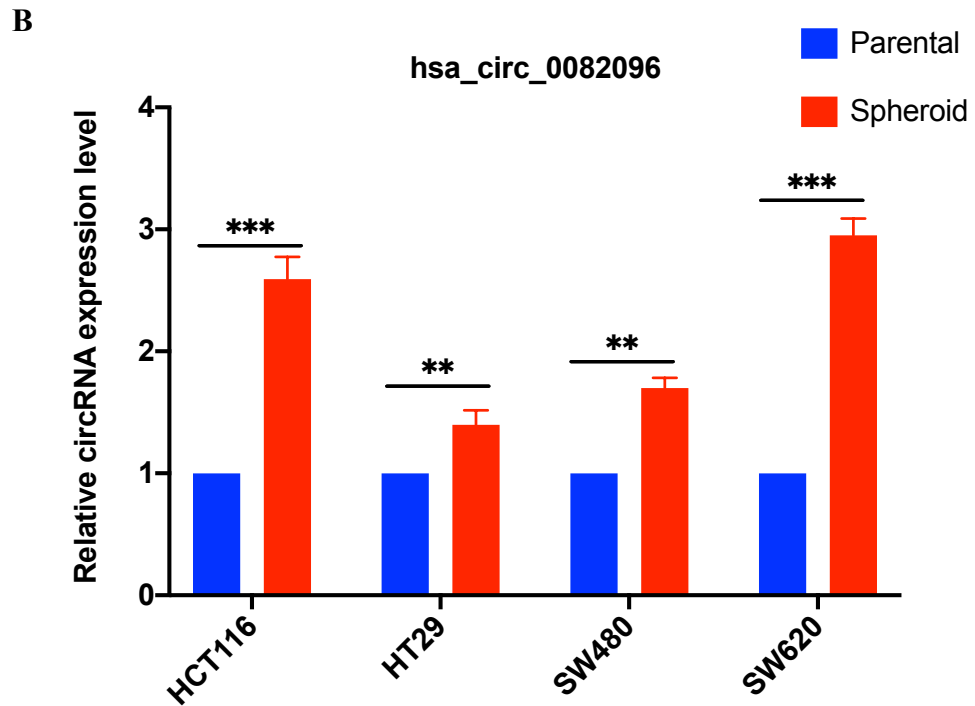
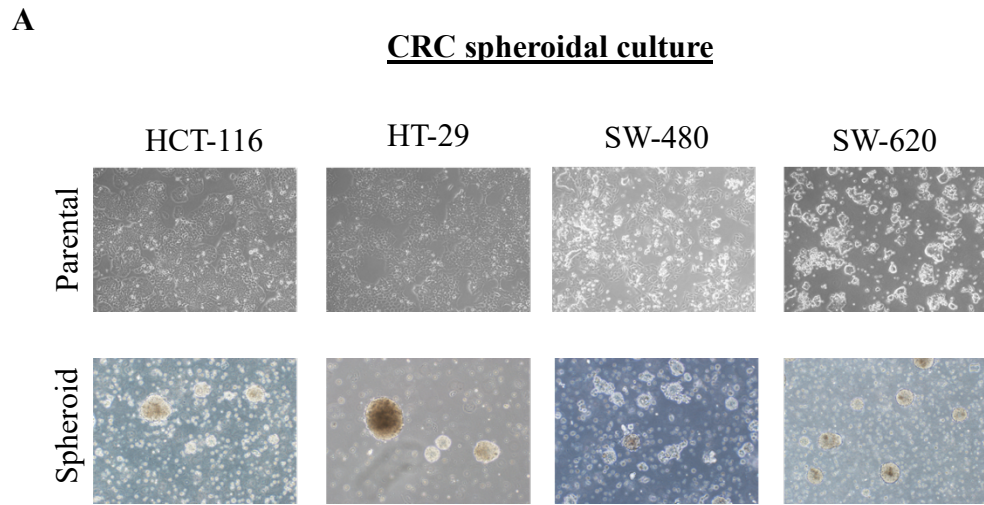


Figure 4.11 Expression of hsa_circ_0082096 in spheroidal cells derived from various CRC lines. Morphology (A) and qRT-PCR analysis (B) of hsa_circ_0082096 expression in spheroidal cells generated from various CRC cell lines. * $p < 0.05$, ** $p < 0.01$ and *** $p < 0.001$ were values relative to the parental cells.

Table 4.4 Molecular characteristics of circZNF800 and circDCBLD2

Molecular characteristic	CircZNF800/ZNF800	Hsa_circ_0066631/DCBLD2
	Circular RNA	
Organism	Human	Human
CircBase ID	hsa_circ_0082096	hsa_circ_0066631
Gene name nomenclature	circZNF800	circDCBLD2
Size	1,837 nucleotides	366 nucleotides
Host-gene sequence retained	Exons 4 - 5	Exons 2 - 3
CircRNA sequence	See Figure 4.12	GTGATGGATGTGGACACACTGTACTAGGCC CTGAGAGTGGAACCCTTACATCCATAAACT ACCCACAGACCTATCCCAACAGCACTGTTT GTGAATGGGAGATCCGTGTAAAGATGGGA GAGAGAGTTCGCATCAAATTTGGTGACTTT GACATTGAAGATTCTGATTCTTGTCACHTTA ATTACTTGAGAATTTATAATGGAATTGGAG TCAGCAGAAGTAAATAGGCAAATACTGTG GTCTGGGGTTGCAAATGAACCATTC AATTG AATCAAAAGGCAATGAAATCACATTGCTGT TCATGAGTGG AATCCATGTTTCTGGACGCG GATTTTTGGCCTCATACTCTGTTATAGATAA ACAAG

Table 4.4 (Cont'd)

	Host gene	
Host gene	Zinc finger protein 800 (<i>ZNF800</i>)	Discoidin, CUB and LCCL domain containing 2 (<i>DCBLD2</i>)
Chromosomal location	Chr7:127342859-127431924	Chr3:98795941-98901695
Host transcript (Accession number)	<i>ZNF800</i> (NM_176814)	<i>DCBLD2</i> (NM_080927)
No. exons in host gene	6	16
Predicted total no. circRNAs	8	24
Predicted circRNA isoforms	hsa_circ_0133240; hsa_circ_0133241; hsa_circ_0133242; hsa_circ_0082095; hsa_circ_0082096; hsa_circ_0082097; hsa_circ_0082098; hsa_circ_0082099	hsa_circ_0004968; hsa_circ_0066610; hsa_circ_0066611; hsa_circ_0066612; hsa_circ_0066613; hsa_circ_0066614; hsa_circ_0066615; hsa_circ_0066616; hsa_circ_0066617; hsa_circ_0066618; hsa_circ_0066619; hsa_circ_0066620; hsa_circ_0066621; hsa_circ_0066622; hsa_circ_0066623; hsa_circ_0066624; hsa_circ_0066625; hsa_circ_0066626; hsa_circ_0066627; hsa_circ_0066628; hsa_circ_0066629; hsa_circ_0066630; hsa_circ_0066631; hsa_circ_0124847

Information in the table is derived from CircBase and CircInteractome.

To date, none of the eight *ZNF800* circRNAs has been reported in characterisation and functional studies. In line with the common nomenclature practice of naming a circular RNA using the name of the host gene (Costa and Enguita, 2020; Vromman, Vandesompele and Volders, 2021), *hsa_circ_0082096* is also designated as *circZNF800* in this first study on the circRNA. The use of uppercase letters, *ZNF800*, in the designation is also in line with the long-standing practice of capitalising human gene names. As such, the “*hsa_*” prefix is dropped from *circZNF800*. For a *Znf800* circRNA derived from mouse, the gene-name nomenclature would be *mmu_circZnf800*, and the like for other animals. The basic molecular characteristics of *circZNF800* are summarised in Table 4.4. The full-length sequence of *circZNF800* is shown in Figure 4.12.

1	GAACTAAACA	ACTTAAGCAT	ATTTTATTAA	AAGATGTGGA	CACTATTTTT	GAATGTAAGT	TATGCCGCAG	TCTCTTCAGA	GGATTACCAA	ATTTAATTAC
101	CCATAAAAAA	TTCTACTGCC	CACCAAGTCT	CCAGATGGAT	GACAACCTTC	CTGATGTAAA	TGATAAACAA	AGCCAAGCCA	TAAATGATCT	CCTAGAAGCC
201	ATATATCCAA	GTGTGGACAA	ACGAGAATAT	ATTATTAAGC	TAGAACCCAT	AGAAACTAAT	CAAAATGCAG	TATTTCAATA	TATTTCGAGG	ACTGATAATC
301	CTATTGAAGT	CACAGAGTCA	AGCAGTACTC	CTGAACAAAC	CGAAGTTCAG	ATACAGGAAA	CTAGCACTGA	ACAGTCAAAA	ACAGTACCGG	TTACAGATAC
401	AGAGGTGGAA	ACTGTAGAGC	CCCCTCCTGT	TGAGATTGTT	ACAGATGAAG	TTGCACCTAC	ATCTGATGAA	CAACCTCAGG	AGTCGCAGGC	TGACTTGGAA
501	ACTTCTGACA	ATTCTGATTT	TGGTCACCAG	TTGATATGTT	GTCTTTGTAG	AAAAGAATTC	AATTCTAGAC	GAGGTGTTCG	CCGTCACATT	CGAAAAGTAC
601	ACAAGAAAAA	GATGGAAGAA	CTAAAAAAGT	ACATTGAAAC	ACGAAAAGAAT	CCAAACCAAT	CCTCTAAAGG	ACGCAGTAAAG	AATGTTCTAG	TTCCATTAAG
701	TAGGAGTTGT	CCAGTATGTT	GTAATCATT	TGCTACAAAA	GCGAATGTAA	GGAGGCATTT	TGATGAAGTT	CATAGAGGAC	TAAGGAGGGA	TTCAATTACT
801	CCTGATATAG	CAACAAAGCC	TGGGCAACCT	TTGTTCTGG	ATTCTATTTT	TCCTAAAAAA	TCTTTTAAGA	CTCGAAAAACA	AAAGTCTTCT	TCAAAGGCTG
901	AATACAATTT	AACTGCATGC	AAATGCCTCC	TTTGCAAGAG	GAAATATAGT	TCACAAATAA	TGCTTAAAAG	ACATATGCAA	ATTGTCCACA	AGATAACTCT
1001	TTCTGGAACA	AACTCTAAAA	GAGAAAAAGG	CCCTAATAAT	ACTGCCAACA	GTTTCAGAAAT	AAAAGTAAA	GTTGAACCAG	CAGATTCTGT	AGAATCTTCA
1101	CCCCCTTCCA	TTACCCATTC	TCCACAGAAT	GAATTAAAGG	GAACAAATCA	TTCAAATGAA	AAAAAGAACA	CACCGGCAGC	ACAGAAAAAT	AAAGTTAAAC
1201	AAGACTCTGA	AAGCCCTAAA	TCAACTAGTC	CGTCGGCTGC	AGGTGGCCAG	CAAAAAACCA	GAAAACCAA	ACTTTCAGCT	GGCTTTGACT	TTAAGCAACT
1301	TTACTGTAAA	CTTTGTAAAC	GTCAGTTTAC	TTCCAAACAG	AACTTGACTA	AACACATCGA	GTTGCACACA	GATGGAAATA	ACATTTATGT	TAAATTTCTAC
1401	AAGTGTCTCT	TTTGCACTTA	TGAAACTCGT	CGGAAACGTG	ATGTGATACG	ACATATAACT	GTGGTTCATA	AAAAGTCATC	TCGTTATCTT	GGGAAAATAA
1501	CAGCCAGTTT	AGAGATCAGA	GCTATAAAAA	AGCCTATTGA	TTTTGTTCTA	AATAAAGTGG	CAAAAAGAGG	CCCTTCGAGG	GATGAAGCAA	AACATAGTGA
1601	TTCAAAACAT	GATGGCACTT	CTAACTCTCC	TAGTAAAAAG	TATGAAGTAG	CTGACGTCGG	TATTGAAGTA	AAAGTCACAA	AAAACTTTTC	TCTTCACAGA
1701	TGCAATAAAT	GTGGAAGGC	ATTTGCCAAA	AAGACTTACC	TTGAACATCA	TAAGAAAAC	CATAAGGCAA	ATGCTTCCAA	TTCACCTGAA	GGAAACAAAA
1801	CCAAAGGCCG	AAGTACAAGA	TCTAAGGCTC	TTGTCTG						

Figure 4.12 Full-length sequence of circZNF800. The sequence was obtained from CircInteractome database and aligned based on the length.

4.7 CircZNF800 exhibited common features of circular RNA

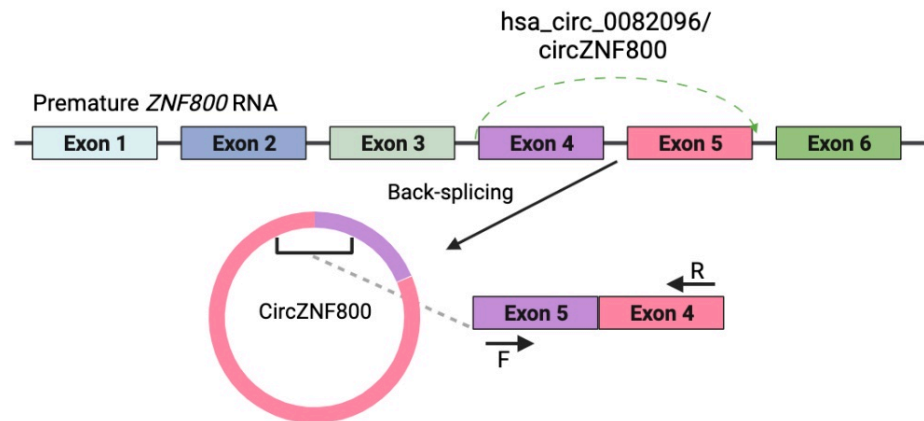
4.7.1 Sanger sequencing validated the circZNF800 backsplicing junction

The backsplicing junction was verified to validate the circularisation of the circZNF800 RNA sequence. The transcript of the host gene, *ZNF800*, consists of six exons (Figure 4.13A). circZNF800 was predicted to be derived from exons four and five of *ZNF800*. To validate the backsplice junction, a divergent primer pair was designed based on the sequence of the joining of exons five and four (Figure 4.13A). The resulting PCR product generated using the divergent primers was subjected to Sanger sequencing, confirming the predicted backsplicing junction sequence (Figure 4.13B).

4.7.2 CircZNF800 was RNase R resistant with longer half-life

CircRNAs are resistant to endonuclease RNase R due to the lack of 5' or 3' UTR region and a polyA tail (Sakshi *et al.*, 2021). RNA extracted from HCT-15 and WiDr cells were subjected to RNase R treatment, followed by qRT-PCR analysis. The host transcript *ZNF800* was significantly degraded on RNase R treatment; however, circZNF800 levels remained stable upon RNase R treatment in the two CRC cell lines tested (Figure 4.14A), confirming that circZNF800 is RNase R resistant.

A



B

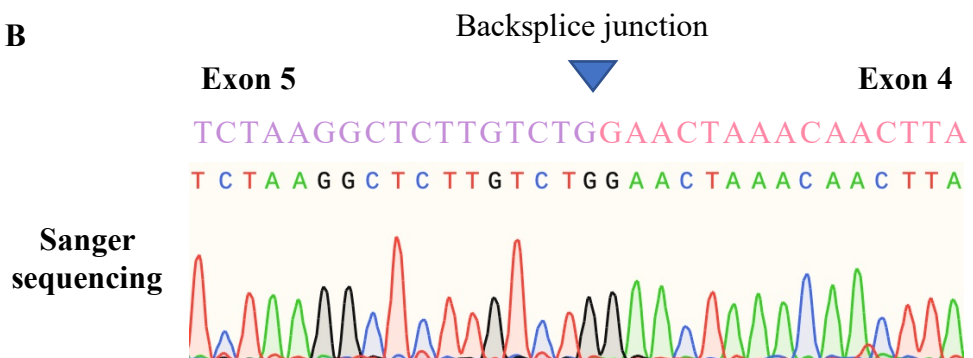


Figure 4.13 Experimental validation of circZNF800 backsplice junction. (A) Illustration of the generation of circZNF800 from host transcript, *ZNF800* via backsplicing. Divergent primer design of circZNF800 spanning the backsplice junction is illustrated as arrows in the lower panel. F denotes the forward primer, and R denotes the reverse primer location. (B) Alignment of the Sanger sequencing data and predicted backsplice junction of circZNF800. The Sanger sequencing was performed on the PCR product generated using the divergent primer.

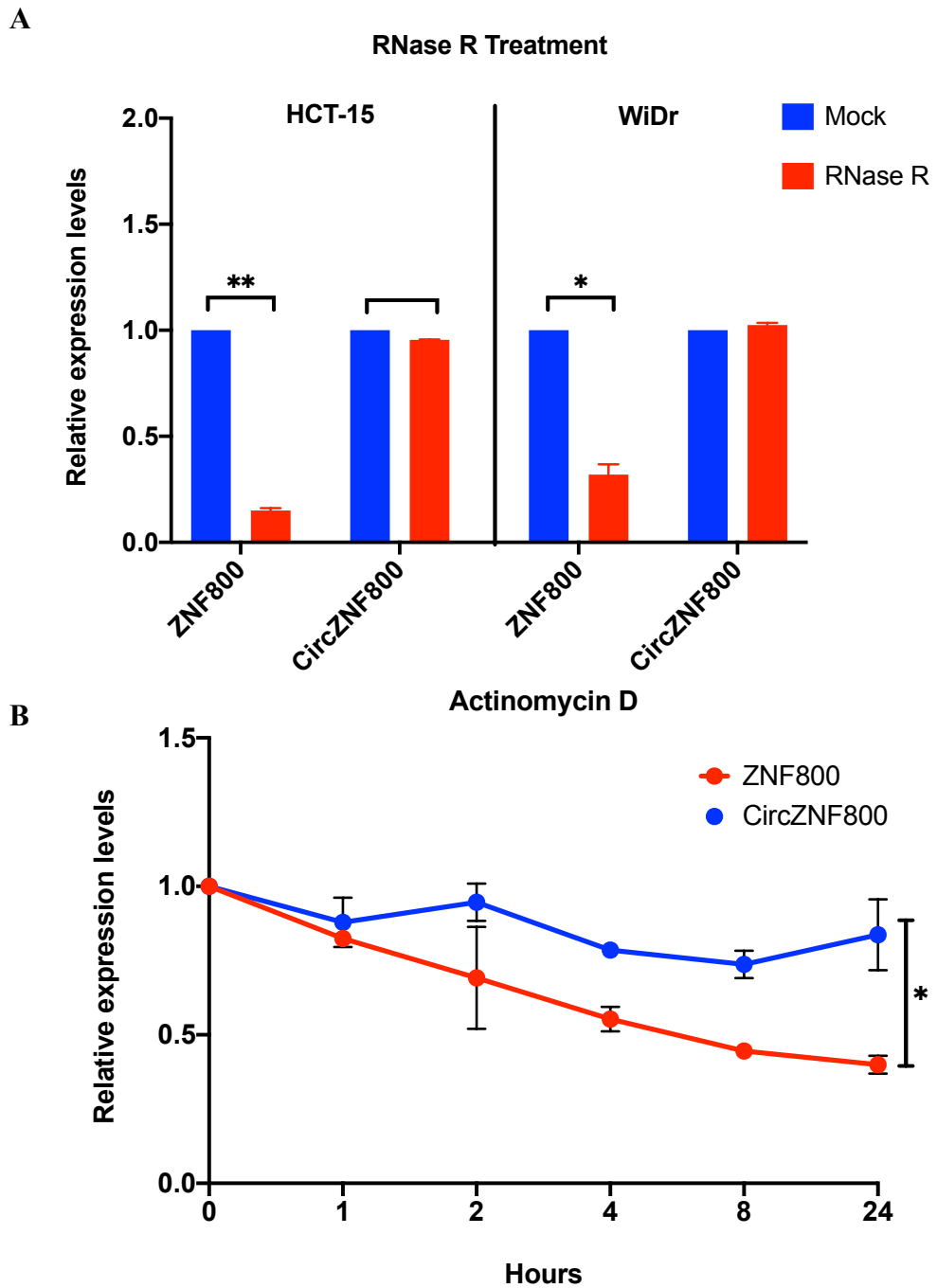


Figure 4.14 Characterisation of hsa_circ_0082096 for distinct circular RNA properties. qRT-PCR analysis of host transcript, *ZNF800* and hsa_circ_0082096 on (A) RNase R treatment and (B) actinomycin D treatments on WiDr cells. * $p < 0.05$ and ** $p < 0.01$ were values relative to the parental cells.

Another distinctive characteristic of circRNAs is a longer life-span of compared to host transcripts (Eneka *et al.*, 2016). Hence, the half-life of the circZNF800 relative to the host transcript *ZNF800* was determined. By treating the cells with Actinomycin D to inhibit the synthesis of new RNA in the cells (Vo *et al.*, 2019), qRT-PCR analysis was performed on cells harvested at different time points of treatment. The analysis revealed that the levels of the host transcript, *ZNF800*, reduced by 50% within 24 hours of Actinomycin D treatment (Figure 4.14B). In contrast, the circZNF800 expression levels were stable up to 24 hours post-treatment, thus demonstrating higher stability of circZNF800 compared to *ZNF800*.

4.8 CircZNF800 expression levels were significantly higher in CRC clinical tissues compared to the host transcript

To establish the clinical relevance of circZNF800 expression with CRC, qRT-PCR analysis was performed on tumour and adjacent tissues of CRC patients (Figure 4.15). *ZNF800* transcript showed no significant differential expression in the adjacent normal and CRC tissues (n=20) (Figure 4.15A, left panel). On the other hand, circZNF800 expression levels were significantly higher in CRC tissues relative to the adjacent normal tissues (Figure 4.15A, right panel). The mean expression levels of circZNF800 in the tumour tissues were approximately 0.5 times higher than those in the adjacent normal tissues, suggesting circZNF800 could act as a possible oncogenic epigenetics regulator.

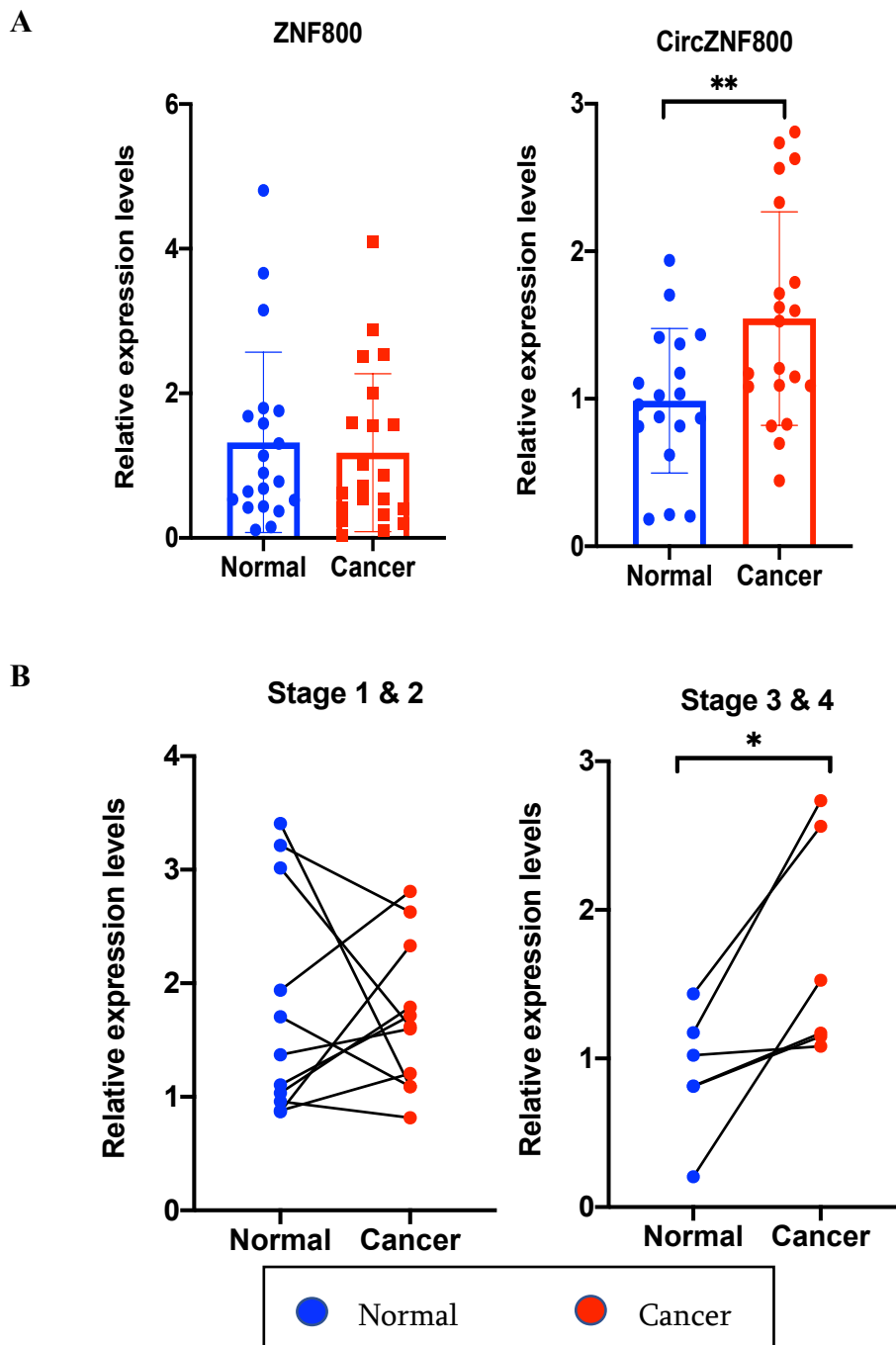


Figure 4.15 Expression of *ZNF800* and circ*ZNF800* in CRC patient samples.

(A) qRT-PCR analysis of the expression levels of *ZNF800* and circ*ZNF800* on normal adjacent and CRC patient tissue samples (N=20). (B) CRC stage-dependent analysis of circ*ZNF800* based patient clinical reports. * $p < 0.05$ and ** $p < 0.01$ were values relative to the parental cells.

To further investigate the expression patterns of circZNF800 in relation to different tumour stages, the CRC patients were grouped based on the clinical staging. CircZNF800 did not show any significant difference between the adjacent normal and the tumour tissues in tissue samples of stages 1 and 2 (Figure 4.15B, left panel). However, tissue samples of stages 3 and 4 showed significant elevated expression of circZNF800 relative to normal adjacent tissues (Figure 4.15B, right panel). CircZNF800 could play a role in late-stage CRC progression compared to early stages in the tumorigenesis process.

4.8.1 Expression of circZNF800 coincided with high proliferative tumour cell population in CRC tissues and in intestinal stem cell population in normal tissues

To validate the qRT-PCR analysis of circZNF800 expression in the clinical samples (Figure 4.15), RNA FISH (fluorescent *in situ* hybridisation) assay was performed. The red fluorescence tag, Cyanine-7, was conjugated with an anti-sense DNA sequence that targeted circZNF800. Corroborating the qRT-PCR analysis, the RNA FISH showed lower circZNF800 expression in paired normal tissues compared to paired tumours tissues (Figure 4.16).

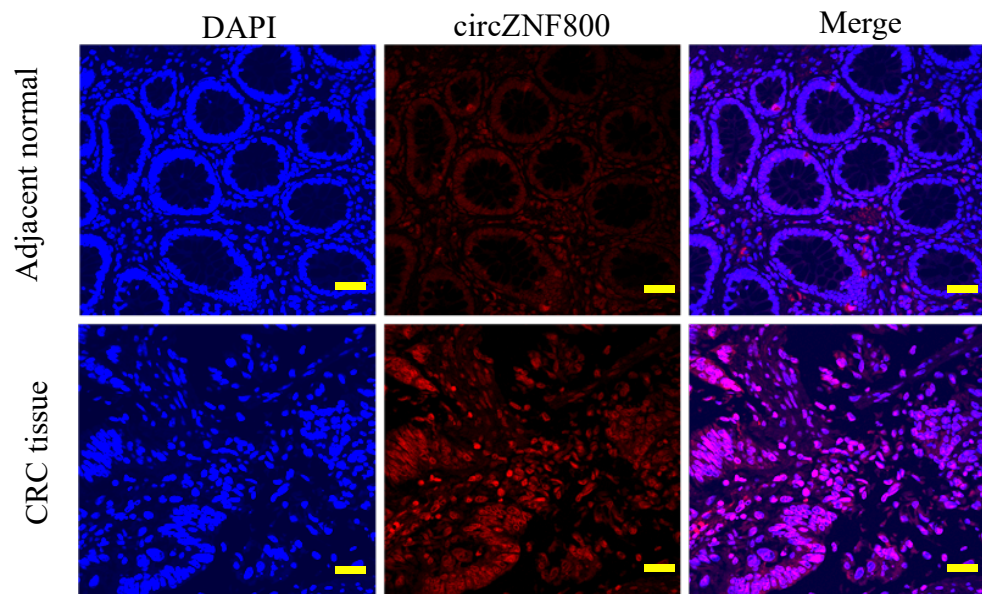


Figure 4.16 RNA FISH analysis of circZNF800 expression in CRC patient tissues. Fluorescence in situ hybridisation (FISH) assay was performed with a specific probe targeting circZNF800 (tagged with red fluorescence, Cyanine 7) on adjacent normal and CRC tissues of the same patient. DAPI was used to stain the nuclei of the tissues. Bar represents 100 μ m.

To further understand the types of cells in the colon tissue that expresses high levels of circZNF800 in both the normal and tumour tissues, dual immunofluorescence assay was performed. As bioinformatics analysis had predicted circZNF800 involvement in the regulation of stemness, co-localisation of circZNF800 in intestinal stem cell population was investigated. Leucine-rich repeat-containing G-protein coupled receptor 5 (Lgr5) and SRY-Box Transcription Factor 9 (Sox9) have been reported to be the markers of intestinal stem cells that reside in crypt base columnar cells (Formeister *et al.*, 2009; Roche *et al.*, 2015).

In the normal colon tissue, the dual immunofluorescence assay revealed that cells that expressed high levels of circZNF800 were co-localised with Lgr5- and Sox9-positive cells (Figure 4.17A). The results suggest that circZNF800 could be a biomarker for mapping the intestinal stem-cell population in normal colon tissues. In the CRC tumour, co-localisation of circZNF800 with proliferative marker Ki-67 was investigated. CircZNF800-expressing cells in CRC tissues were also positive for the Ki-67 marker (Figure 4.17B), suggesting that circZNF800 could be involved in CRC cancer progression as an oncogenic epigenetic regulator.

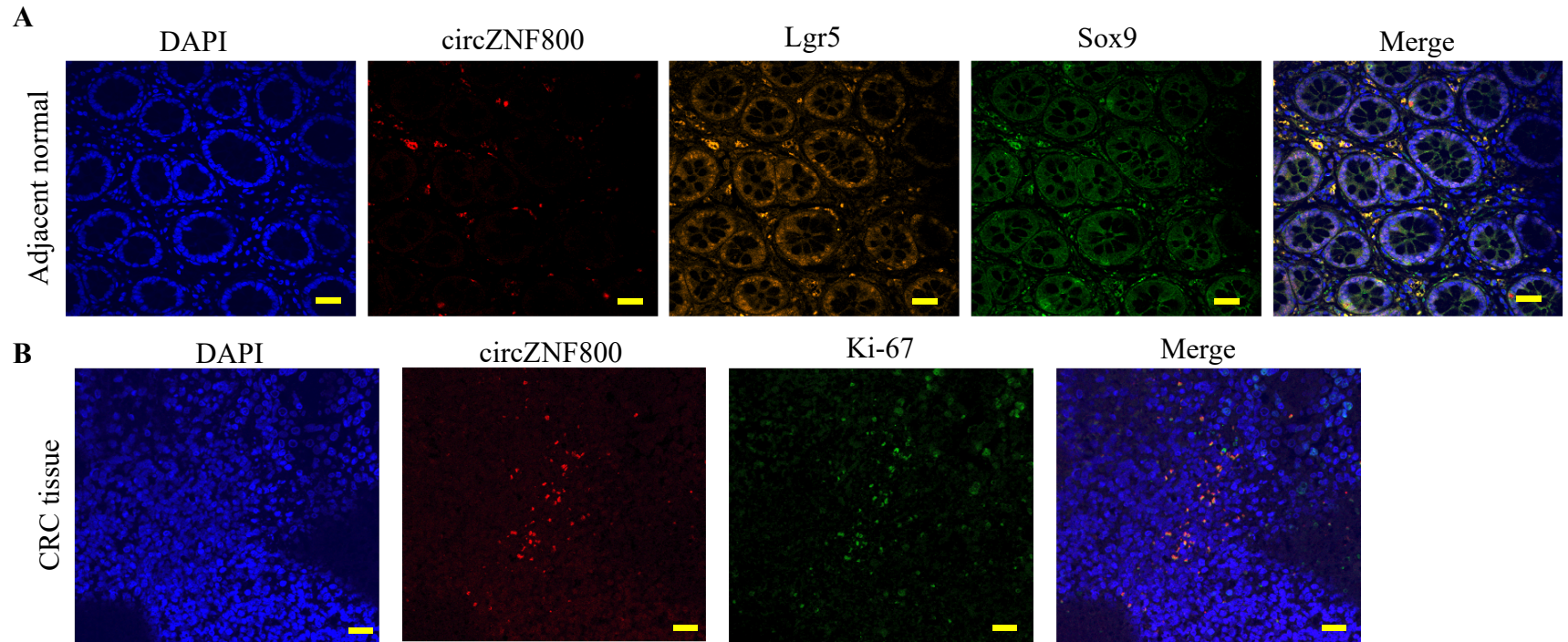


Figure 4.17 Co-localisation analysis of circZNF800 with intestinal cells and proliferative markers. Dual immunofluorescent assays of RNA FISH and protein immunofluorescent on (A) adjacent normal and (B) corresponding CRC tissues. In the adjacent normal tissues in (A), circZNF800 (in red) was co-stained with antibodies specific for Lgr5 (orange) and Sox9 (green) proteins, which are specific for intestinal stem cell population (A). In CRC tissue, circZNF800 was co-stained with Ki-67 (green) to represent high proliferative population (Bar= 100 μ m).

Part 3A: Functional modulation of circZNF800 in relation to stemness regulation: circZNF800 overexpression analysis

4.9 Establishment of an ectopic overexpression system of circZNF800

Group one introns of T4 phage of *thymidylate synthase* gene are able to yield circularised introns during the exon splicing process (Ford and Ares, 1994). By permutating the introns to flank an exon, and through autocatalytic splicing process via chemical transesterification reactions, the flanked exon can be circularised (Chen *et al.*, 2017). A similar strategy was employed in the present study. A matured sequence of circZNF800 was cloned into a permuted *td* gene plasmid carrying a T7 promoter that flanks introns (3' and 5' splice sites) of the T4 phage (Figure 4.18).

Using *in vitro* transcription reactions, linear RNA was generated with the intron splice sites intact. Subsequently, autocatalytic splicing process to induce transesterification was performed using excess guanosine-5'-triphosphate (GTP) and magnesium chloride (MgCl₂) to generate circularised RNA molecules encoding the circZNF800 sequence.

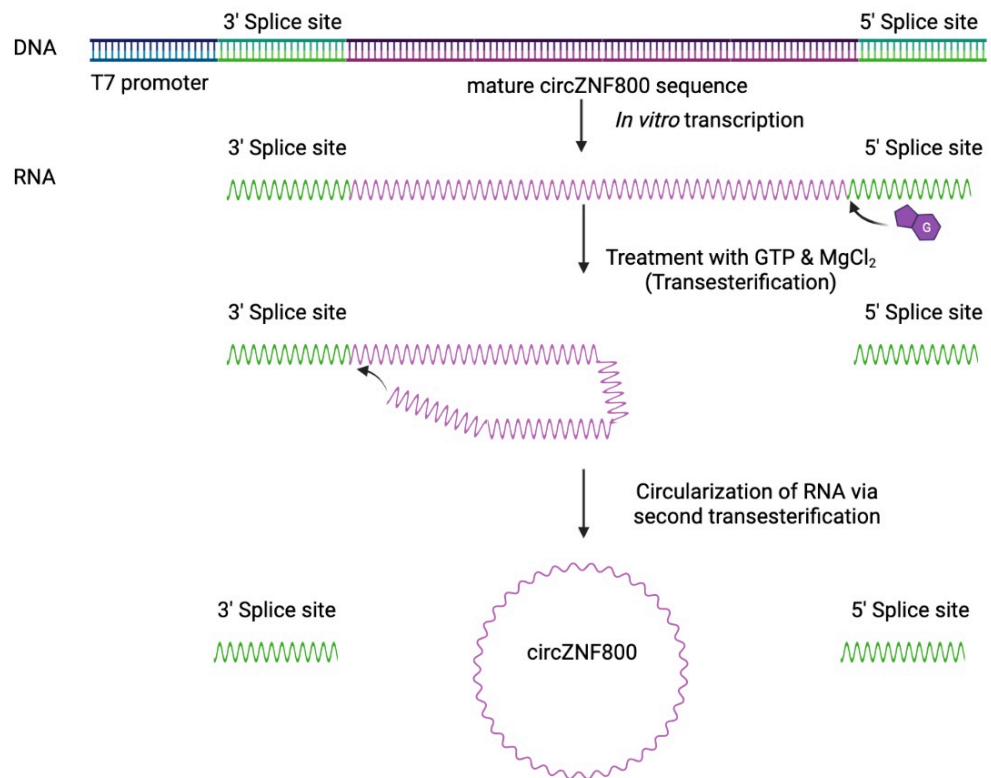


Figure 4.18 Illustration of circZNF800 overexpression generation system.

Using permuted autocatalytic self-splicing group 1 introns, circZNF800 sequence was cloned into permuted *td* gene vector in between the 3'- and 5' splice sites. On *in vitro* RNA transcription, the resulting linear RNA was chemically treated with excess guanosine-5'-triphosphate (GTP) and magnesium chloride (MgCl₂) to induce circularisation.

4.9.1 Generation and validation of *in vitro* transcribed self-circularising circZNF800

Using the aforementioned method, the *in vitro* transcription-generated circZNF800 RNA was treated with RNase R enzyme for validation of circularisation. The resulting RNA was purified and separated in 2% MOPS gel electrophoresis (Figure 4.19A). *In vitro* transcription and the subsequent transesterification-induced circularisation yield of RNA products were within the expected lengths of ~1,800 nucleotides (Figure 4.19A, 2nd and 3rd lanes). Upon RNase R treatment, the resulting RNA showed similar band size compared to the untreated group (Figure 4.19A 3rd and 4th lanes), suggesting RNase R resistance, and the transcribed RNA was circularised.

To further investigate if the *in vitro* transcribed circZNF800 was indeed circularised, Sanger sequencing on the PCR product was performed. As predicted, the 5'- and 3'-ends of the circZNF800 sequence encoding for exons four and five, respectively, were joined (Figure 4.19B). A “GCAG: tetra-nucleotides leftover from the 5' splice site was also detected in the Sanger sequencing result. Collectively, the results indicated that using the autocatalytic splicing introns, a circularised full-length sequence of circZNF800 was generated via *in vitro* transcription.

4.9.2 Successful cellular uptake of circZNF800 in chemical transfection

The transfection of large RNA (> 1,500 nucleotides) has been a major limitation in circRNA studies (Obi and Chen, 2021; Chen and Lu, 2021). To evaluate the uptake efficiency of circZNF800 RNA by CRC cells, *in vitro* transcribed circZNF800 was tagged with the green fluorescent Cyanine-3 (Cy3). CircZNF800-Cy3 was chemically transfected into WiDr cells (as described in Section 3.7.4) and was visualised through fluorescence microscopy 12 h post-transfection. The fluorescence images suggest that the transfected circZNF800 overlapped with the CRC cells (Figure 4.20A) suggesting successful circZFP800 uptake by the cells.

To further measure the circZNF800 uptake efficiency, flowcytometry analysis was performed through fluorescence quenching. Trypan blue is known to quench the green fluorescence (Avelar-Freitas *et al.*, 2014). Furthermore, trypan blue can be used as an exclusion assay to identify cells with intact cell membrane (Shilova, Shilov and Deyev, 2017). By combining these properties, trypan blue was used to determine if the transfected circZNF800 tagged with green fluorescence Cy3 was residing inside the cells, thus measuring the uptake efficiency.

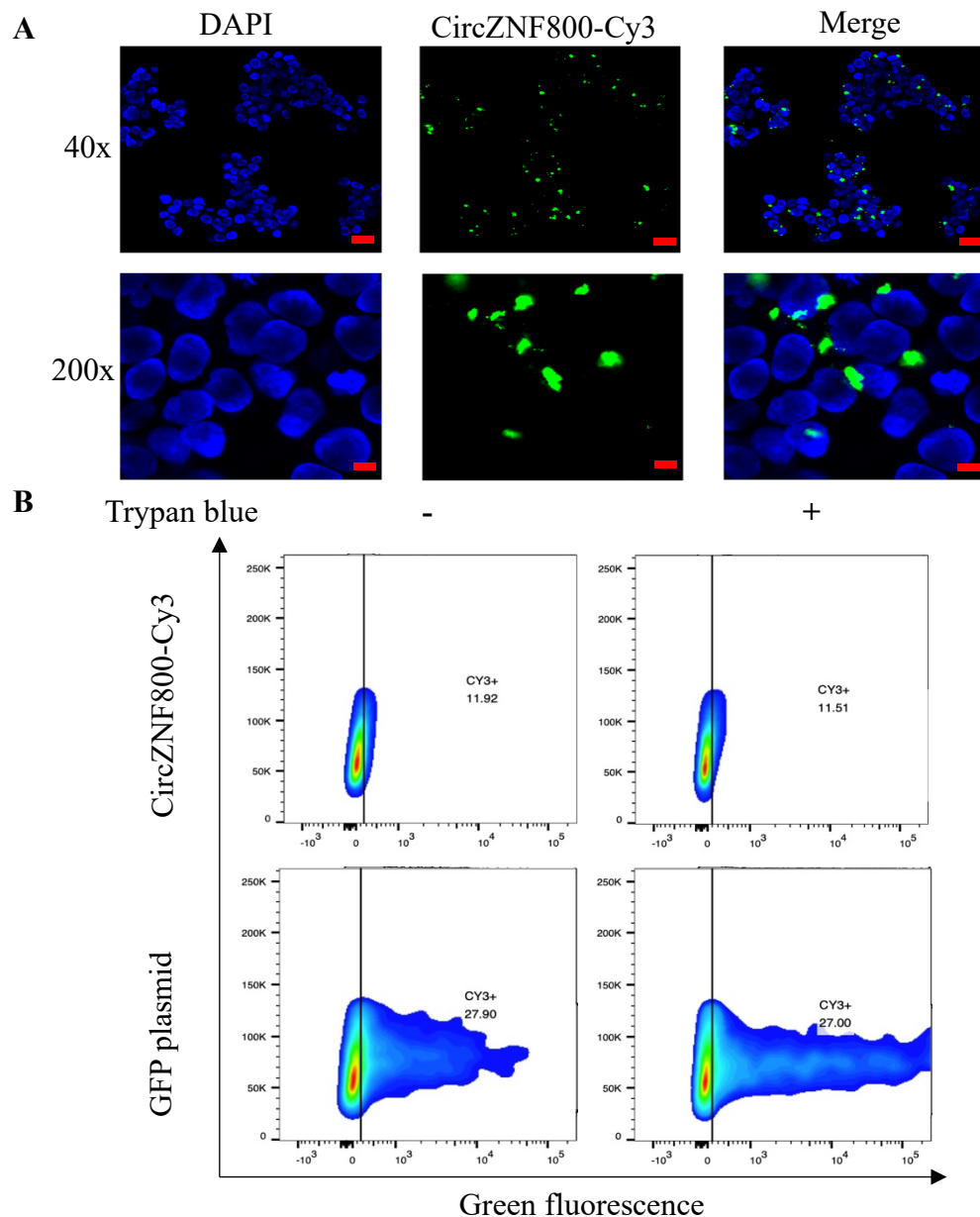


Figure 4.20 Evaluation of the transfection efficiency of *in vitro* transcribed circZNF800. (A) Visualisation of *in vitro* transcribed circZNF800 in cells. circZNF800 was tagged with Cyanine-3 (Cy3; green fluorescent) and was transfected into WiDr cells for observation under a fluorescence microscope at different magnifications using fluorescent microscopy. Scale bars represent 100 μ m. (B) Flowcytometry analysis of green fluorescence emission upon *in vitro* transcribed circZNF800-Cy3 RNA and DNA plasmid tagged with green fluorescent protein (GFP) before and after treatment with 0.4% trypan blue.

Upon transfecting WiDr cells with circZNF800-Cy3, flowcytometry analysis was performed to assess the green fluorescence emitted by the RNA. As a control, a green fluorescence protein (GFP)-expressing DNA plasmid was used. The green emitted fluorescence levels were measured with or without the treatment with 0.4% trypan blue. The expression levels of the RNA-Cy3 were around 11% and 27% in the GFP-transfected cells, for both the untreated and treated group (Figure 4.20B). While these results do not equate to the efficiency of RNA transfection, Cy3 green fluorescence levels remain stable regardless of the trypan blue treatment, suggesting a successful uptake of the circZNF800 RNA by the cells.

4.10 Ectopic overexpression of circZNF800 enhanced CSC-like properties in WiDr cells

Using the *in vitro* transcribed circZNF800, CSC-related properties in CRC cells were investigated. Proliferation assay and expression of cancer stem cells (CSC) and intestinal stem cells (ISC) markers were evaluated upon circZNF800 RNA transfection (Figs. 4.22 & 4.23, see below). Proliferation assays were performed using EdU assays. CD44 and CD133 were evaluated to analyse the changes in CSC markers (Tsunekuni *et al.*, 2019). Lrg5 and Sox9 were used to evaluate the expression levels of ISC population (Formeister *et al.*, 2009). Due to the transient effects of circZNF800 transfection, other cellular phenotypic assays involving CSC properties such as colony-forming and sphere-forming assays were not performed.

4.10.1 CircZNF800 increased cell proliferation

The cell proliferative effects of circZNF800 on the CRC cells were evaluated using EdU assay, which measures the DNA synthesis levels by labelling the newly incorporated thymidine analogue, 5-ethynyl-2'-deoxyuridine, EdU (Mead and Lefebvre, 2014). The EdU levels are measured by a click reaction where fluorescently tagged molecules interact with the incorporated EdU analogue and the results were evaluated using flowcytometry.

Upon transfection of *in vitro* transcribed circZNF800 in WiDr cells, there was a marked increase in EdU⁺ cells compared to the vehicle and the circGFP RNA control groups (Figure 4.21). Transfection with circZNF800 significantly increased the levels of EdU⁺ cells close to 17% compared to the vehicle group at approximately 11%. High RNA-induced toxicity was observed in the circGFP RNA transfected group (Liu *et al.*, 2018) compared to the vehicle group where the number of EdU⁺ cells was reduced by almost half. Despite this, the higher EdU⁺ cell levels in the circZNF800-transfected samples were higher suggesting that circZNF800 promoted cellular proliferation in CRC WiDr cells in the experiments.

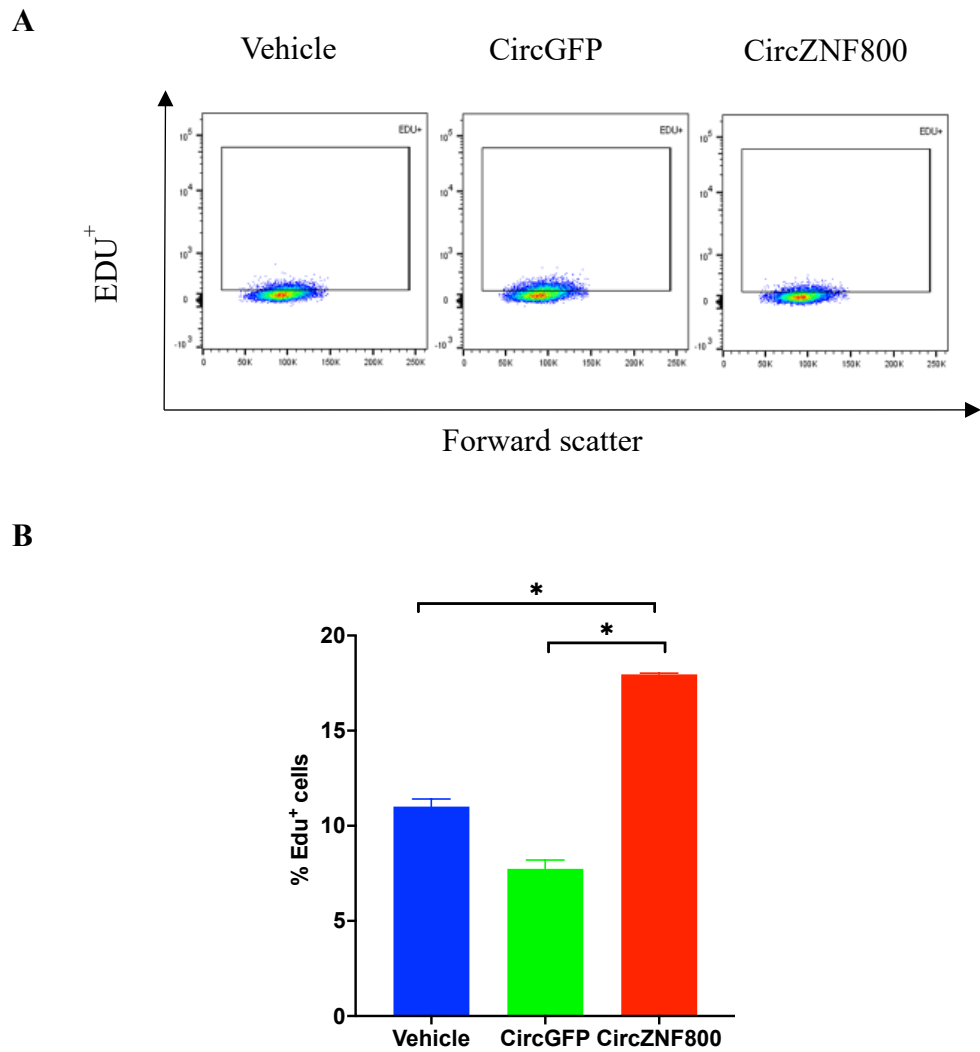


Figure 4.21 Effects of circZNF800 overexpression on CRC cell proliferation.

Flowcytometry analysis of EdU-positive WiDr cell population on transfection with vehicle, circGFP and circZNF800 RNA. (A) Representative flowcytometry contour plots are shown in left 3 panels for each treatment group. (B) The bar graph represents the average data from triplicated independent experiments.

** $p < 0.01$ and *** $p < 0.001$ were obtained by comparing to the vehicle-treated group.

4.10.2 CircZNF800 up-regulated cancer and intestinal stem cell markers

To establish the effects of circZNF800 on cancer stem cell properties, CD44 and CD133 expression levels were evaluated on circZNF800 transfection. Compared to the vehicle group, WiDr cells over-expressing circZNF800 showed significant up-regulation of CD44 and CD133 markers (Figure 4.22A). CD44 expression levels increased from an average of 52% to about 81%. Similarly, CD133 expression levels doubled from 42% to 87% (Figure 4.22B). The up-regulation of CD44 and CD133 are consistent with that circZNF800 is involved in the regulation of CSC properties as predicted in the bioinformatics analysis (Figure 4.9).

RNA FISH analysis on CRC patient tissue samples showed co-localisation of circZNF800 with intestinal stem cell population (Figure 4.17A). Furthermore, flowcytometry analysis revealed that both the intestinal stem cell markers Lgr5 and Sox9 were significantly up-regulated on circZNF800 ectopic overexpression (Figure 4.23A). Lgr5 expression levels increased from 32% to 93% in the treated group, while Sox9 expression from 48% to 82% (Figure 4.23B). The up-regulation of ISC population is indicative that circZNF800 regulates adult stem cell properties in CRC cells.

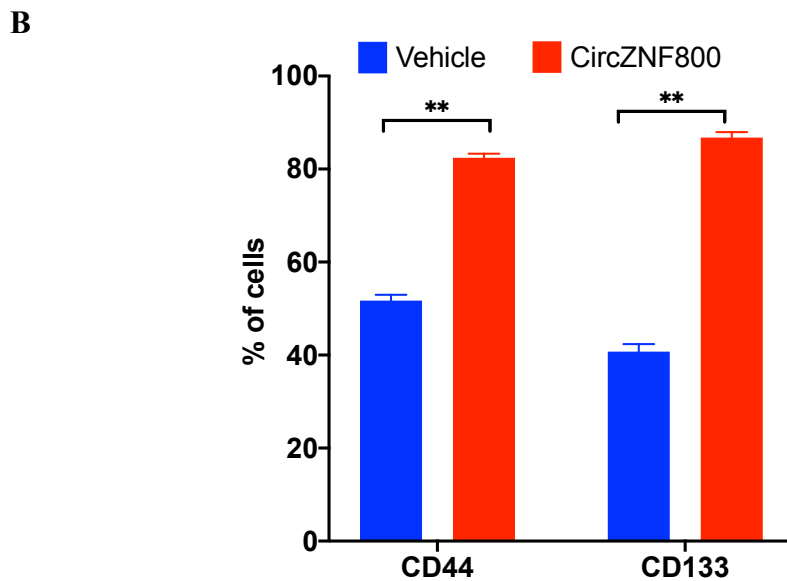
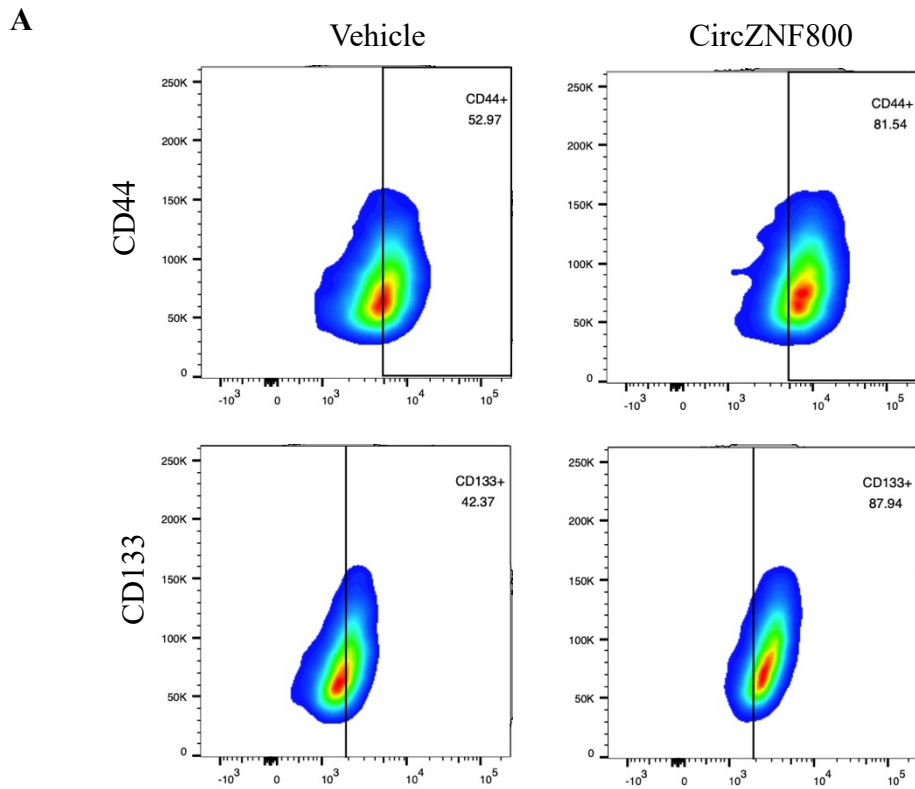
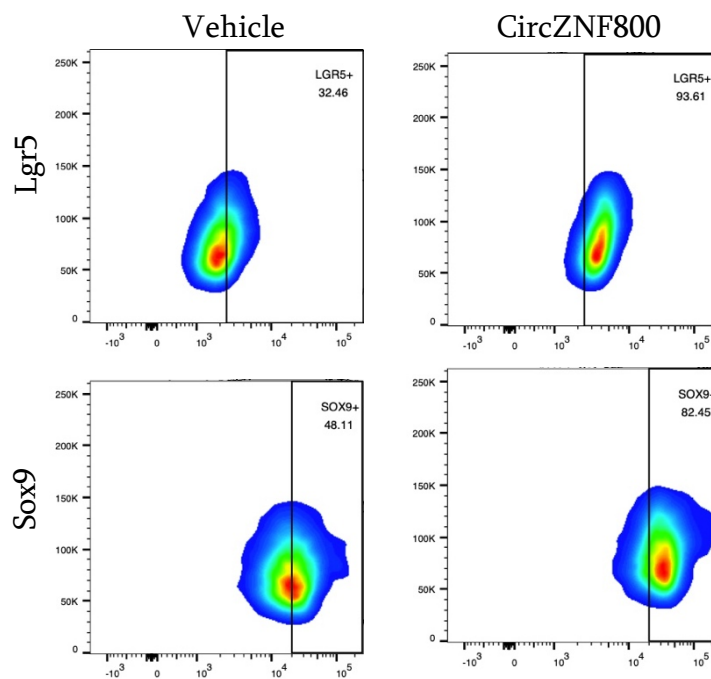


Figure 4.22 Effects of circZNF800 overexpression on CSC markers expression levels. (A) Representative contour plots of flowcytometry analysis of CD44 and CD133 on circZNF800 overexpression in WiDr cells. (B) Bar graph of the average data from triplicated independent experiments. $**p < 0.01$ and $***p < 0.001$ were obtained by comparing to the vehicle-treated group.

A



B

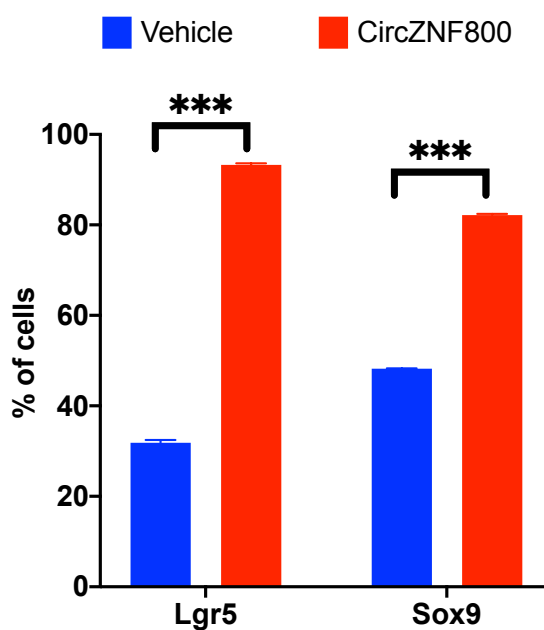


Figure 4.23 Effects of circZNF800 overexpression on expression levels of intestinal stem cell markers. (A) Representative contour plots of flowcytometry analysis of Lgr5 and Sox9 upon circZNF800 overexpression in WiDr cells. **(B)** Bar graph of the average data from triplicated independent experiments. $**p < 0.01$ and $***p < 0.001$ were obtained by comparing to the vehicle-treated group.

4.10.3 CircZNF800 up-regulated expression of stemness markers in CRC cells

The pluripotency regulation of embryonic and induced pluripotent stem cells involves the transcriptional factors Oct4, Sox2, Klf4, cMyc and Nanog (van Schaijik *et al.*, 2018). Previous reports have associated these pluripotency transcriptional factors with the maintenance of stemness in CSC population, including colorectal cancer stem cell populations (Munro *et al.*, 2019; Munro *et al.*, 2018; Zhang *et al.*, 2020b).

To investigate the effects of circZNF800 overexpression on these transcription factors, qRT-PCR analysis was performed. The results showed that on circZNF800 ectopic overexpression, *OCT4*, *SOX2* and *NANOG* expression levels were significantly up-regulated (Figure 4.24). However, *KLF4* and *cMYC* showed no significant difference between the overexpression and the vehicle groups. The results are in line with the increased CSC and intestinal stem cell markers (Figure 4.22), suggesting that circZNF800 is able to reprogramme CRC cells into a high state of cellular potency.

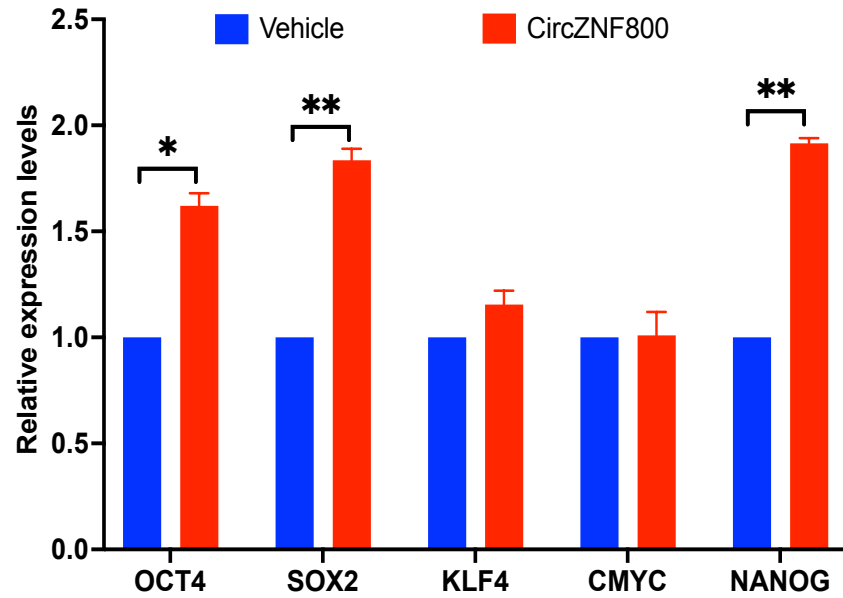


Figure 4.24 Effects of circZNF800 overexpression on expression levels of pluripotency markers. qRT-PCR analysis of selected pluripotency genes was performed on circZNF800 overexpression cells. ** $p < 0.01$ were values relative to the vehicle-treated cells.

4.11 CircZNF800 enhanced tumourigenicity in mice

The most significant property of a CSC population is enhanced tumourigenicity (Vales *et al.*, 2019). The tumourigenicity properties induced by circZNF800 were investigated in a mouse model. As illustrated in the schematic in Figure 4.25, WiDr cells were subcutaneously transplanted into each flank of the nude mice, at 2.5×10^6 cells/flank. The mice were divided into three groups; vehicle group treated with saline and two groups treated with either circGFP or circZNF800 RNA. CircGFP RNA and circZNF800 RNA were administered four times over 8 days, each at 10 μ g RNA per treatment. The vehicle group was treated with saline. Tumour growth was monitored every fourth day up to 20 days.

The tumour growth analysis revealed that mice treated with circGFP RNA showed slower tumour growth compared to the vehicle and circZNF800 RNA group (Figure 4.26A, Appendix C). In contrast, circZNF800-injected treated mice showed significantly enhanced tumour growth compared to the vehicle- and circGFP RNA-treated groups. Furthermore, tumour volume analysis showed that the circZNF800 treated group developed larger tumours compared to other groups (Figure 4.26B). The tumourigenicity *in vivo* data echoed the observation from the *in vitro* proliferation assays in which circZNF800 was shown to promote cellular proliferation. Taken together, the results indicate that circZNF800 promotes cellular proliferation, up-regulates expression of CSC and intestinal stem cell markers and up-regulates pluripotency-associated transcriptional factors, which are all linked to enhanced tumourigenicity.

Subcutaneous transplantation for *in vivo* RNA treatment

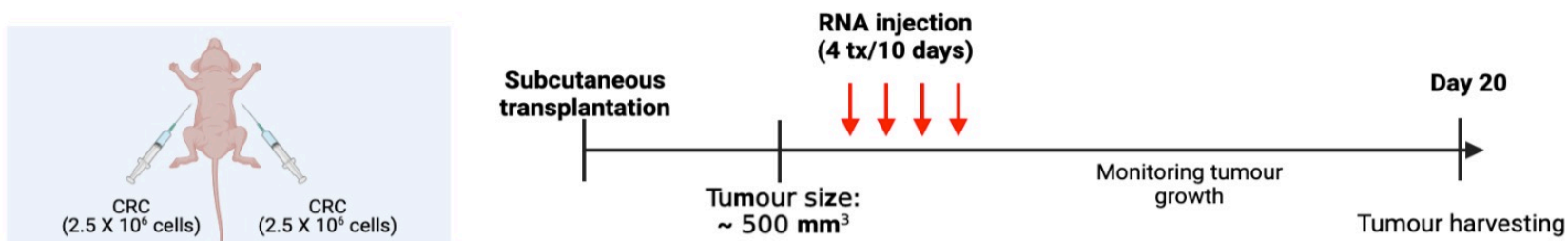


Figure 4.25 Schematic illustration of the mouse model used to study the effects of circZNF800 overexpression on tumorigenicity.

WiDr cells were first transplanted subcutaneously into nude mice. The mice were divided into three groups: the vehicle group and the two groups injected either with circZNF800 RNA or circGFP RNA (see right panel) ($n=3$ for each group). When the tumours reached $\sim 500 \text{ mm}^3$, each group was injected four times with $10 \mu\text{g}$ of RNA in the treatment groups, or saline as in the vehicle group. Tumours were allowed to grow up to 0 days before the tumours were harvested for further analysis.

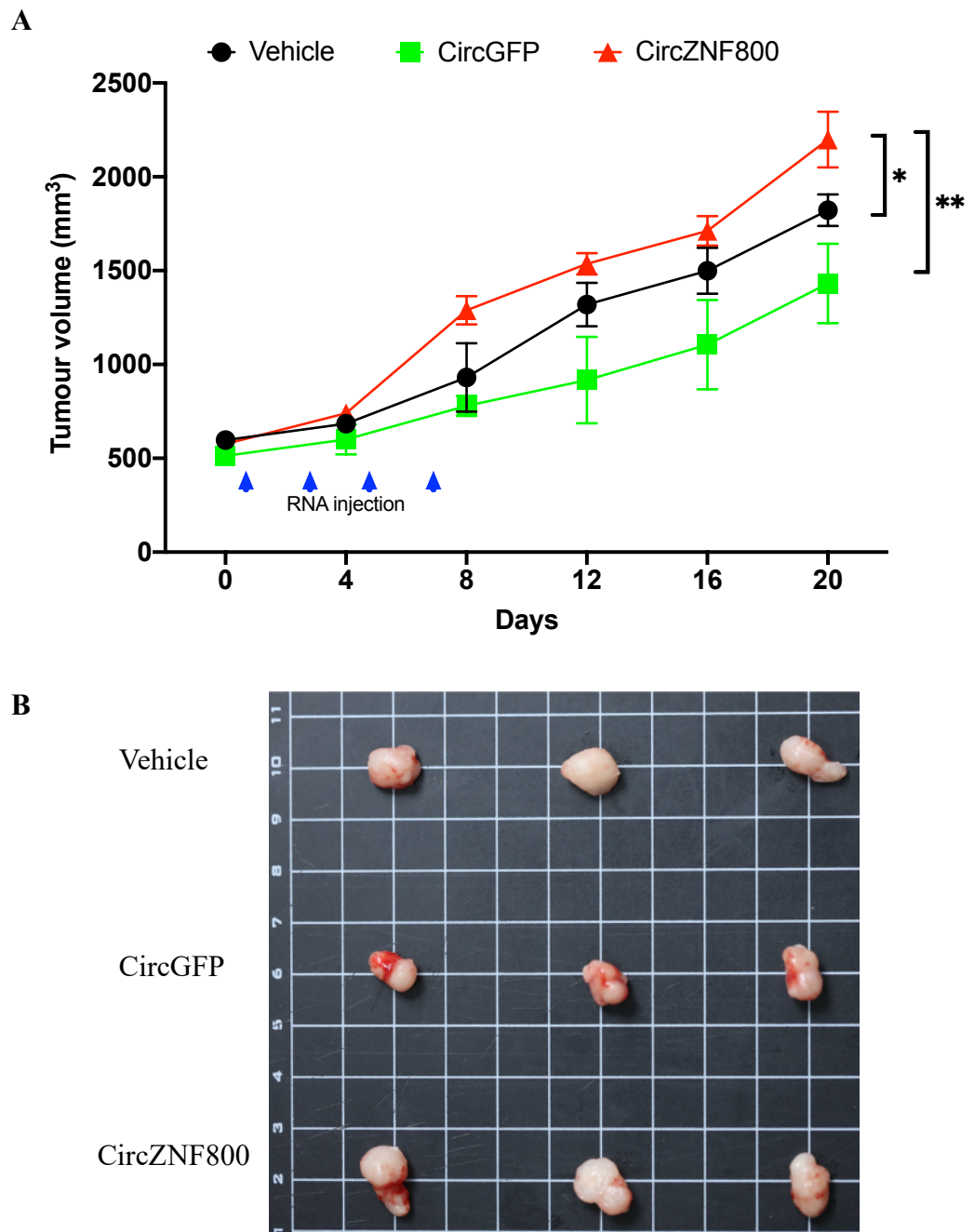


Figure 4.26 Effects of circZNF800 overexpression on tumorigenicity in mice.

(A) Average tumour growth in mice of different treatment groups of subcutaneously WiDr cells as shown in Fig. 4.26. * $p < 0.05$ and ** $p < 0.01$ were values relative to the vehicle-treated group ($n=3$ for each group). (B) Images of the harvested subcutaneous CRC tumours on day 20 of different treatment groups.

Part 3B: Functional molecular modulations of circZNF800 overexpression

4.12 CircZNF800 down-regulated the expression of targeted miRNAs to positively regulate downstream genes of the predicted pluripotency pathways

The bioinformatics analysis predicted a regulatory network of circRNA-miRNA-mRNA axis that controls pluripotency-associated pathways (Figure 4.9). Hsa_circ_0066631 and circZNF800 were predicted to sponge hsa-miR-140-3p, -miR-224, -miR-382, -miR-548c-3p and -miR-579. Based on our prediction, circZNF800 only interacts with miR-140-3p, miR-382 and miR-579 (Table 4.5). Bioinformatics analysis of pairing using the RNAhybrid prediction tool supports that circZNF800 competitively binds the miRNAs (Table 4.6).

4.12.1 CircZNF800 sponges the predicted tumour suppressive miRNAs hsa-miR-140-3p, -miR-382 and -miR-579

To validate the predicted sponging activities of circZNF800 on miR-140-3p, miR-382 and miR-579, RNA pulldown assay was performed. Biotinylated-circZNF800 RNA and a scramble RNA were generated using *in vitro* transcription assay (see Section 3.7.2). were incubated with cell lysates of HCT-15 and WiDr cells and the purified pulled-down miRNAs were identified using stem loop qRT-PCR analysis.

Table 4.5. Interactions of the circZNF800 with the predicted core miRNAs

miRNA	CircZNF800	Hsa_circ_0066631
hsa-miR-140-3p	+	+
hsa-miR-224	-	+
hsa-miR-382	+	-
hsa-miR-548c-3p	-	+
hsa-miR-579	+	+

“+”, predicted binding; “-“, no predicted binding.

The results indicated that circZNF800 RNA pulldown was enriched miR-140-3p, miR-382 and miR-579 in both HCT-15 and WiDr cells compared to the scramble RNA, with hsa-miR-140-3p the most enriched (Figure 4.27). Stem loop qRT-PCR analysis further showed that on ectopic circZNF800 overexpression, miR-140-3p, miR-382 and miR-579 were significantly down-regulated (Figure 4.28). Taken together, circZNF800 is able to sponge and down-regulate these miRNAs.

4.12.2 CircZNF800 up-regulated pluripotency-associated target transcripts of the miRNAs

The effects of circZNF800 on the expression of the downstream transcripts of the predicted pluripotency pathways (Figure 4.9) were next investigated. *ALKF7*, *FZD3*, *IL6ST*, *SKIL*, *SMAD2* and *WNT5A* were predicted to be regulated by circZNF800 and hsa_circ_0066631 via the predicted miRNAs. Ectopic circZNF800 overexpression significant up-regulated the *ALKF7*, *FZD3* and *WNT5A* transcript levels of the predicted pluripotency-associated pathways (Figure 4.29). However, *IL6ST* and *SMAD2* were slightly up-regulation, albeit not significantly. *SKIL* showed no differential expression between the vehicle and circZNF800 overexpression group.

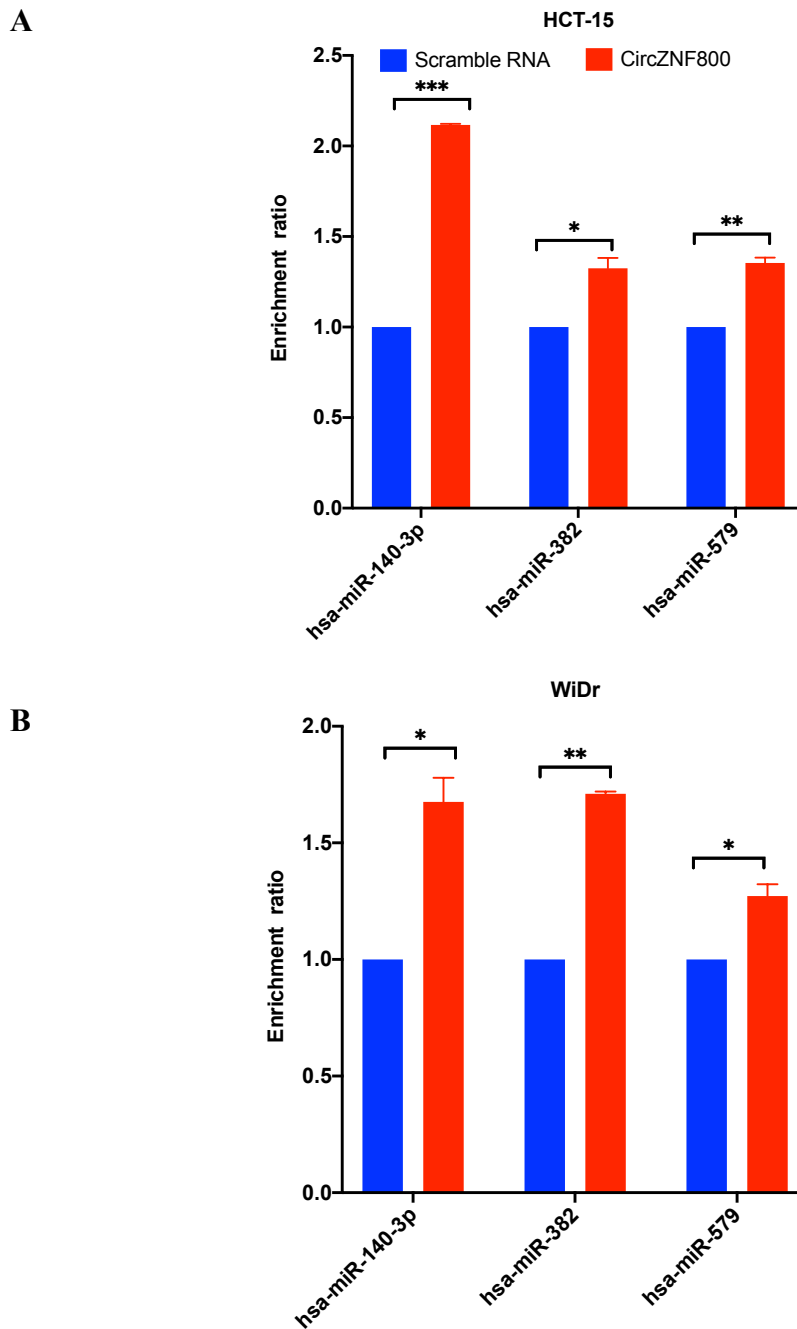


Figure 4.27 CircZNF800 RNA pulldown analysis of predicted miRNAs.

Biotinylated circZNF800 RNA was used in pulldown assay to identify the predicted interacting miRNAs in (A) HCT-15 and (B) WiDr cell lines. Stem loop qRT-PCR analysis was performed on the target miRNAs. The enrichment ratios of the miRNAs were identified based on the relative expression levels of the scramble RNA and circZNF800 RNA pulldown. * $p < 0.05$ and ** $p < 0.01$ were obtained by comparing to the scramble group.

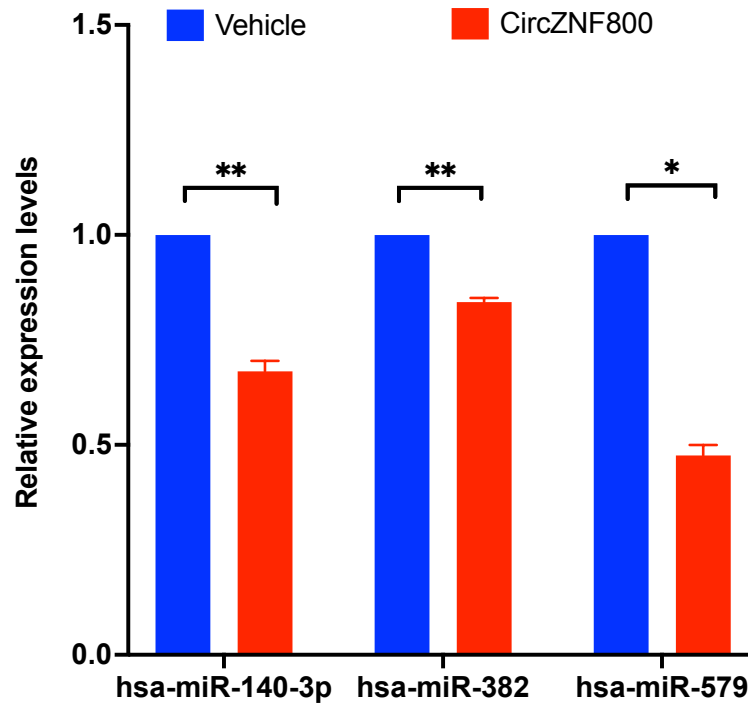


Figure 4.28 Effects of circZNF800 overexpression on the expression levels of the predicted miRNAs. Stem loop qRT-PCR analysis of hsa-miR-140-3p, miR-382 and miR-579 on circZNF800 RNA transfection of WiDr cells for 48 hrs. * $p < 0.05$ and ** $p < 0.01$ were obtained by comparing to the vehicle group.

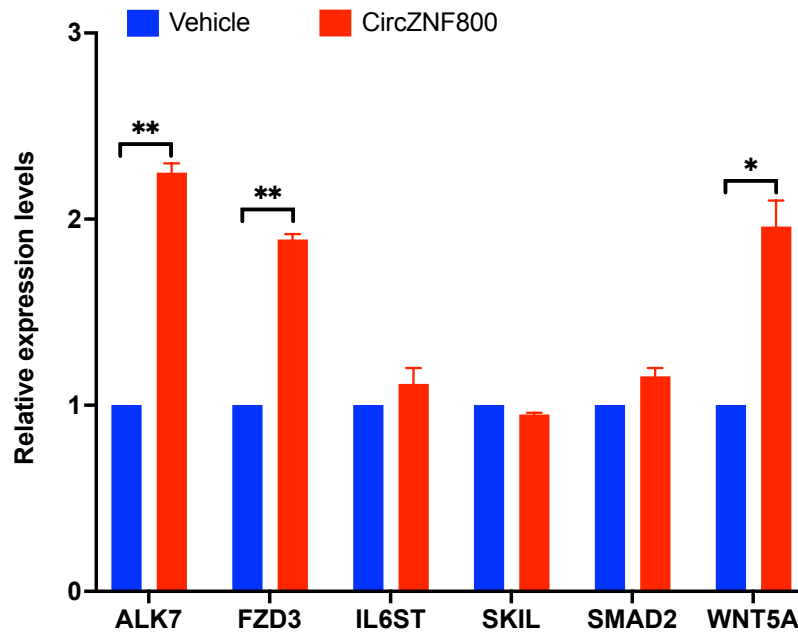


Figure 4.29 Expression analysis of predicted pluripotency-associated pathways upon circZNF800 RNA overexpression. The expression levels of *ALK7*, *FZD3*, *IL6ST*, *SKIL*, *SMAD2* and *WNT5A* were analysed using qRT-PCR. The expression levels are relative to the vehicle treated group. * $p < 0.05$ and ** $p < 0.01$ were obtained by comparing to the vehicle group.

In summary, the results demonstrate that circZNF800 sponges tumour suppressive miRNAs hsa-miR-140-3p, miR-382 and miR-579, which in turn, up-regulates the expression of downstream transcripts, *ALKF7*, *FZD3* and *WNT5A* previously reported to be involved in various pluripotency-associated pathways (see Table 4.3). CircZNF800 acts as a potent stemness regulator in CRC cells.

Part 3C: Phenotypic and genotypic modulations of circZNF800 knockdown in relation to stemness regulation

4.13 CircZNF800 knockdown via CRISPR Cas13d suppressed CSC-like properties

RNA interference (RNAi) tools, including siRNA and shRNA, are often used to induce knockdown of circRNAs (Mumtaz *et al.*, 2020). The RNAi tools are designed based on the backsplice junction of a candidate circRNA to induce knockdown without affecting the expression levels of the host transcript. However, RNAi is known to have high off-target effects (He *et al.*, 2021). The recent development of CRISPR (Clustered Regularly Interspaced Short Palindromic Repeats) systems as RNA editing tools has gained growing attention. Citing enhanced targeting specificity and low off-target effects, CRISPR Cas13d is a potent tool to induce circRNA knockdown, both *in vitro* and *in vivo* (Gupta *et al.*, 2022).

4.13.1 Construction and validation of CRISPR Cas13d-mediated knockdown of circZNF800

In the present study, the CRISPR Cas13d system was established to induce knockdown in circZNF800. Based on the backsplice junction of circZNF800, two crRNA sequences (crRNAs) were generated. The sequences were designed to be in reverse complementary matches, each with 24 nucleotides in length (Figure 4.30A). By the binding activities of these crRNAs on circZNF800, the CRISPR Cas13d endonuclease would induce degradation of circZNF800.

The efficiency of the circZNF800 knockdown using the CRISPR Cas13d was evaluated using qRT-PCR assay (Figure 4.30B). The CRISPR Cas13d plasmid cloned with either a scramble or a specific crRNA sequence was transfected into WiDr cells. qRT-PCR analysis was performed 48 hours post-transfection. Both crRNA 1 and 2 were able to induce significant knockdown of circZNF800, with little to no effect on the host transcript, *ZNF800*. A specific knockdown of circZNF800 was achieved, with up to 40% knockdown efficiency. The successful generation of a specific knockdown model for circZNF800 using CRISPR Cas13d was used for the downstream analysis.

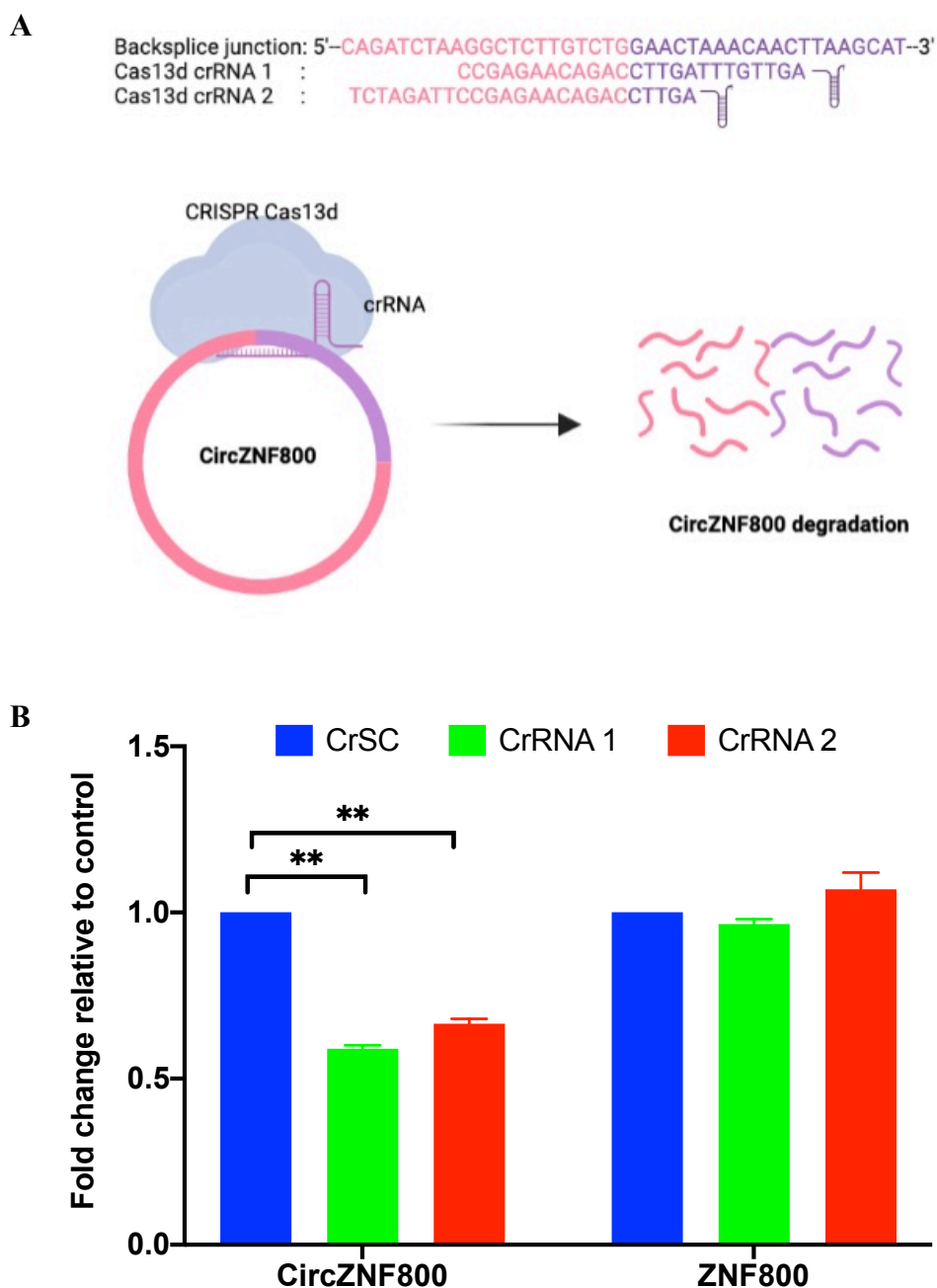


Figure 4.30 Establishment and validation of circZNF800 knockdown system.

(A) Schematic illustration of the CRISPR Cas13d RNA system to target circZNF800. The backsplice junction and complementary crRNA sequences that target circZNF800 are illustrated. (B) Knockdown efficiency of circZNF800 using CRISPR Cas13d system via qRT-PCR analysis. Relative expression analysis of circZNF800 and host transcript, *ZNF800* to CrSC group. ** $p < 0.01$ was obtained by comparing to the scramble group.

4.13.2 Knockdown of circZNF800 diminished stemness properties in CRC cells

The reversal of the enrichment of stemness observed on circZNF800 overexpression was investigated using the established CRISPR Cas13d system. Proliferation assay, CSC and intestinal stem cell markers analysis, sphere- and colony-forming assays, and *in vivo* tumourigenicity assay was performed using the circZNF800 knockdown cells.

The EdU proliferation assay revealed circZNF800 knockdown cells showed a significant reduction in cellular proliferation (Figure 3.31). Compared to CrSC transfected cells, there was a reduction of up to 9% of EdU⁺ cells upon circZNF800 knockdown. The lower proliferation rate is in line with the data obtained upon circZNF800 overexpression (Figure 4.21). Flowcytometry analysis of CSC markers, CD44 and CD133, and intestinal stem cell markers, Lgr5 and Sox9 were also significantly down-regulated upon circZNF800 knockdown. The expression levels of CD44 and CD133 were reduced by up to 50% on circZNF800 knockdown (Figures 4.32). Similarly, Lgr5 and Sox9 expression levels were also reduced in circZNF800 down-regulated cells (Figure 4.33). The results suggest that the circZNF800 knockdown induced a reduction in CSC-related properties. Pluripotency factors *OCT4*, *SOX2* and *NANOG* were likewise significantly down-regulated in circZNF800 crRNAs-transfected cells compared to CrSC cells (Figure 4.34), confirming the involvement of circZNF800 in regulating stemness properties in CRC cells.

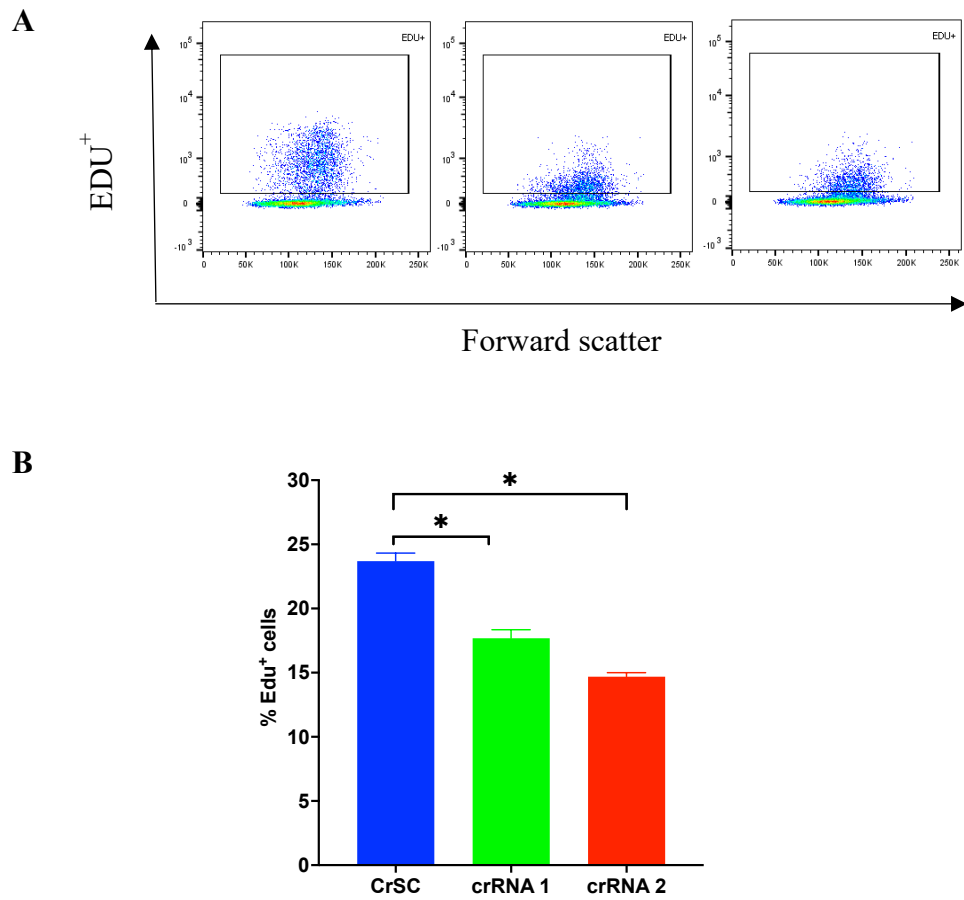


Figure 4.31 Effects on CRC cell proliferation upon circZNF800 knockdown.

(A) Flowcytometry analysis of EdU-positive population on WiDr cells upon circZNF800 knockdown. Representative flowcytometry contour plots are shown in left panels for each treatment group. (B) Bar graph (right panel) represents the average data from triplicated independent experiments. * $p < 0.05$ was obtained by comparing the CrSC with crRNA 1 or crRNA 2 transfected cells.

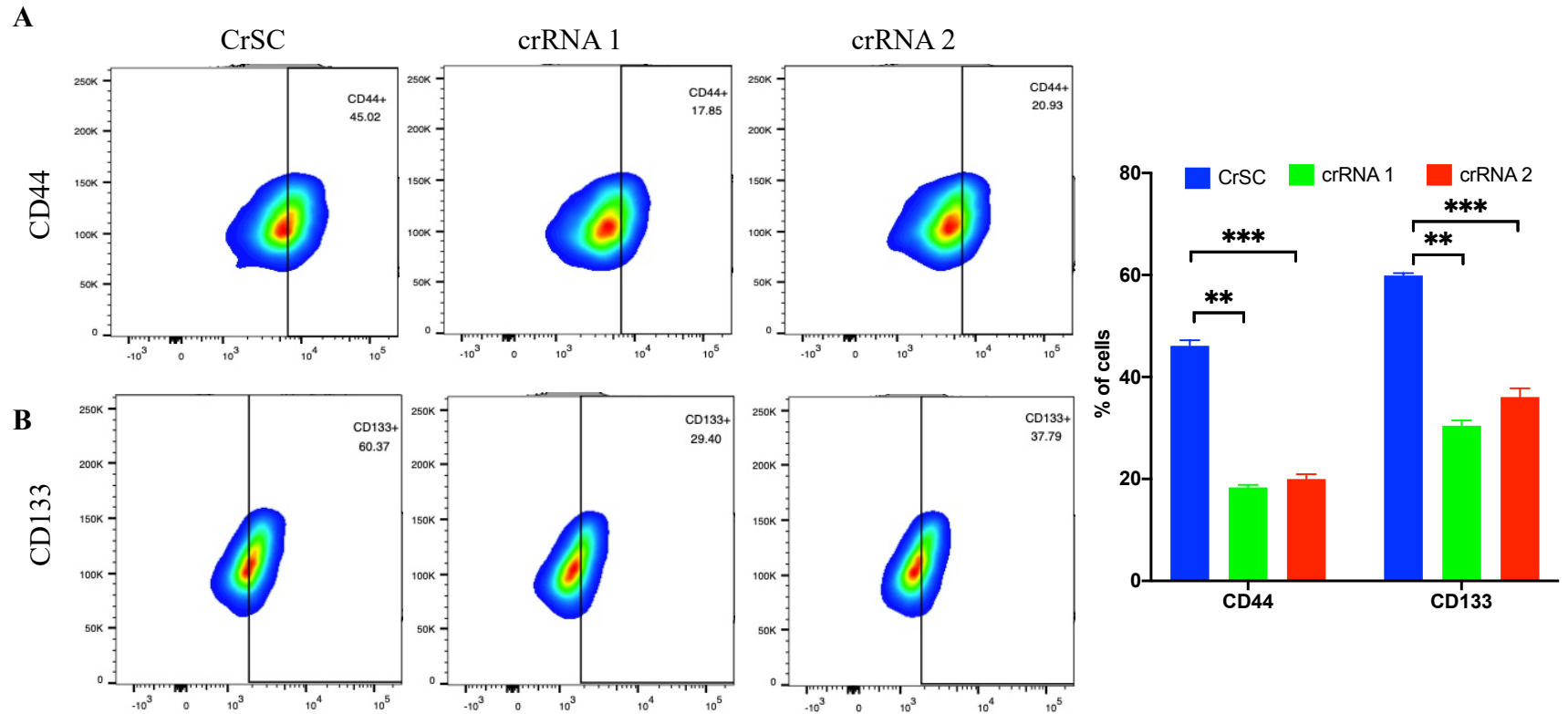


Figure 4.32 Effects on CSC markers expression levels upon circZNF800 knockdown. (A) Representative contour plots of flowcytometry analysis of CD44 and CD133 upon circZNF800 knockdown in WiDr cells. (B) Bar graph (right panel) represents the average data from triplicated independent experiments. ** $p < 0.01$ and *** $p < 0.001$ were obtained by comparing to the CrSC transfected cells.

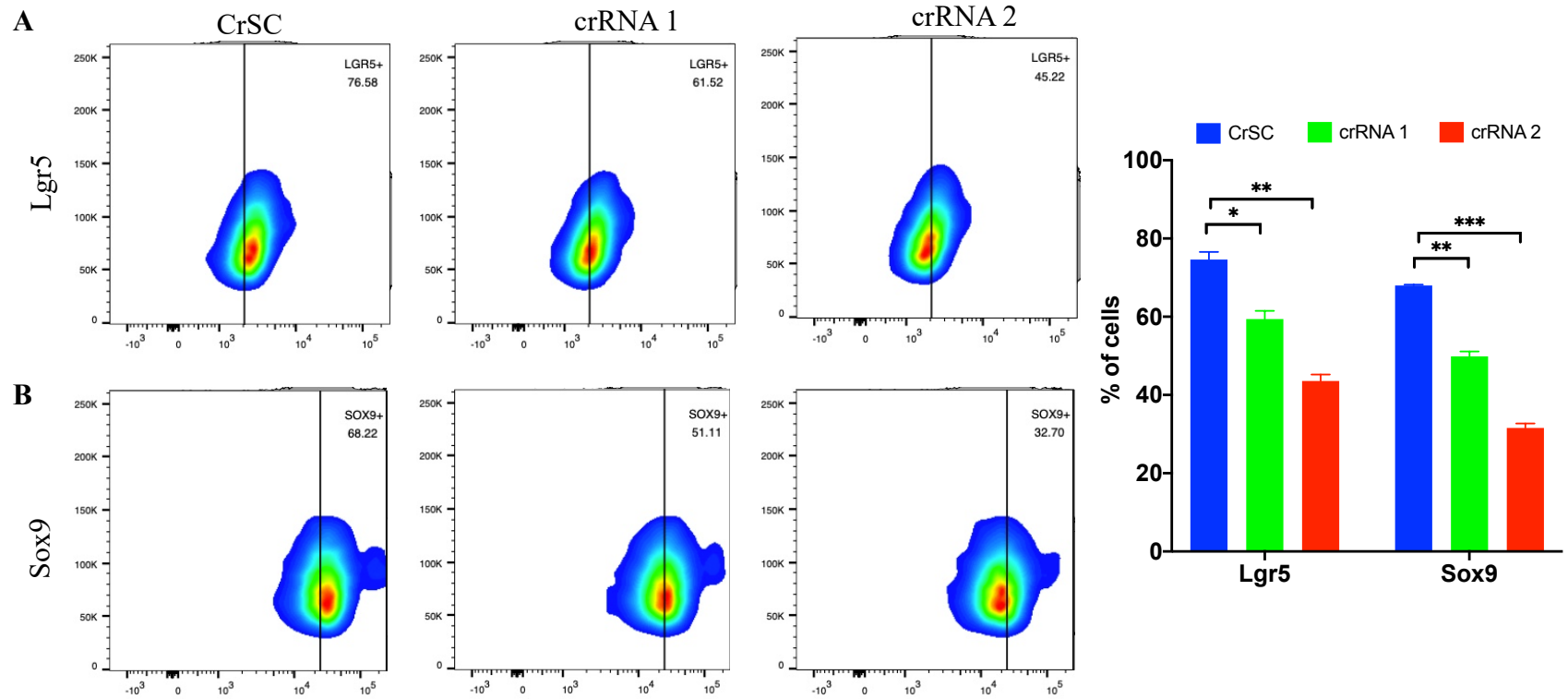


Figure 4.33 Effects on intestinal stem cells markers expression levels upon circZNF800 knockdown. (A) Representative contour plots of flowcytometry analysis of Lgr5 and Sox9 upon circZNF800 knockdown in WiDr cells. (B) Bar graph (right panel) represents the average data from triplicated independent experiments. * $p < 0.05$, ** $p < 0.01$ and *** $p < 0.001$ were obtained by comparing to the CrSC transfected cells.

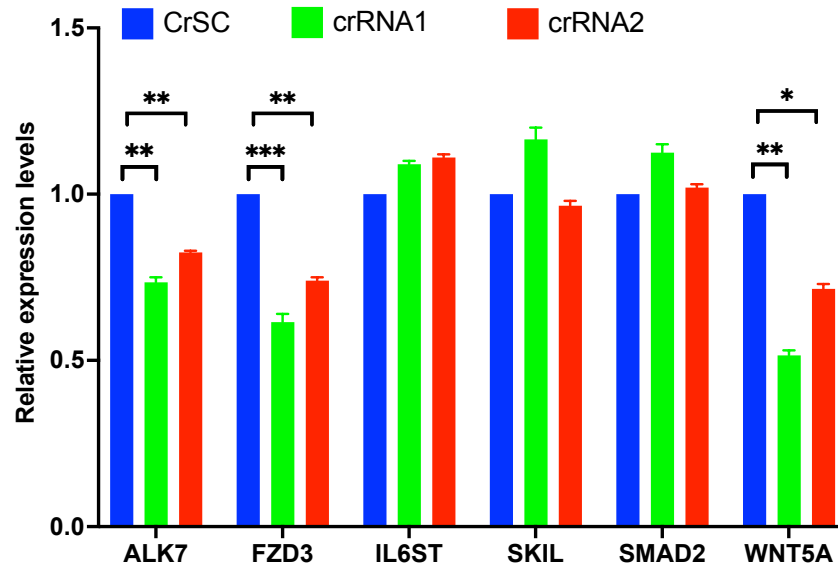


Figure 4.34 Evaluation of core pluripotency markers upon circZNF800 knockdown. qRT-PCR analysis of selected pluripotency genes upon circZNF800 knockdown. * $p < 0.05$, ** $p < 0.01$ and *** $p < 0.001$ were values relative to the CrSC transfected cells.

To investigate the effects of the circZNF800 knockdown on sphere- and colony-forming abilities, stable circZNF800-knockdown cells were seeded for the sphere- and colony-forming culture conditions for 10 days. The results indicated that, compared to the control group (CrSC), circZNF800-knockdown cells (crRNA 1 and crRNA 2) showed a reduction in the ability to form spheroids (Figure 4.35), and the colony-forming abilities were also impaired in CRC cells (Figure 4.36). The data further illustrated that circZNF800 knockdown impairs the CSC features of spheroid and colony formation in CRC cells.

4.13.3 Impaired tumour-forming abilities in a mice model transplanted with circZNF800 knockdown cells

The effects of circZNF800 knockdown on *in vivo* tumorigenicity were further evaluated. CircZNF800 knockdown WiDr cells were subcutaneously transplanted into nude mice at 2.5×10^6 cells/flank (Figure 4.37, Appendix D). Three flanks were used for each of the CrSC, crRNA 1 and crRNA 2 groups. The transplanted cells were left to form xenograft tumours up to 30 days and the tumour size was measured at least twice per week before the animals were sacrificed for further analysis (Figure 4.37). Mice injected with the control CrSC cells showed the fastest tumour growth rate than the mice injected with the crRNA 1- and crRNA 2-expressing cells (Figure 4.38A). CrSC cells yield the largest tumour size relative to crRNA 1 and crRNA 2 cells (Figure 4.38B). The impairment of tumour growth on circZNF800 knockdown is in line with the data that circZNF800 reduces CSC properties.

Sphere-forming abilities

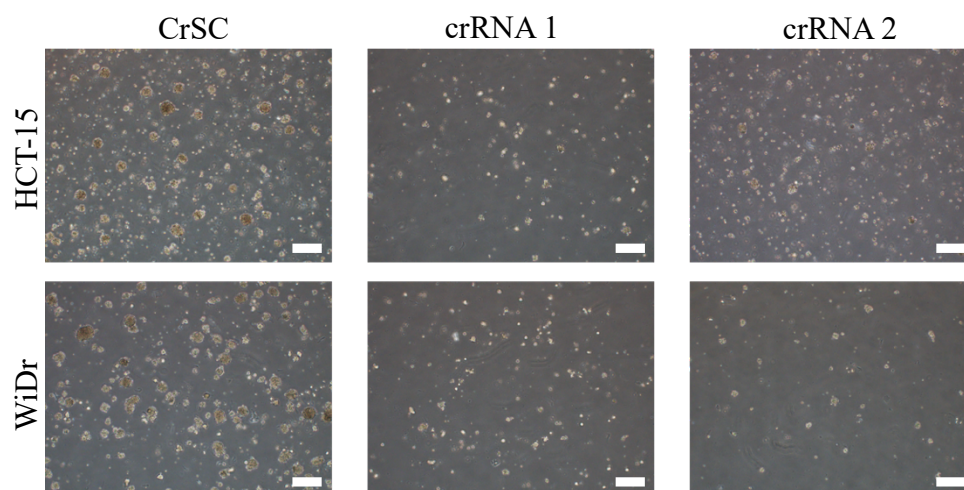


Figure 4.35 Evaluation of sphere-forming abilities on circZNF800 knockdown cells. Morphological images of the spheroids forming in the suspension culture upon circZNF800 knockdown. Images were taken after 10 days in the spheroid culture condition. Bar represents 100 μm .

Colony-forming abilities

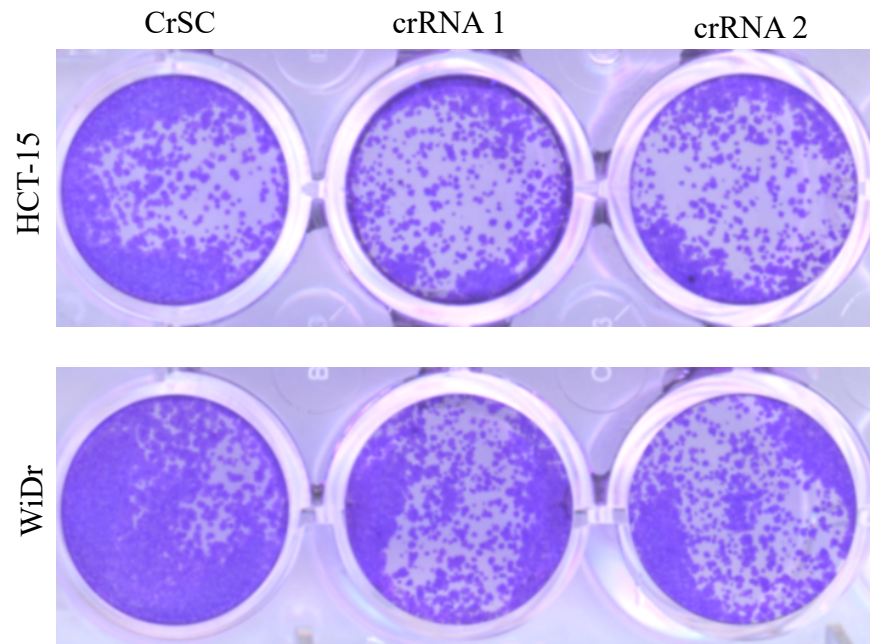


Figure 4.36 Effects of circZNF800 knockdown on colony-forming abilities. Stable circZNF800 knockdown cells were seeded in 6 well plate for colony-forming assay. Images show the colonies stained with crystal violet.

Subcutaneous transplantation of stable circZNF800 knockdown CRC cells

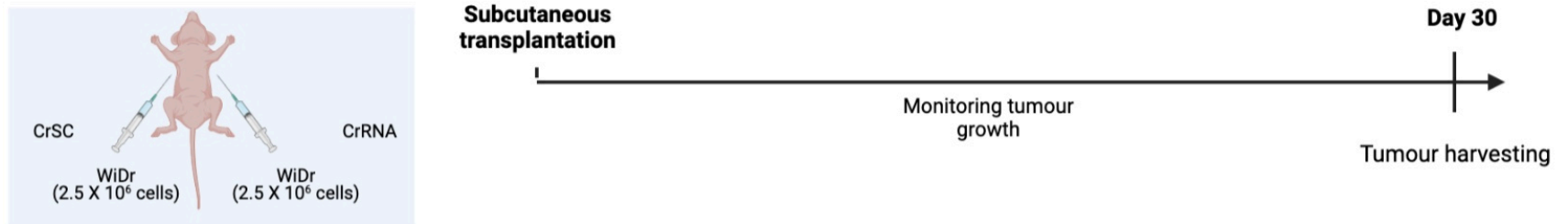


Figure 4.37 Schematic illustration of mouse model used to study the effects of circZNF800 knockdown on tumorigenicity. Stably circZNF800-knockdown cells were transplanted subcutaneously into nude mice. The tumour growth was monitored for 30 days (n=3 per group). In the left panel, CrSC represents the control group while crRNA may be crRNA 1 or crRNA 2 circZNF800 knockdown cells (see Fig. 4.30A for construction).

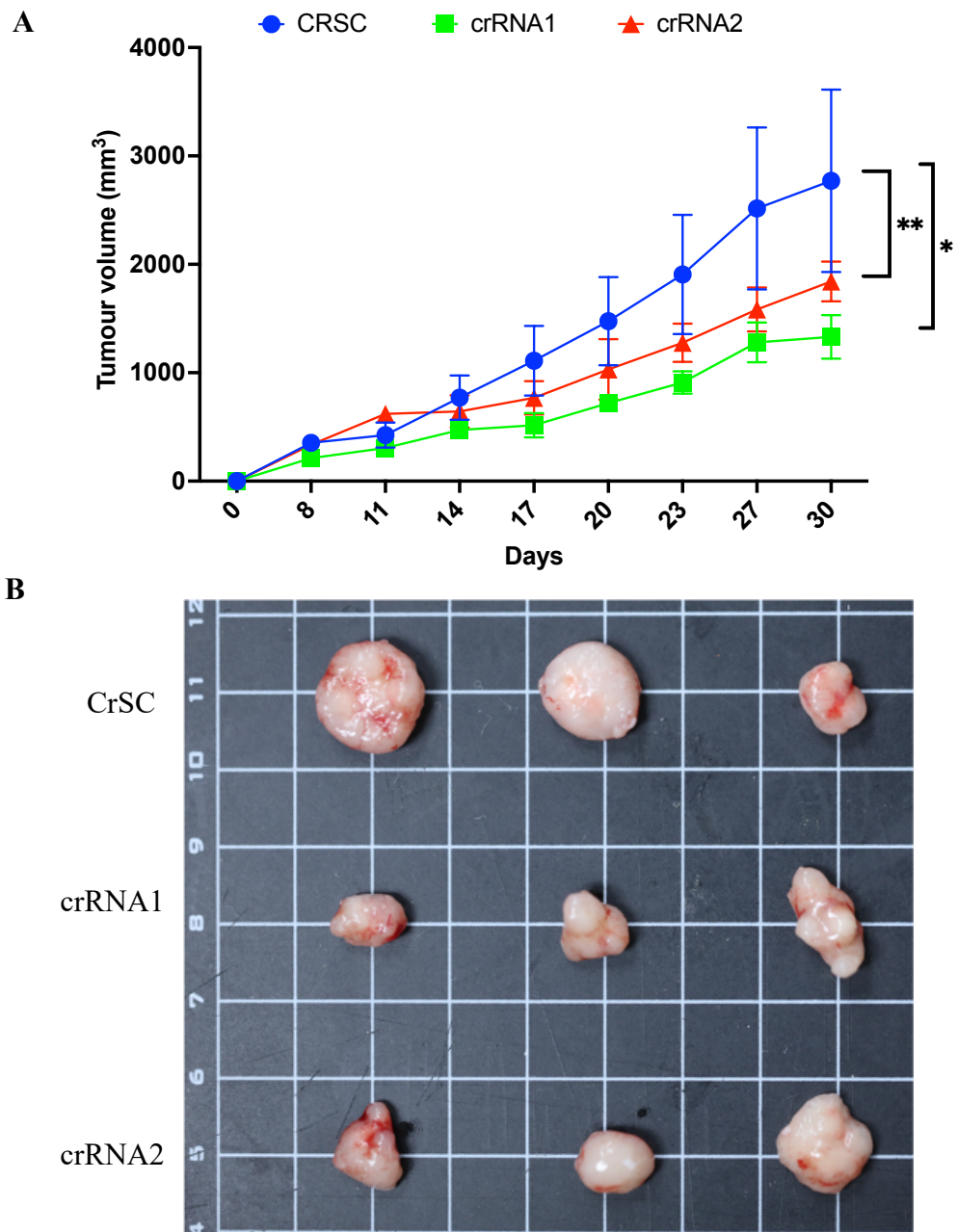


Figure 4.38 Effects on tumorigenicity on circZNF800 knockdown in mice. (A) Average tumour growth of different treatment groups of subcutaneously WiDr cells. * $p < 0.05$ and ** $p < 0.01$ were values relative to the control group ($n=3$ for each group). (B) Images of the harvested subcutaneous CRC tumours on day 30 of different treatment groups.

Part 3D: Functional molecular modulations of circZNF800 knockdown

4.14 Knockdown of circZNF800 up-regulated expression levels of tumour suppressive miRNAs and down-regulated transcripts of pluripotency-associated pathways

In circRNA profiling analysis (Figure 4.9) miR-140-3p, miR-382 and miR-579 were predicted to be sponged by circZNF800. To establish the molecular modulation of circZNF800, on the expression of the predicted miRNAs, stem loop qRT-PCR analysis was performed. The results indicated that circZNF800 knockdown significant up-regulated the expression levels of miR-140-3p, miR-382 and miR-579 compared to the control (Figure 4.39), collaborating with circZNF800 sponging of the miRNAs.

Expression of the downstream transcripts *ALK7*, *FZD3* and *WNT5A* was also predicted to be modulated by circZNF800 via miR-140-3p, miR-382 and miR-579 (Figure 4.9). Upon knockdown of circZNF800, the expression levels of *ALK7*, *FZD3* and *WNT5A* were significantly lower compared to the control group qRT-PCR analysis (Figure 4.40). Since these transcripts encode important factors in pluripotency-associated pathways (Figure 4.9), the data corroborate with the proposition that circZNF800 negatively modulates CSC phenotypes.

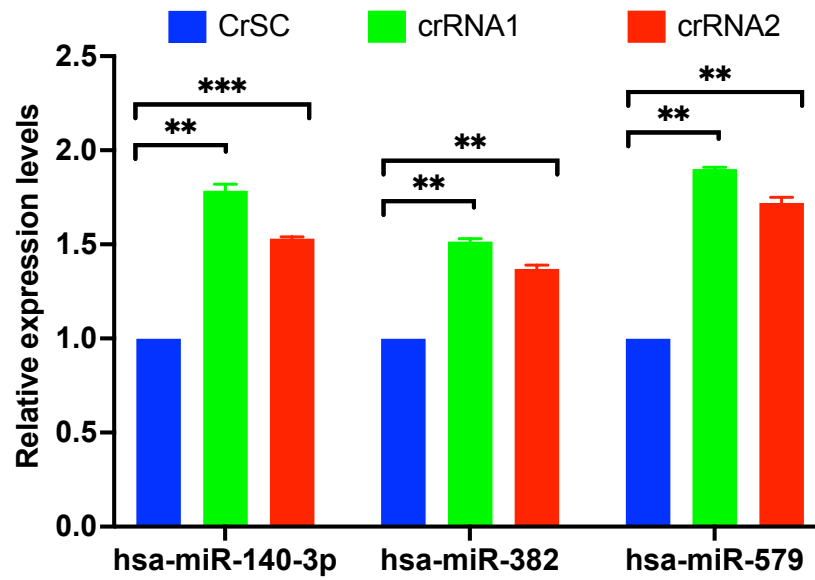


Figure 4.39 Validation of the expression levels of miRNAs upon circZNF800 knockdown. Stem loop qRT-PCR analysis of hsa-miR-140-3p, miR-382 and miR-579 on circZNF800 knockdown WiDr cells. $**p < 0.01$ and $***p < 0.001$ were obtained by comparing to the control group.

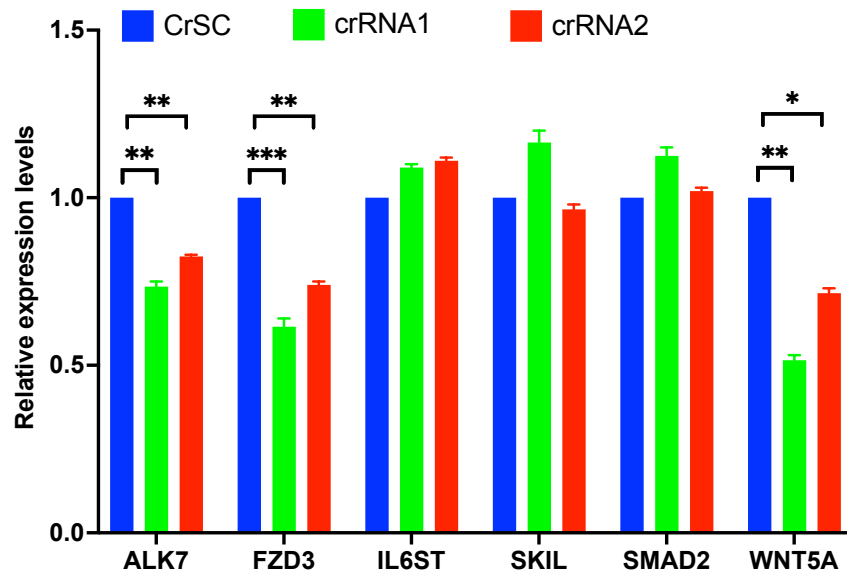


Figure 4.40 Expression analysis of predicted pluripotency-associated pathways upon circZNF800 knockdown. The expression levels of *ALK7*, *FZD3*, *IL6ST*, *SKIL*, *SMAD2* and *WNT5A* were analysed using qRT-PCR. The expression levels are relative to the control group. * $p < 0.05$, ** $p < 0.01$ and *** $p < 0.001$ were obtained by comparing to the vehicle group.

CHAPTER 5

DISCUSSION

5.1 Use of spheroidal culture in the study of cancer stem cells

The rarity of colorectal cancer stem cell (CrCSC) population in the tumour mass warrants the development of novel approaches to enrich and cultivate the CrCSC population. The use of 3D spheroidal culture as a CSC enrichment model has been well accepted as a simple and potent *in vitro* tool (as reviewed by (Ishiguro *et al.*, 2017). In our previous investigation, CrCSC-like population was enriched in CRC cell lines using spheroidal culture, and the CSC properties validated (Rengganaten, 2016).

In the previous work (Rengganaten, 2016), enrichment of CrCSC population was achieved by subjecting the CRC cells to serial passaging in spheroidal culture. CSC properties including chemoresistance and pluripotency genes were enhanced on a passage-dependent manner in the CRC spheroidal cells. Other CSC properties were also shown, including enhanced self-renewal abilities and up-regulation of CSC markers, CD133, CD44 and ALDH1 in the CRC spheroidal cells compared to the parental cells (Rengganaten, 2016). Serum-induced differentiation of the CRC spheroidal cells reversed the enrichment of CSC properties, suggesting that spheroidal culture could effectively enrich and maintain the CSC properties in CRC cells. The collective data confirmed that CRC cells with

CSC properties were enriched in the spheroidal culture, echoing other reports (Barisam *et al.*, 2022; Ishiguro *et al.*, 2017). The established CRC-derived spheroidal cultures were used in this work to characterise circRNA involvement in the regulation of stem cell properties.

5.2 Integrative analysis of circRNA unveiled a complex post-transcriptional gene regulation network in cancer stem cells

Cancer recurrence mediated by cancer stem cell (CSC) population poses a major clinical drawback (Chen *et al.*, 2020a). The up-regulation of stemness properties in CSC population that give rise to enhanced differentiation and proliferation abilities have been a major therapeutic target (Prasad *et al.*, 2020). However, the underlying mechanisms mediating the potency maintenance in colorectal CSC (CrCSC) population remains poorly understood (Zhao *et al.*, 2018).

To date, there is a lack of circRNA profiling work on understanding the distribution of circRNAs in CrCSC population. However, circRNA profiling works have been performed on stem cell populations of other cancers, including breast (Yan *et al.*, 2017) and hepatocellular cancer (Chen *et al.*, 2020b). In both studies, CSC population enrichment was achieved using 3D spheroidal culture, as in the present study.

In the present work, RNA sequencing and extensive bioinformatics analysis were performed, which led to the identification of over 8,000 differentially expressed circRNAs in CRC spheroidal cells (Figure 4.1), suggesting that circRNAs play an extensive role in a large number biological processes involving oncogenicity and stemness regulation in CrCSC cells. Furthermore, based on the top 4 up- and down-regulated circRNAs identified, a complex network of circRNA-miRNA-mRNA interaction was elucidated (Figure 4.4).

KEGG analysis of downstream transcripts suggested that various signalling pathways were regulated by the differentially expressed circRNAs. Among these, the Wnt and ErbB signalling pathways, which were implicated in the KEGG analysis, have previously been associated with regulating CSC properties (de Sousa and Vermeulen, 2016; Clark *et al.*, 2012). Wnt signalling pathways have been reported to control epithelial-mesenchymal transition (EMT), cellular proliferation and to mediate various transcriptional factors involved in enhancing stemness properties in cancer cells (Chang *et al.*, 2015; Malladi *et al.*, 2016). Likewise, ErbB signalling pathways regulate cellular differentiation, proliferation and migratory properties in cancer cells, which are often enhanced in CSC population (Arteaga, 2011; Appert-Collin *et al.*, 2015). The bioinformatics prediction of the present work highlights the addition of another tier of post-transcriptional regulators to the existing understanding of the regulation of CSC properties in CRC cells.

Other studies have proposed circRNA-miRNA-mRNA networks in different cancer populations. Dong et al. illustrated six circRNAs that were predicted to sponge 15 miRNAs and were involved in regulating tumour-associated signalling pathways in gastric cancer (Dong *et al.*, 2021). A similar network of circRNA-miRNA-mRNA was constructed involving macrophage infiltration in hepatocellular carcinoma (Zhou *et al.*, 2020). However, both these studies focused only on bioinformatics analysis to predict the network with little or no functional assays to validate the predicted network. The present study experimentally validated all interacting members of the selected network and performed extensive downstream functional assays to confirm the prediction.

5.3 CircRNA-mediated regulation is involved in activities of the pluripotency pathways

The KEGG analysis accentuated important signalling pathways mediating pluripotency. The bioinformatics analysis revealed two potential candidate circRNAs, hsa_circ_0066631 and circ_0082096 (later denoted as circZNF800) to be major regulators of signalling pathways of pluripotency (Figure 4.6). Very little is known about the two circRNAs, except for a few reports briefly mentioning possible involvements in viral infection and atrial fibrillation in a whole transcriptomics study (Zhang, Sun and Li, 2020).

Hsa_circ_0066631 is derived from exons 2 and 3 of the host transcript, DCBLD2 (CUB and LCCL domain containing 2; NM_080927), which harbours 16 exons. There are no literature reports on the functional role of hsa_circ_0066631. Based on the host transcript literature analysis, the DCBLD2 protein acts as major regulator of tumorigenesis (Schmoker, Ebert and Ballif, 2019). In terms of CRC development, DCBLD2 is up-regulated in CRC patients, and is linked with poor prognosis (He *et al.*, 2020b). The up-regulated expression of DCBLD2 in CRC patients is in agreement with up-regulated levels of the derived hsa_circ_0066631 in the CrCSC population reported in the present work.

On the other hand, circ_0082096 (circZNF800) is derived from exons 4 and 5 of the host transcript zinc-finger protein 800 (ZFN800); NM_176814. The ZNF800 protein has only been reported as a candidate master regulator in adipose gene expression and cardio-metabolic traits (Civelek *et al.*, 2017). ZNF800 involvement in cancers and oncogenicity has yet to be demonstrated. In the present work, the addition of circ_0066631 and circZNF800 to the short list of circRNAs involved in regulating cancer stemness highlights the relevance of circRNAs in understanding the pathological features of cancer stem cells (Zhang *et al.*, 2021a).

In the identified signalling pathways of pluripotency, hsa_circ_0066631 and circZNF800 were predicted to sponge five miRNAs, hsa-miR-140-3p, miR-224, miR-382, miR-548c-3p and miR-579 (Figure 4.6). Literature analysis revealed that all the predicted miRNAs are tumour suppressors and inhibit various CSC-related properties, including cancer progression, chemoresistance and migration (Li *et al.*, 2018a; Wang *et al.*, 2019; Kalthori *et al.*, 2019; Yao *et al.*, 2019). Correlating with

literature reports, expression of these miRNAs was down-regulated in CRC spheroidal cells and up-regulated upon serum-induced differentiation, indicating involvement in stemness. Up-regulation of hsa_circ_0066631 and circZNF800 in CRC spheroidal cells supports the predicted sponging of the five miRNAs.

The KEGG analysis also identified six core mRNAs, *ACVR1C*, *FZD3*, *IL6ST*, *SKIL*, *SMAD2* and *WNT5A*, that were collectively targeted by the circRNA–miRNA axis in the regulation of pluripotency. The suppression of the five miRNAs by the sponging activities of two circRNAs was predicted to promote the translation of the downstream transcripts of the pluripotency signalling pathways (Figure 4.8), reinforcing the bioinformatics prediction of the circRNAs being the major class of regulators of CSC properties in CRC cells.

The six mRNA transcripts have been associated with the regulation of diverse CSC-related properties, ranging from cellular proliferation, migration, chemoresistance to tumour growth (Tsuneyoshi *et al.*, 2012; Kaufman-Francis *et al.*, 2014; Dahle and Kuehn, 2016; Bertero *et al.*, 2018; Bourillot *et al.*, 2020). As described in Table 4.3, these transcripts are involved in the modulation of major signalling pathways that regulate numerous CSC-associated properties observed in the enriched CSC population of CRC spheroidal cells. Interestingly, some of the mRNA transcripts have been reported to have dual promoter and repressor functions in cancer. *ACVR1C/ALK7* has been reported as a tumour suppressor in breast cancer but promotes cancer growth in prolactinoma and retinoblastoma (Asnaghi *et al.*, 2019; Hu *et al.*, 2017; Principe *et al.*, 2018b). The GP130/Stat, Activin/Nodal,

TGF- β /Smad and Wnt/ β -catenin signalling pathways have been shown to increase CSC-like features in cancer population (full reference available in Table 4.3).

5.4 CircZNF800 mediates CSC-like properties in CRC cells

Hsa_circ_0066631 and circZNF800 were identified as potential regulators of stemness in CRC. Hsa_circ_0066631 showed higher expression levels in CRC spheroidal cells; however, the expression levels were inconsistent across increasing passages of CRC spheroidal culture (Figure 4.10B). Due to the lack any literature on hsa_circ_0066631, the current result indicates that hsa_circ_0066631 could be a non-specific regulator of stemness in CRC. CircZNF800 was selected as the candidate circRNA for downstream analysis based on the consistent up-regulated expression in CRC spheroidal cells and CRC patient tissues (Figures 4.10 – 4.15). The collective results indicate that circZNF800 is involved in the maintenance of CSC properties of CRC spheroidal cells and oncogenicity observed by enhanced expression of circZNF800 in tumour tissues of CRC patients.

While there is a general lack of studies involving circRNA in CRC population, various circRNAs have been reported to be associated with CSC population of other cancers. Circ_CCDC666 (hsa_circ_0001313) was reported to be up-regulated in renal carcinoma spheroidal cells (Yang *et al.*, 2020), parallel to the findings of the present work. CircPRMT5 (hsa_circ_0031250) showed higher expression levels in the tumour parts of urothelial carcinoma of the bladder compared to the noncancerous tissues (Chen *et al.*, 2018). Interestingly, as

circPRMT5 was linked with EMT regulation, the expression levels of circPRMT5 were significantly enriched in the metastatic bladder cancer cells compared to the nonmetastatic group of patients (Chen *et al.*, 2018).

Co-localisation analysis of circZNF800 with proliferation and stem cell markers (Figure 4.17) also highlights the potential use of circRNAs in identifying specific stem cell populations of interest. CircZNF800 co-localised with intestinal stem cell (ISC) population in normal colonic tissues while in high proliferative population in cancerous tissues. Due to the enhanced plasticity of ISC population and higher expression of ISC markers in CRC cancerous region, CSC population in CRC is believed to arise from mutated ISC (van der Heijden and Vermeulen, 2019). Reports on mouse model suggested that the common mutation of *APC* (adenomatous polyposis coli) gene in CRC could only form adenoma when introduced to ISC population (Sangiorgi and Capecchi, 2008; Barker *et al.*, 2009). The reports resonate well with the present data that circZNF800 marks the ISC population and the CSC population in normal and CRC cancer regions, respectively, indicating the prospect as a dual biomarker.

In this work, the hallmarks of CSC properties, including cellular proliferation, CSC and ISC markers, were enhanced upon circZNF800 overexpression (Figures 4.21 – 4.24), and suppressed on circZNF800 knockdown (Figures 4.31 – 4.33). Due to the transient nature of ectopic overexpression of circZNF800 RNA, colony- and sphere-forming properties of CSC were not investigated. Overexpression of circZNF800 accelerated while knockdown of circZNF800 retarded the tumour growth in mice. The *in vivo* tumorigenicity assay

in the mouse model provided a solid understanding of circZNF800 in enriching tumorigenicity abilities in CRC cells (Figure 4.26). Taken together, data suggest that circZNF800 augments CSC properties in CRC cells.

Involvement of circRNA in mediating CSC properties, including stemness, has been reported in other cell types, including induced pluripotent, and cancer stem cells (reviewed by (Lu *et al.*, 2022)). Overexpression of circBIRC6 promotes and maintains the pluripotency state of human embryonic stem cells (Yu *et al.*, 2017a). Likewise, in gastric CSC population, overexpression of circNOTCH1 (hsa_circ_0089547) maintains CSC stemness properties (Zhao *et al.*, 2020b). These reports resonate with the current finding that circRNAs act as gene expression modulators to exert potent cellular effects in various biological processes.

Besides the enhanced phenotypic properties of CSC, core pluripotent transcriptional factors, *OCT4*, *SOX2* and *NANOG* were significantly up-regulated upon ectopic circZNF800 overexpression (Figure 4.24), consistent with genotypic profile of a CSC population. Some, if not all, of the Yamanaka transcriptional factors, Oct4, Sox2, Klf4, cMyc and Nanog are generally up-regulated in CSC-enriched population (Muller *et al.*, 2016). In other studies, circVRK1 (hsa_circ_0141206) was shown to regulate the expression levels of *OCT4*, *SOX2* and *NANOG* in breast CSC (Yan *et al.*, 2017).

Functional analysis using RNA pulldown assay supports the bioinformatics prediction that circZNF800 sponges miR-140-3p, miR-382 and miR-579 (Figure 4.27). The circRNA sponging activities of miRNAs have been well described; however, the exact mechanisms of degradation of the sponged miRNAs remain unclear (Kim and Pak, 2020). Biologically, the sponging activities of circZNF800 of miR-140-3p, miR-382 and miR-579, which are known tumour suppressors, confers further evidence that circZNF800 plays an oncogenic role in CRC (Zhou *et al.*, 2016; Yu *et al.*, 2016; Kalhori *et al.*, 2019) (Table 4.2).

The circZNF800-induced sponging of the miRNAs increased the expression levels of selected downstream target transcripts in the CrCSC cells (Figure 4.29). *ALK7*, *FZD3* and *WNT5A* were significantly up-regulated upon circZNF800 overexpression, in agreement with the literature on the involvement of these transcripts in various CSC-related properties, as summarised in Table 4.3. These transcripts are involved in the regulation of the Activin/Nodal and Wnt/ β -catenin signalling pathways essential in the modulation of CSC properties (Tsuneyoshi *et al.*, 2012; Suwannakul *et al.*, 2020), and promotion of CSC properties by circZNF800. In summary, circZNF800 overexpression increased sponging activities of tumour suppressive miRNAs to increase *ALK7*, *FZD3* and *WNT5A* transcript levels, and resulting in enhanced CSC properties.

5.5 Targeted knockdown of circZNF800 may be a potential therapeutic approach in CRC treatment

CircRNA knockdown approaches that are commonly used in RNA interference (RNAi) are siRNA or shRNA (Li *et al.*, 2018). Using a similar mechanism in mRNA transcript knockdown, the RNAi approach has been applied in circRNA targeting by the use of specific anti-sense RNAs based on the circRNA backsplicing junctional sequences. There have also been reports highlighting the use of RNAi technology delivered using lipid-based polymer and nanoparticle as tools for circRNA knockdown (He *et al.*, 2021). However, the major drawback of using the RNAi undesired knockdown on the host transcript (Pamudurti *et al.*, 2020). Hence, the use of RNAi technology for therapeutic targeting of oncogenic circRNA in clinics remains a challenge. An alternative solution to overcome this problem is by utilizing the recently discovered RNA-editing CRISPR Cas13d system (Zhang *et al.*, 2021b), as has been used in this work.

The present work optimised the CRISPR Cas13d system to mediate specific circZNF800 knockdown with little to no effects on the host transcript, *ZNF800* (Figure 4.30). To date, there are only two other reports on the use of CRISPR Cas13d to knockdown circRNAs (Zhang *et al.*, 2021b; Li *et al.*, 2021b). Zhang *et al.* reported that even a single mismatch in the crRNA targeting sequence of a circRNA could significantly reduce knockdown efficiency, thus highlighting the high specificity of the CRISPR Cas13d system (Zhang *et al.*, 2021b). The highly selective knockdown of circZNF800 by CRISPR Cas13d used in the present study

enabled investigations on the loss-of-function phenotypes of various CSC properties.

The knockdown of circZNF800 diminished all the explored CSC hallmarks (Figures 4.31– 4.38). CircZNF800-knockdown cells were suppressed in cellular proliferation and expression levels of CSC and ISC markers. Furthermore, the sphere- and colony-forming abilities, were also affected, suggesting reduced self-renewal abilities. CircZNF800 knockdown also resulted in reduced expression of the pluripotent transcriptional factors, *OCT4*, *SOX2* and *NANOG* reduced *in vivo* tumorigenicity abilities, all of which were reversed on circZNF800 overexpression. The reduced CSC properties upon circZNF800 knockdown could be explained by the down-regulation of *ALK7*, *FZD3* and *WNT5A* based on the involvement of these transcripts in maintaining proliferative and self-renewal abilities in CSC population (Longati *et al.*, 2013; Principe *et al.*, 2018a; Xia *et al.*, 2018).

The suppression of circZNF800 functions mediated by CRISPR Cas13d may shed light on clinical application potential of the current work. The significant reduction of tumour growth upon circZNF800 knockdown in mice may postulate potential clinical intervention in CRC progression by targeting circZNF800. As the CRISPR Cas13d system used in the present study is highly specific for circZNF800 with no known off-target effect, integrating the current system into a clinically compatible vector, such as adeno-associated virus (AAV), could be beneficial (Wells, 2017). An AAV vector elicits only mild or no immunogenic response *in vivo* compared to other vectors (Wang, Zhang and Gao, 2020). Recent work on integrating CRISPR Cas13d into AAV vector to target *Pcsk9* in mouse hepatocytes

successfully lowered serum cholesterol levels in mice, hinting clinical application potentials (He *et al.*, 2020a). Coupling the CRISPR Cas13d and an AAV vector to target circZNF800 for clinical treatment of CRC is being explored in our laboratory.

CHAPTER 6

CONCLUSIONS

6.1 Conclusions

In our previous work, colorectal cancer (CRC) CRC spheroidal culture was used to enrich CRC cells with enhanced stemness properties, mimicking colorectal cancer stem cell (CrCSC) population. Circular RNA (circRNA) profiling was performed to understand the molecular regulations of the stemness in CrCSC population. A vast majority of 15,000 circRNAs identified was differentially expressed in the CRC spheroidal cells compared to the parental cells, suggesting the potential involvement of circRNAs in mediating biological process of CrCSC population.

Further bioinformatics analysis identified a complex network of post-transcriptional control of circRNAs via microRNA (miRNA) sponging activities in governing pluripotency-associated pathways. CircRNAs, *hsa_circ_0066631* (circDCBLD2) and *circZNF800* (*hsa_circ_0082096*), sponged five tumour suppressive miRNAs, *hsa-miR-140-3p*, *miR-224*, *miR-382*, *miR-548c-3p* and *miR-579m*. The miRNA sponging was predicted to inhibit post-transcriptional suppression of six downstream mRNA transcripts, *ACVR1C/ALK7*, *FZD3*, *IL6ST/GP130*, *SKIL/SNON*, *SMAD2* and *WNT5A*, which are involved in pluripotency-associated pathways. The predicted network was experimentally validated and was consistent with the bioinformatics predictions, suggesting the

potential involvement of the identified network in the enrichment in CSC properties in CRC spheroidal cells.

CircZNF800 was shown to be consistently overexpressed in various CRC spheroidal cells and significantly up-regulated in CRC region compared to adjacent normal in CRC tissue samples. Modulation of circZNF800 expression levels affected CSC-related properties. Overexpression of circZNF800 increased cell proliferation and self-renewal abilities in CRC cells. *In vivo* investigation in mouse model showed overexpression of circZNF800 significantly increased the tumorigenicity of CRC cells. However, these phenotypes were reversed in circZNF800-knockdown cells, suggesting that circZNF800 plays an important role in maintaining CSC properties in CRC cells. Functionally, circZNF800 was shown to sponge, hsa-miR-140-3p, miR-382 and miR-579m and reduced the bioavailability of these miRNAs in CRC cells. Consequently, suppression of the three tumour suppressive miRNAs increased expression levels of the downstream targets *ALK7*, *FZD3* and *WNT5A*, which were shown to up-regulate CSC properties. The overview of the regulation of circZNF800 is presented in Figure 6.1

In summary, the present study has shown that circZNF800 which sponges various tumour suppressive miRNA, resulting in increased expression levels of downstream pluripotency-associated transcripts, could be further explored as a therapeutic target.

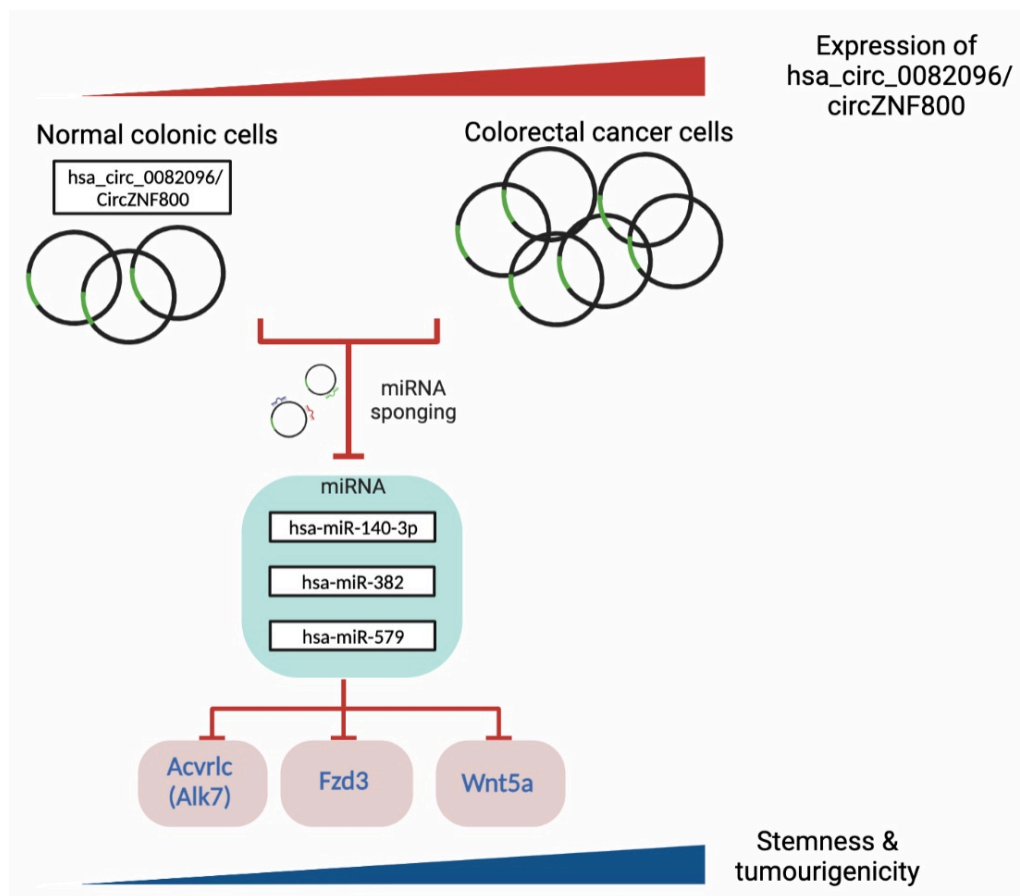


Figure 6.1 Overview of the biological findings of the present work. CircZNF800 was identified to be differentially expressed in tumour tissues of CRC patients. By sponging the tumour suppressor miRNAs, hsa-miR-140-3p, miR-382 and miR-579, circZNF800 up-regulated expression of the downstream targets involved in the CSC regulation in CRC cells. The red and deep blue wedges shown at the top and bottom show increasing enhancement of stemness and tumorigenicity properties on increasing circZNF800 expression.

6.2 Limitations of the study

In this study, CRC cells were enriched for CSC properties using spheroidal cells. The resulting CRC spheroidal cells exhibited classical CSC properties including enhanced stemness markers, self-renewal abilities and chemoresistance (Rengganaten, 2016). While spheroidal culture is a simple robust approach to enrich CSC population, there are limitations in using cell-line derived CRC spheroidal cells in this work. Cell lines often represent specific phenotypes of the original cancer due to adaptation to the 2D culture environment (Białkowska *et al.*, 2020). Hence, the cultured cells do not truly reflect tumour heterogeneity of the cancer patient. The use of patient-derived organoids model would have improved the representation of the tumour population (Zhu *et al.*, 2022).

The downstream miRNA and mRNA targets presented in this work were predicted based on bioinformatics and profiling tools. The prediction has unveiled a new regulatory pathway of stemness properties in CRC. The use of bioinformatics tools to identify downstream targets allows for a comprehensive approach for identifying a large number of candidates in expression profiling works. However, such an approach limits the prediction to only previously annotated interactions, missing other potentially important mediators. Additional screening approaches, such as single-cell sequencing, could be utilised in expanding the current work (Hwang, Lee and Bang, 2018).

Furthermore, technical improvements on the generation of *in vitro* transcribed circRNA are warranted to improve the quality of data presented in this work. In the present study, the naïve form of circZNF800 was used in the cellular transfection. RNA modifications have been implicated with various biological process involving RNA stability (Ye *et al.*, 2021). The scope of the present study did not include modification of circRNA generation. Therefore, by further understanding the potential endogenous modifications of circZNF800, a deeper understanding on the biological functions and actions of circZNF800 may be achieved.

6.3 Future investigations

The current work explored the circRNA differentially expression profile of CRC spheroidal cells and identified circZNF800 as a potential regulator of stemness in the CRC population. As CrCSC population hinders the efficacy of the current therapeutic treatment, the data of the present work could be further explored for development of alternative therapeutic protocols for CRC treatment. Since modulation of circZNF800 levels significantly affected tumour growth in animal models, additional clinical explorations may validate the potential use of circZNF800 as a CRC therapeutic intervention target.

The use of CRISPR Cas13d system to induce knockdown of circZNF800 has demonstrated a significant reduction of tumour-forming abilities in CRC cells. Current clinical applications of other CRISPR systems, such as CRISPR Cas9 in various diseases such as β -thalassemia and sickle-cell anaemia, is at various stages of clinical trial (Liu *et al.*, 2021). Coupled with effective delivery vectors, such as adeno-associated virus (AAV), more studies are warranted to further explore the clinical advantages of *in vivo* knockdown of circZNF800 using CRISPR Cas13d-AAV approach in intervention treatment of CRC, and open the way in targeting other oncogenic circRNAs in other cancers and human diseases.

REFERENCES

- Adeshakin, F. O., Adeshakin, A. O., Afolabi, L. O., Yan, D., Zhang, G. and Wan, X. (2021) 'Mechanisms for Modulating Anoikis Resistance in Cancer and the Relevance of Metabolic Reprogramming', *Front Oncol*, 11, pp. 626577.
- Agliano, A., Calvo, A. and Box, C. 'The challenge of targeting cancer stem cells to halt metastasis'. *Seminars in Cancer Biology*: Academic Press, 25-42.
- Ahmad, R., Kumar, B., Chen, Z., Chen, X., Müller, D., Lele, S. M., Washington, M. K., Batra, S. K., Dhawan, P. and Singh, A. B. 2017. Loss of claudin-3 expression induces IL6/gp130/Stat3 signaling to promote colon cancer malignancy by hyperactivating Wnt/ β -catenin signaling. *Oncogene*. Nature Publishing Group.
- Alhulais, R. A. and Ralph, S. J. (2019) 'Cancer stem cells, stemness markers and selected drug targeting: metastatic colorectal cancer and cyclooxygenase-2/prostaglandin E2 connection to WNT as a model system', *Journal of Cancer Metastasis and Treatment*, 2019.
- Amankwatia, E. B., Chakravarty, P., Carey, F. A., Weidlich, S., Steele, R. J. C., Munro, A. J., Wolf, C. R. and Smith, G. 2015. MicroRNA-224 is associated with colorectal cancer progression and response to 5-fluorouracil-based chemotherapy by KRAS-dependent and-independent mechanisms. *British Journal of Cancer*. Nature Publishing Group.
- Amersi, F., Agustin, M. and Ko, C. Y. (2005) 'Colorectal cancer: epidemiology, risk factors, and health services', *Clin Colon Rectal Surg*, 18(3), pp. 133-140.
- Amini, S., Fathi, F., Mobalegi, J., Sofimajidpour, H. and Ghadimi, T. (2014) 'The expressions of stem cell markers: Oct4, Nanog, Sox2, nucleostemin, Bmi, Zfx, Tc11, Tbx3, Dppa4, and Esrrb in bladder, colon, and prostate cancer, and certain cancer cell lines', *Anat Cell Biol*, 47(1), pp. 1-11.
- Angius, A., Scanu, A. M., Arru, C., Muroli, M. R., Rallo, V., Deiana, G., Ninniri, M. C., Carru, C., Porcu, A., Pira, G., Uva, P., Cossu-Rocca, P. and De Miglio, M. R. (2021) 'Portrait of Cancer Stem Cells on Colorectal Cancer: Molecular Biomarkers, Signaling Pathways and miRNAome', *Int J Mol Sci*, 22(4), pp. 1603.
- Aponte, P. M. and Caicedo, A. (2017) 'Stemness in cancer: Stem cells, cancer stem cells, and their microenvironment', *Stem Cells International*, 2017.

Appert-Collin, A., Hubert, P., Cremel, G. and Bennisroune, A. (2015) 'Role of ErbB Receptors in Cancer Cell Migration and Invasion', *Front Pharmacol*, 6, pp. 283.

Arima, Y., Nobusue, H. and Saya, H. (2020) 'Targeting of cancer stem cells by differentiation therapy', *Cancer Sci*, 111(8), pp. 2689-2695.

Arnold, M., Sierra, M. S., Laversanne, M., Soerjomataram, I., Jemal, A. and Bray, F. (2017) 'Global patterns and trends in colorectal cancer incidence and mortality', *Gut*, 66(4), pp. 683-691.

Arteaga, C. L. (2011) 'ERBB receptors in cancer: signaling from the inside', *Breast Cancer Res*, 13(2), pp. 304.

Asnaghi, L., White, D. T., Key, N., Choi, J., Mahale, A., Alkatan, H., Edward, D. P., Elkhamary, S. M., Al-Mesfer, S., Maktabi, A., Hurtado, C. G., Lee, G. Y., Carcaboso, A. M., Mumm, J. S., Safieh, L. A. and Eberhart, C. G. (2019) 'ACVR1C/SMAD2 signaling promotes invasion and growth in retinoblastoma', *Oncogene*, 38(12), pp. 2056-2075.

Avelar-Freitas, B. A., Almeida, V. G., Pinto, M. C., Mourao, F. A., Massensini, A. R., Martins-Filho, O. A., Rocha-Vieira, E. and Brito-Melo, G. E. (2014) 'Trypan blue exclusion assay by flow cytometry', *Braz J Med Biol Res*, 47(4), pp. 307-315.

Balaguer, F., Link, A., Lozano, J. J., Cuatrecasas, M., Nagasaka, T., Boland, C. R. and Goel, A. (2010) 'Epigenetic silencing of miR-137 is an early event in colorectal carcinogenesis', *Cancer Res*, 70(16), pp. 6609-6618.

Barisam, M., Niavol, F. R., Kinj, M. A., Saidi, M. S., Ghanbarian, H. and Kashaninejad, N. (2022) 'Enrichment of cancer stem-like cells by controlling oxygen, glucose and fluid shear stress in a microfluidic spheroid culture device', *Journal of Science: Advanced Materials and Devices*, 7(2), pp. 100439.

Barker, N., Ridgway, R. A., Van Es, J. H., Van De Wetering, M., Begthel, H., Van Den Born, M., Danenberg, E., Clarke, A. R., Sansom, O. J. and Clevers, H. (2009) 'Crypt stem cells as the cells-of-origin of intestinal cancer', *Nature*, 457(7229), pp. 608-611.

Baylin, S. B. and Jones, P. A. (2016) 'Epigenetic Determinants of Cancer', *Cold Spring Harb Perspect Biol*, 8(9), pp. a019505.

Bertero, A., Brown, S., Madrigal, P., Osnato, A., Ortmann, D., Yiangou, L., Kadiwala, J., Hubner, N. C., De Los Mozos, I. R., Sadée, C., Lenaerts, A. S.,

Nakanoh, S., Grandy, R., Farnell, E., Ule, J., Stunnenberg, H. G., Mendjan, S. and Vallier, L. 2018. The SMAD2/3 interactome reveals that TGF β controls m 6 A mRNA methylation in pluripotency. *Nature*. Nature Publishing Group.

Białkowska, K., Komorowski, P., Bryszewska, M. and Miłowska, K. (2020) 'Spheroids as a Type of Three-Dimensional Cell Cultures—Examples of Methods of Preparation and the Most Important Application', *International Journal of Molecular Sciences*, 21(17), pp. 6225.

Biller, L. H. and Schrag, D. (2021) 'Diagnosis and Treatment of Metastatic Colorectal Cancer: A Review', *JAMA*, 325(7), pp. 669-685.

Bitarte, N., Bandres, E., Boni, V., Zarate, R., Rodriguez, J., Gonzalez-Huarriz, M., Lopez, I., Javier Sola, J., Alonso, M. M., Fortes, P. and Garcia-Foncillas, J. (2011) 'MicroRNA-451 is involved in the self-renewal, tumorigenicity, and chemoresistance of colorectal cancer stem cells', *Stem Cells*, 29(11), pp. 1661-1671.

Blondy, S., David, V., Verdier, M., Mathonnet, M., Perraud, A. and Christou, N. (2020) '5-Fluorouracil resistance mechanisms in colorectal cancer: From classical pathways to promising processes', *Cancer Science*, 111, pp. 3142-3154.

Bojkova, D., Wagner, J. U. G., Shumliakivska, M., Aslan, G. S., Saleem, U., Hansen, A., Luxán, G., Günther, S., Pham, M. D., Krishnan, J., Harter, P. N., Ermel, U., Frangakis, A., Zeiher, A. M., Milting, H., Cinatl, J., Dendorfer, A., Eschenhagen, T., Ciesek, S. and Dimmeler, S. 2020. SARS-CoV-2 infects and induces cytotoxic effects in human cardiomyocytes. *bioRxiv*. Cold Spring Harbor Laboratory.

Bourillot, P. Y., Santamaria, C., David, L. and Savatier, P. 2020. GP130 signaling and the control of naïve pluripotency in humans, monkeys, and pigs. *Experimental Cell Research*. Elsevier Inc.

Bradshaw, A., Wickremsekera, A., Tan, S. T., Peng, L., Davis, P. F. and Itinteang, T. (2016) 'Cancer Stem Cell Hierarchy in Glioblastoma Multiforme', *Front Surg*, 3, pp. 21.

Bray, F., Ferlay, J., Soerjomataram, I., Siegel, R. L., Torre, L. A. and Jemal, A. 2018. Global cancer statistics 2018: GLOBOCAN estimates of incidence and mortality worldwide for 36 cancers in 185 countries. *CA: A Cancer Journal for Clinicians*. Wiley.

Burdon, T., Stracey, C., Chambers, I., Nichols, J. and Smith, A. 1999. Suppression of SHP-2 and ERK signalling promotes self-renewal of mouse embryonic stem cells. *Developmental Biology*. Academic Press Inc.

Cai, J., Xia, L., Li, J., Ni, S., Song, H. and Wu, X. 2019. Tumor-associated macrophages derived TGF- β -induced epithelial to mesenchymal transition in colorectal cancer cells through Smad2,3-4/Snail signaling pathway. *Cancer Research and Treatment*. Korean Cancer Association.

Cascella, M., Bimonte, S., Barbieri, A., Del Vecchio, V., Caliendo, D., Schiavone, V., Fusco, R., Granata, V., Arra, C. and Cuomo, A. (2018) 'Dissecting the mechanisms and molecules underlying the potential carcinogenicity of red and processed meat in colorectal cancer (CRC): an overview on the current state of knowledge', *Infect Agent Cancer*, 13(1), pp. 3.

Chang, Y. W., Su, Y. J., Hsiao, M., Wei, K. C., Lin, W. H., Liang, C. L., Chen, S. C. and Lee, J. L. (2015) 'Diverse Targets of beta-Catenin during the Epithelial-Mesenchymal Transition Define Cancer Stem Cells and Predict Disease Relapse', *Cancer Res*, 75(16), pp. 3398-3410.

Chen, J., Li, X., Yang, L., Li, M., Zhang, Y. and Zhang, J. (2020a) 'CircASH2L Promotes Ovarian Cancer Tumorigenesis, Angiogenesis, and Lymphangiogenesis by Regulating the miR-665/VEGFA Axis as a Competing Endogenous RNA', *Front Cell Dev Biol*, 8(1405), pp. 595585.

Chen, J., Yang, J., Fei, X., Wang, X. and Wang, K. (2021) 'CircRNA ciRS-7: a Novel Oncogene in Multiple Cancers', *Int J Biol Sci*, 17(1), pp. 379-389.

Chen, L., Kong, R., Wu, C., Wang, S., Liu, Z., Liu, S., Li, S., Chen, T., Mao, C. and Liu, S. (2020b) 'Circ-MALAT1 Functions as Both an mRNA Translation Brake and a microRNA Sponge to Promote Self-Renewal of Hepatocellular Cancer Stem Cells', *Adv Sci (Weinh)*, 7(4), pp. 1900949.

Chen, X., Chen, R. X., Wei, W. S., Li, Y. H., Feng, Z. H., Tan, L., Chen, J. W., Yuan, G. J., Chen, S. L., Guo, S. J., Xiao, K. H., Liu, Z. W., Luo, J. H., Zhou, F. J. and Xie, D. (2018) 'PRMT5 Circular RNA Promotes Metastasis of Urothelial Carcinoma of the Bladder through Sponging miR-30c to Induce Epithelial-Mesenchymal Transition', *Clin Cancer Res*, 24(24), pp. 6319-6330.

Chen, X. and Lu, Y. (2021) 'Circular RNA: Biosynthesis in vitro', *Front Bioeng Biotechnol*, 9, pp. 787881.

Chen, Y., Yang, F., Fang, E., Xiao, W., Mei, H., Li, H., Li, D., Song, H., Wang, J., Hong, M., Wang, X., Huang, K., Zheng, L. and Tong, Q. (2019) 'Circular RNA circAGO2 drives cancer progression through facilitating HuR-repressed functions of AGO2-miRNA complexes', *Cell Death Differ*, 26(7), pp. 1346-1364.

Chen, Y. G., Kim, M. V., Chen, X., Batista, P. J., Aoyama, S., Wilusz, J. E., Iwasaki, A. and Chang, H. Y. (2017) 'Sensing Self and Foreign Circular RNAs by Intron Identity', *Mol Cell*, 67(2), pp. 228-238 e225.

Civelek, M., Wu, Y., Pan, C., Raulerson, C. K., Ko, A., He, A., Tilford, C., Saleem, N. K., Stancakova, A., Scott, L. J., Fuchsberger, C., Stringham, H. M., Jackson, A. U., Narisu, N., Chines, P. S., Small, K. S., Kuusisto, J., Parks, B. W., Pajukanta, P., Kirchgessner, T., Collins, F. S., Gargalovic, P. S., Boehnke, M., Laakso, M., Mohlke, K. L. and Lusis, A. J. (2017) 'Genetic Regulation of Adipose Gene Expression and Cardio-Metabolic Traits', *Am J Hum Genet*, 100(3), pp. 428-443.

Clark, P. A., Iida, M., Treisman, D. M., Kalluri, H., Ezhilan, S., Zorniak, M., Wheeler, D. L. and Kuo, J. S. 2012. Activation of multiple ERBB family receptors mediates glioblastoma cancer stem-like cell resistance to EGFR-targeted inhibition. *Neoplasia (United States)*. Elsevier B.V.

Colombo, E. and Cattaneo, M. G. (2021) 'Multicellular 3D Models to Study Tumour-Stroma Interactions', *Int J Mol Sci*, 22(4), pp. 1633.

Conciatori, F., Bazzichetto, C., Falcone, I., Ferretti, G., Cognetti, F., Milella, M. and Ciuffreda, L. (2019) 'Colorectal cancer stem cells properties and features: evidence of interleukin-8 involvement', *Cancer Drug Resist*, 2(4), pp. 968-979.

Costa, M. C. and Enguita, F. J. (2020) 'Towards a universal nomenclature standardization for circular RNAs', *Non-coding RNA Investigation*, 4, pp. 2-2.

Dahle, Ø. and Kuehn, M. R. 2016. Inhibiting Smad2/3 signaling in pluripotent mouse embryonic stem cells enhances endoderm formation by increasing transcriptional priming of lineage-specifying target genes. *Developmental Dynamics*. John Wiley and Sons Inc.

Dai, X., Ge, J., Wang, X., Qian, X., Zhang, C. and Li, X. (2013) 'OCT4 regulates epithelial-mesenchymal transition and its knockdown inhibits colorectal cancer cell migration and invasion', *Oncol Rep*, 29(1), pp. 155-160.

Das, P. K., Islam, F. and Lam, A. K. (2020) 'The Roles of Cancer Stem Cells and Therapy Resistance in Colorectal Carcinoma', *Cells*, 9(6), pp. 1392.

De Angelis, M. L., Francescangeli, F., Zeuner, A. and Baiocchi, M. (2021) 'Colorectal Cancer Stem Cells: An Overview of Evolving Methods and Concepts', *Cancers (Basel)*, 13(23), pp. 5910.

De Robertis, M., Poeta, M. L., Signori, E. and Fazio, V. M. (2018) 'Current understanding and clinical utility of miRNAs regulation of colon cancer stem cells', *Semin Cancer Biol*, 53, pp. 232-247.

De Sousa, E. M. F. and Vermeulen, L. (2016) 'Wnt Signaling in Cancer Stem Cell Biology', *Cancers (Basel)*, 8(7), pp. 60.

Demšar, J., Curk, T., Erjavec, A., Gorup, Č., Hočevar, T., Milutinovič, M., Možina, M., Polajnar, M., Toplak, M. and Starič, A. (2013) 'Orange: data mining toolbox in Python', *the Journal of machine Learning research*, 14(1), pp. 2349-2353.

Deng, Y., Zhou, J., Fang, L., Cai, Y., Ke, J., Xie, X., Huang, Y., Huang, M. and Wang, J. (2014) 'ALDH1 is an independent prognostic factor for patients with stages II-III rectal cancer after receiving radiochemotherapy', *Br J Cancer*, 110(2), pp. 430-434.

Dieter, S. M., Ball, C. R., Hoffmann, C. M., Nowrouzi, A., Herbst, F., Zavidij, O., Abel, U., Arens, A., Weichert, W., Brand, K., Koch, M., Weitz, J., Schmidt, M., Von Kalle, C. and Glimm, H. (2011) 'Distinct types of tumor-initiating cells form human colon cancer tumors and metastases', *Cell Stem Cell*, 9(4), pp. 357-365.

Dong, W., Yao, C., Teng, X., Chai, J., Yang, X. and Li, B. 2016. MiR-140-3p suppressed cell growth and invasion by downregulating the expression of ATP8A1 in non-small cell lung cancer. *Tumor Biology*. Springer Netherlands.

Dong, Z., Liu, Z., Liang, M., Pan, J., Lin, M., Lin, H., Luo, Y., Zhou, X. and Yao, W. (2021) 'Identification of circRNA-miRNA-mRNA networks contributes to explore underlying pathogenesis and therapy strategy of gastric cancer', *J Transl Med*, 19(1), pp. 226.

Du, L., Wang, H., He, L., Zhang, J., Ni, B., Wang, X., Jin, H., Cahuzac, N., Mehrpour, M., Lu, Y. and Chen, Q. (2008) 'CD44 is of functional importance for colorectal cancer stem cells', *Clin Cancer Res*, 14(21), pp. 6751-6760.

Du, W. W., Yang, W., Liu, E., Yang, Z., Dhaliwal, P. and Yang, B. B. (2016) 'Foxo3 circular RNA retards cell cycle progression via forming ternary complexes with p21 and CDK2', *Nucleic Acids Res*, 44(6), pp. 2846-2858.

Dudekula, D. B., Panda, A. C., Grammatikakis, I., De, S., Abdelmohsen, K. and Gorospe, M. (2016) 'CircInteractome: a web tool for exploring circular RNAs and their interacting proteins and microRNAs', *RNA biology*, 13(1), pp. 34-42.

Dunagin, M., Cabili, M. N., Rinn, J. and Raj, A. (2015) 'Visualization of lncRNA by single-molecule fluorescence in situ hybridization', *Nuclear Bodies and Noncoding RNAs*: Springer, pp. 3-19.

Edwards, B. K., Ward, E., Kohler, B. A., Ehemann, C., Zauber, A. G., Anderson, R. N., Jemal, A., Schymura, M. J., Lansdorp-Vogelaar, I., Seeff, L. C., Van Ballegooijen, M., Goede, S. L. and Ries, L. A. (2010) 'Annual report to the nation on the status of cancer, 1975-2006, featuring colorectal cancer trends and impact of interventions (risk factors, screening, and treatment) to reduce future rates', *Cancer*, 116(3), pp. 544-573.

Enuka, Y., Lauriola, M., Feldman, M. E., Sas-Chen, A., Ulitsky, I. and Yarden, Y. (2016) 'Circular RNAs are long-lived and display only minimal early alterations in response to a growth factor', *Nucleic Acids Res*, 44(3), pp. 1370-1383.

Fang, D., Nguyen, T. K., Leishear, K., Finko, R., Kulp, A. N., Hotz, S., Van Belle, P. A., Xu, X., Elder, D. E. and Herlyn, M. 2005. A tumorigenic subpopulation with stem cell properties in melanomas. *Cancer Research*. American Association for Cancer Research.

Fattore, L., Mancini, R., Acunzo, M., Romano, G., Laganà, A., Pisanu, M. E., Malpicci, D., Madonna, G., Mallardo, D., Caponea, M., Fulciniti, F., Mazzucchelli, L., Botti, G., Croce, C. M., Ascierto, P. A. and Ciliberto, G. 2016. miR-579-3p controls melanoma progression and resistance to target therapy. *Proceedings of the National Academy of Sciences of the United States of America*. National Academy of Sciences.

Fekir, K., Dubois-Pot-Schneider, H. E., Desert, R., Daniel, Y., Glaise, D., Rauch, C., Morel, F., Fromenty, B., Musso, O., Cabillic, F. and Corlu, A. 2019. Retrodifferentiation of human tumor hepatocytes to stem cells leads to metabolic reprogramming and chemoresistance. *Cancer Research*. American Association for Cancer Research Inc.

Feng, Y. H. and Tsao, C. J. (2016) 'Emerging role of microRNA-21 in cancer', *Biomed Rep*, 5(4), pp. 395-402.

Feng, Y. H., Wu, C. L., Tsao, C. J., Chang, J. G., Lu, P. J., Yeh, K. T., Uen, Y. H., Lee, J. C. and Shiau, A. L. (2011) 'Deregulated expression of sprouty2 and microRNA-21 in human colon cancer: Correlation with the clinical stage of the disease', *Cancer Biol Ther*, 11(1), pp. 111-121.

Ford, E. and Ares, M., Jr. (1994) 'Synthesis of circular RNA in bacteria and yeast using RNA cyclase ribozymes derived from a group I intron of phage T4', *Proc Natl Acad Sci U S A*, 91(8), pp. 3117-3121.

Formeister, E. J., Sionas, A. L., Lorance, D. K., Barkley, C. L., Lee, G. H. and Magness, S. T. (2009) 'Distinct SOX9 levels differentially mark stem/progenitor populations and enteroendocrine cells of the small intestine epithelium', *Am J Physiol Gastrointest Liver Physiol*, 296(5), pp. G1108-1118.

Frank, M. H., Wilson, B. J., Gold, J. S. and Frank, N. Y. (2021) 'Clinical Implications of Colorectal Cancer Stem Cells in the Age of Single-Cell Omics and Targeted Therapies', *Gastroenterology*, 160(6), pp. 1947-1960.

French, R. and Pauklin, S. (2021) 'Epigenetic regulation of cancer stem cell formation and maintenance', *Int J Cancer*, 148(12), pp. 2884-2897.

Fulci, V., Chiaretti, S., Goldoni, M., Azzalin, G., Carucci, N., Tavoraro, S., Castellano, L., Magrelli, A., Citarella, F., Messina, M., Maggio, R., Peragine, N., Santangelo, S., Mauro, F. R., Landgraf, P., Tuschl, T., Weir, D. B., Chien, M., Russo, J. J., Ju, J., Sheridan, R., Sander, C., Zavolan, M., Guarini, A., Foa, R. and Macino, G. (2007) 'Quantitative technologies establish a novel microRNA profile of chronic lymphocytic leukemia', *Blood*, 109(11), pp. 4944-4951.

Gheytauchi, E., Naseri, M., Karimi-Busheri, F., Atyabi, F., Mirsharif, E. S., Bozorgmehr, M., Ghods, R. and Madjd, Z. (2021) 'Morphological and molecular characteristics of spheroid formation in HT-29 and Caco-2 colorectal cancer cell lines', *Cancer Cell Int*, 21(1), pp. 204.

Gisina, A. M., Kim, Y. S., Potashnikova, D. M., Tvorogova, A. V., Yarygin, K. N. and Lupatov, A. Y. (2019) 'Proliferative Activity of Colorectal Cancer Cells with Different Levels of CD133 Expression', *Bull Exp Biol Med*, 167(4), pp. 541-545.

Grady, W. M. and Carethers, J. M. (2008) 'Genomic and epigenetic instability in colorectal cancer pathogenesis', *Gastroenterology*, 135(4), pp. 1079-1099.

Grady, W. M. and Markowitz, S. D. (2015) 'The molecular pathogenesis of colorectal cancer and its potential application to colorectal cancer screening', *Dig Dis Sci*, 60(3), pp. 762-772.

Gupta, R., Bhatt, L. K., Johnston, T. P. and Prabhavalkar, K. S. (2019) 'Colon cancer stem cells: Potential target for the treatment of colorectal cancer', *Cancer Biol Ther*, 20(8), pp. 1068-1082.

Gupta, R., Ghosh, A., Chakravarti, R., Singh, R., Ravichandiran, V., Swarnakar, S. and Ghosh, D. (2022) 'Cas13d: A New Molecular Scissor for Transcriptome Engineering', *Front Cell Dev Biol*, 10, pp. 866800.

Hadjimichael, C., Chanoumidou, K., Papadopoulou, N., Arampatzi, P., Papamatheakis, J. and Kretsovali, A. (2015) 'Common stemness regulators of embryonic and cancer stem cells', *World J Stem Cells*, 7(9), pp. 1150-1184.

Harper, K. L., McDonnell, E. and Whitehouse, A. (2019) 'CircRNAs: From anonymity to novel regulators of gene expression in cancer (Review)', *Int J Oncol*, 55(6), pp. 1183-1193.

He, A. T., Liu, J., Li, F. and Yang, B. B. (2021) 'Targeting circular RNAs as a therapeutic approach: current strategies and challenges', *Signal Transduct Target Ther*, 6(1), pp. 185.

He, B., Peng, W., Huang, J., Zhang, H., Zhou, Y., Yang, X., Liu, J., Li, Z., Xu, C., Xue, M., Yang, H. and Huang, P. (2020a) 'Modulation of metabolic functions through Cas13d-mediated gene knockdown in liver', *Protein Cell*, 11(7), pp. 518-524.

He, J., Huang, H., Du, Y., Peng, D., Zhou, Y., Li, Y., Wang, H., Zhou, Y. and Nie, Y. (2020b) 'Association of DCBLD2 upregulation with tumor progression and poor survival in colorectal cancer', *Cell Oncol (Dordr)*, 43(3), pp. 409-420.

He, Q. Z., Luo, X. Z., Wang, K., Zhou, Q., Ao, H., Yang, Y., Li, S. X., Li, Y., Zhu, H. T. and Duan, T. 2014. Isolation and characterization of cancer stem cells from high-grade serous ovarian carcinomas. *Cellular Physiology and Biochemistry*. Cell Physiol Biochem Press.

Henrikson, N. B., Webber, E. M., Goddard, K. A., Scrol, A., Piper, M., Williams, M. S., Zallen, D. T., Calonge, N., Ganiats, T. G., Janssens, A. C., Zauber, A., Lansdorp-Vogelaar, I., Van Ballegooijen, M. and Whitlock, E. P. (2015) 'Family history and the natural history of colorectal cancer: systematic review', *Genet Med*, 17(9), pp. 702-712.

Herrmann, D., Conway, J. R., Vennin, C., Magenau, A., Hughes, W. E., Morton, J. P. and Timpson, P. (2014) 'Three-dimensional cancer models mimic cell-matrix interactions in the tumour microenvironment', *Carcinogenesis*, 35(8), pp. 1671-1679.

Hill, D. G., Yu, L., Gao, H., Balic, J. J., West, A., Oshima, H., Mcleod, L., Oshima, M., Gallimore, A., D'costa, K., Bhathal, P. S., Sievert, W., Ferrero, R. L., Jenkins, B. J. and Jones, G. W. 2018. Hyperactive gp130/STAT3-driven gastric tumourigenesis promotes submucosal tertiary lymphoid structure development. *International Journal of Cancer*. Wiley-Liss Inc.

Hnatyszyn, A., Hryhorowicz, S., Kaczmarek-Rys, M., Lis, E., Slomski, R., Scott, R. J. and Plawski, A. (2019) 'Colorectal carcinoma in the course of inflammatory bowel diseases', *Hered Cancer Clin Pract*, 17(1), pp. 18.

Hoarau-Vechot, J., Rafii, A., Touboul, C. and Pasquier, J. (2018) 'Halfway between 2D and Animal Models: Are 3D Cultures the Ideal Tool to Study Cancer-Microenvironment Interactions?', *Int J Mol Sci*, 19(1), pp. 181.

Holle, A. W., Young, J. L. and Spatz, J. P. (2016) 'In vitro cancer cell-ECM interactions inform in vivo cancer treatment', *Adv Drug Deliv Rev*, 97, pp. 270-279.

Hu, T., Su, F., Jiang, W. and Dart, D. A. (2017) 'Overexpression of Activin Receptor-like Kinase 7 in Breast Cancer Cells Is Associated with Decreased Cell Growth and Adhesion', *Anticancer Research*, 37(7), pp. 3441.

Huang, H., Wang, Y., Li, Q., Fei, X., Ma, H. and Hu, R. 2019. miR-140-3p functions as a tumor suppressor in squamous cell lung cancer by regulating BRD9. *Cancer Letters*. Elsevier Ireland Ltd.

Huels, D. J. and Sansom, O. J. (2015) 'Stem vs non-stem cell origin of colorectal cancer', *British Journal of Cancer*, 113, pp. 1-5.

Hwang, B., Lee, J. H. and Bang, D. (2018) 'Single-cell RNA sequencing technologies and bioinformatics pipelines', *Experimental & Molecular Medicine*, 50(8), pp. 1-14.

Ibarrola-Villava, M., Cervantes, A. and Bardelli, A. (2018) 'Preclinical models for precision oncology', *Biochim Biophys Acta Rev Cancer*, 1870(2), pp. 239-246.

Ishiguro, T., Ohata, H., Sato, A., Yamawaki, K., Enomoto, T. and Okamoto, K. (2017) 'Tumor-derived spheroids: Relevance to cancer stem cells and clinical applications', *Cancer Sci*, 108(3), pp. 283-289.

Itatani, Y., Kawada, K. and Sakai, Y. (2019) 'Transforming Growth Factor-beta Signaling Pathway in Colorectal Cancer and Its Tumor Microenvironment', *Int J Mol Sci*, 20(23), pp. 5822.

Iyer, D. N., Sin, W. Y. and Ng, L. (2019) 'Linking stemness with colorectal cancer initiation, progression, and therapy', *World Journal of Stem Cells*, 11, pp. 519-534.

Jacky Lam, W. K. and Dennis Lo, Y. M. (2019) 'Circular RNAs as Urinary Biomarkers', *Clin Chem*, 65(10), pp. 1196-1198.

Jiang, K., Ren, C. and Nair, V. D. (2013) 'MicroRNA-137 represses Klf4 and Tbx3 during differentiation of mouse embryonic stem cells', *Stem Cell Res*, 11(3), pp. 1299-1313.

Jiang, W., Li, T., Wang, J., Jiao, R., Shi, X., Huang, X. and Ji, G. 2019. miR-140-3p suppresses cell growth and induces apoptosis in colorectal cancer by targeting PD-L1. *OncoTargets and Therapy*. Dove Medical Press Ltd.

Kalhuri, M. R., Irani, S., Soleimani, M., Arefian, E. and Kouhkan, F. 2019. The effect of miR-579 on the PI3K/AKT pathway in human glioblastoma PTEN mutant cell lines. *Journal of Cellular Biochemistry*. Wiley-Liss Inc.

Kanth, P. and Inadomi, J. M. (2021) 'Screening and prevention of colorectal cancer', *BMJ*, 374, pp. n1855.

Kasi, A., Handa, S., Bhatti, S., Umar, S., Bansal, A. and Sun, W. (2020) 'Molecular Pathogenesis and Classification of Colorectal Carcinoma', *Curr Colorectal Cancer Rep*, 16(5), pp. 97-106.

Kaufman-Francis, K., Goh, H. N., Kojima, Y., Studdert, J. B., Jones, V., Power, M. D., Wilkie, E., Teber, E., Loebel, D. a. F. and Tam, P. P. L. 2014. Differential response of epiblast stem cells to Nodal and Activin signalling: A paradigm of early endoderm development in the embryo. *Philosophical Transactions of the Royal Society B: Biological Sciences*. Royal Society of London.

Keller, K. C., Ding, H., Tieu, R., Sparks, N. R. L., Ehnes, D. D. and Zur Nieden, N. I. 2016. Wnt5a Supports Osteogenic Lineage Decisions in Embryonic Stem Cells. *Stem Cells and Development*. Mary Ann Liebert Inc.

Keum, N. and Giovannucci, E. (2019) 'Global burden of colorectal cancer: emerging trends, risk factors and prevention strategies', *Nat Rev Gastroenterol Hepatol*, 16(12), pp. 713-732.

Kim, C. K. and Pak, T. R. (2020) 'miRNA degradation in the mammalian brain', *Am J Physiol Cell Physiol*, 319(4), pp. C624-C629.

Kim, E., Coelho, D. and Blachier, F. (2013) 'Review of the association between meat consumption and risk of colorectal cancer', *Nutr Res*, 33(12), pp. 983-994.

Kim, J. H. and Kang, G. H. (2014) 'Molecular and prognostic heterogeneity of microsatellite-unstable colorectal cancer', *World J Gastroenterol*, 20(15), pp. 4230-4243.

Kim, Y.-H., Song, Y., Kim, J.-K., Kim, T.-M., Sim, H. W., Kim, H.-L., Jang, H., Kim, Y.-W. and Hong, K.-M. (2019) 'False-negative errors in next-generation sequencing contribute substantially to inconsistency of mutation databases', *PLOS ONE*, 14(9), pp. e0222535.

Kolligs, F. T. (2016) 'Diagnostics and Epidemiology of Colorectal Cancer', *Visc Med*, 32(3), pp. 158-164.

Kozovska, Z., Patsalias, A., Bajzik, V., Durinikova, E., Demkova, L., Jargasova, S., Smolkova, B., Plava, J., Kucerova, L. and Matuskova, M. (2018) 'ALDH1A inhibition sensitizes colon cancer cells to chemotherapy', *BMC Cancer*, 18(1), pp. 656.

Kramer, M. F. (2011) 'Stem-loop RT-qPCR for miRNAs', *Curr Protoc Mol Biol*, Chapter 15, pp. Unit 15 10.

Kuo, C.-N., Liao, Y.-M., Kuo, L.-N., Tsai, H.-J., Chang, W.-C. and Yen, Y. (2020) 'Cancers in Taiwan: Practical insight from epidemiology, treatments, biomarkers, and cost', *Journal of the Formosan Medical Association*, 119(12), pp. 1731-1741.

Lee, S. H., Hong, J. H., Park, H. K., Park, J. S., Kim, B. K., Lee, J. Y., Jeong, J. Y., Yoon, G. S., Inoue, M., Choi, G. S. and Lee, I. K. (2015) 'Colorectal cancer-derived tumor spheroids retain the characteristics of original tumors', *Cancer Lett*, 367(1), pp. 34-42.

Lewandowska, A., Rudzki, G., Lewandowski, T., Strykowska-Gora, A. and Rudzki, S. (2022) 'Title: Risk Factors for the Diagnosis of Colorectal Cancer', *Cancer Control*, 29, pp. 10732748211056692.

Li, A., Wang, W. C., Mcalister, V., Zhou, Q. and Zheng, X. (2021a) 'Circular RNA in colorectal cancer', *J Cell Mol Med*, 25(8), pp. 3667-3679.

Li, J., Zou, K., Yu, L., Zhao, W., Lu, Y., Mao, J., Wang, B., Wang, L., Fan, S., Song, B. and Li, L. 2018a. MicroRNA-140 Inhibits the Epithelial-Mesenchymal Transition and Metastasis in Colorectal Cancer. *Molecular Therapy - Nucleic Acids*. Cell Press.

Li, S., Li, X., Xue, W., Zhang, L., Yang, L. Z., Cao, S. M., Lei, Y. N., Liu, C. X., Guo, S. K., Shan, L., Wu, M., Tao, X., Zhang, J. L., Gao, X., Zhang, J., Wei, J., Li, J., Yang, L. and Chen, L. L. (2021b) 'Screening for functional circular RNAs using the CRISPR-Cas13 system', *Nat Methods*, 18(1), pp. 51-59.

Li, S., Tian, J., Zhang, H., Zhou, S., Wang, X., Zhang, L., Yang, J., Zhang, Z. and Ji, Z. 2018b. Down-regulating IL-6/GP130 targets improved the anti-tumor effects of 5-fluorouracil in colon cancer. *Apoptosis*. Springer New York LLC.

Li, T., Lai, Q., Wang, S., Cai, J., Xiao, Z., Deng, D., He, L., Jiao, H., Ye, Y., Liang, L., Ding, Y. and Liao, W. 2016. MicroRNA-224 sustains Wnt/ β -catenin signaling and promotes aggressive phenotype of colorectal cancer. *Journal of Experimental and Clinical Cancer Research*. BioMed Central Ltd.

Li, X., Wang, J., Zhang, C., Lin, C., Zhang, J., Zhang, W., Zhang, W., Lu, Y., Zheng, L. and Li, X. (2018c) 'Circular RNA circITGA7 inhibits colorectal cancer growth and metastasis by modulating the Ras pathway and upregulating transcription of its host gene ITGA7', *J Pathol*, 246(2), pp. 166-179.

Li, X. N., Wang, Z. J., Ye, C. X., Zhao, B. C., Huang, X. X. and Yang, L. (2019) 'Circular RNA circVAPA is up-regulated and exerts oncogenic properties by sponging miR-101 in colorectal cancer', *Biomed Pharmacother*, 112, pp. 108611.

Li, Z., Huang, C., Bao, C., Chen, L., Lin, M., Wang, X., Zhong, G., Yu, B., Hu, W., Dai, L., Zhu, P., Chang, Z., Wu, Q., Zhao, Y., Jia, Y., Xu, P., Liu, H. and Shan, G. (2015) 'Exon-intron circular RNAs regulate transcription in the nucleus', *Nat Struct Mol Biol*, 22(3), pp. 256-264.

Liu, M., Lang, N., Qiu, M., Xu, F., Li, Q., Tang, Q., Chen, J., Chen, X., Zhang, S., Liu, Z., Zhou, J., Zhu, Y., Deng, Y., Zheng, Y. and Bi, F. (2011) 'miR-137 targets Cdc42 expression, induces cell cycle G1 arrest and inhibits invasion in colorectal cancer cells', *Int J Cancer*, 128(6), pp. 1269-1279.

Liu, W., Li, L., Jiang, J., Wu, M. and Lin, P. (2021) 'Applications and challenges of CRISPR-Cas gene-editing to disease treatment in clinics', *Precis Clin Med*, 4(3), pp. 179-191.

Liu, Y., Chia, Z. H., Liew, J., Or, S. M. and Phua, K. K. L. (2018) 'Modulation of mRNA Translation and Cell Viability by Influenza A Virus Derived Nonstructural Protein 1', *Nucleic Acid Ther*, 28(3), pp. 200-208.

Longati, P., Jia, X., Eimer, J., Wagman, A., Witt, M. R., Rehnmark, S., Verbeke, C., Toftgård, R., Löhr, M. and Heuchel, R. L. 2013. 3D pancreatic carcinoma spheroids induce a matrix-rich, chemoresistant phenotype offering a better model for drug testing. *BMC Cancer*. BioMed Central.

Lu, H., Yao, B., Wen, X. and Jia, B. (2019) 'FBXW7 circular RNA regulates proliferation, migration and invasion of colorectal carcinoma through NEK2,

mTOR, and PTEN signaling pathways in vitro and in vivo', *BMC Cancer*, 19(1), pp. 918.

Lu, H. J., Li, J., Yang, G., Yi, C. J., Zhang, D., Yu, F. and Ma, Z. (2022) 'Circular RNAs in stem cells: from basic research to clinical implications', *Biosci Rep*, 42(1).

Malladi, S., Macalinao, D. G., Jin, X., He, L., Basnet, H., Zou, Y., De Stanchina, E. and Massague, J. (2016) 'Metastatic Latency and Immune Evasion through Autocrine Inhibition of WNT', *Cell*, 165(1), pp. 45-60.

Marhaba, R., Klingbeil, P., Nuebel, T., Nazarenko, I., Buechler, M. W. and Zoeller, M. (2008) 'CD44 and EpCAM: cancer-initiating cell markers', *Curr Mol Med*, 8(8), pp. 784-804.

Massagué, J. and Xi, Q. (2012) 'TGF- β control of stem cell differentiation genes', *FEBS Letters*, 586, pp. 1953-1958.

Matsui, W. H. 2016. Cancer stem cell signaling pathways. *Medicine*. Wolters Kluwer Health.

Mead, T. J. and Lefebvre, V. (2014) 'Proliferation Assays (BrdU and EdU) on Skeletal Tissue Sections', *Methods in Molecular Biology*: Humana Press, pp. 233-243.

Memczak, S., Jens, M., Elefsinioti, A., Torti, F., Krueger, J., Rybak, A., Maier, L., Mackowiak, S. D., Gregersen, L. H., Munschauer, M., Loewer, A., Ziebold, U., Landthaler, M., Kocks, C., Le Noble, F. and Rajewsky, N. 2013. Circular RNAs are a large class of animal RNAs with regulatory potency. *Nature*. Nature Publishing Group.

Meng, C., Zhao, X. and Lao, J. (2018) 'A modified immunofluorescence in situ hybridization method to detect long non-coding RNAs and proteins in frozen spinal cord sections', *Experimental and Therapeutic Medicine*, 15(6), pp. 4623-4628.

Muller, M., Hermann, P. C., Liebau, S., Weidgang, C., Seufferlein, T., Kleger, A. and Perkhofer, L. (2016) 'The role of pluripotency factors to drive stemness in gastrointestinal cancer', *Stem Cell Res*, 16(2), pp. 349-357.

Mumtaz, P. T., Taban, Q., Dar, M. A., Mir, S., Haq, Z. U., Zargar, S. M., Shah, R. A. and Ahmad, S. M. (2020) 'Deep Insights in Circular RNAs: from biogenesis to therapeutics', *Biol Proced Online*, 22(1), pp. 10.

Munro, M. J., Wickremesekera, S. K., Peng, L., Marsh, R. W., Itinteang, T. and Tan, S. T. (2019) 'Cancer stem cell subpopulations in primary colon adenocarcinoma', *PLoS One*, 14(9), pp. e0221963.

Munro, M. J., Wickremesekera, S. K., Peng, L., Tan, S. T. and Itinteang, T. (2018) 'Cancer stem cells in colorectal cancer: a review', *J Clin Pathol*, 71(2), pp. 110-116.

Neumann, J., Bahr, F., Horst, D., Kriegl, L., Engel, J., Luque, R. M., Gerhard, M., Kirchner, T. and Jung, A. (2011) 'SOX2 expression correlates with lymph-node metastases and distant spread in right-sided colon cancer', *BMC Cancer*, 11(1), pp. 518.

Ni, X. F., Zhao, L. H., Li, G., Hou, M., Su, M., Zou, C. L. and Deng, X. 2018. MicroRNA-548-3p and microRNA-576-5p enhance the migration and invasion of esophageal squamous cell carcinoma cells via NRIP1 down-regulation. *Neoplasma*. AEPress, s.r.o.

Nigro, J. M., Cho, K. R., Fearon, E. R., Kern, S. E., Ruppert, J. M., Oliner, J. D., Kinzler, K. W. and Vogelstein, B. (1991) 'Scrambled exons', *Cell*, 64(3), pp. 607-613.

Obi, P. and Chen, Y. G. (2021) 'The design and synthesis of circular RNAs', *Methods*, 196, pp. 85-103.

Pamudurti, N. R., Patop, I. L., Krishnamoorthy, A., Ashwal-Fluss, R., Bartok, O. and Kadener, S. (2020) 'An in vivo strategy for knockdown of circular RNAs', *Cell Discov*, 6(1), pp. 52.

Panda, A. C. (2018) 'Circular RNAs Act as miRNA Sponges', *Adv Exp Med Biol*, 1087, pp. 67-79.

Pandey, P. R., Rout, P. K., Das, A., Gorospe, M. and Panda, A. C. (2019) 'RPAD (RNase R treatment, polyadenylation, and poly(A)⁺ RNA depletion) method to isolate highly pure circular RNA', *Methods*, 155, pp. 41-48.

Pashirzad, M., Sathyapalan, T., Sheikh, A., Kesharwani, P. and Sahebkar, A. (2022) 'Cancer stem cells: An overview of the pathophysiological and prognostic roles in colorectal cancer', *Process Biochemistry*, 115, pp. 19-29.

Peeters, P. J., Bazelier, M. T., Leufkens, H. G., De Vries, F. and De Bruin, M. L. (2015) 'The risk of colorectal cancer in patients with type 2 diabetes: associations with treatment stage and obesity', *Diabetes Care*, 38(3), pp. 495-502.

Prasad, S., Ramachandran, S., Gupta, N., Kaushik, I. and Srivastava, S. K. (2020) 'Cancer cells stemness: A doorstep to targeted therapy', *Biochim Biophys Acta Mol Basis Dis*, 1866(4), pp. 165424.

Principe, M., Chanal, M., Karam, V., Wierinckx, A., Mikaélian, I., Gadet, R., Auger, C., Raverot, V., Jouanneau, E., Vasiljevic, A., Hennino, A., Raverot, G. and Bertolino, P. 2018a. ALK7 expression in prolactinoma is associated with reduced prolactin and increased proliferation. *Endocrine-Related Cancer*. BioScientifica Ltd.

Principe, M., Chanal, M., Karam, V., Wierinckx, A., Mikaélian, I., Gadet, R., Auger, C., Raverot, V., Jouanneau, E., Vasiljevic, A., Hennino, A., Raverot, G. and Bertolino, P. (2018b) 'ALK7 expression in prolactinoma is associated with reduced prolactin and increased proliferation', *Endocrine-Related Cancer*, 25(9), pp. 795-806.

Puglisi, M. A., Tesori, V., Lattanzi, W., Gasbarrini, G. B. and Gasbarrini, A. (2013) 'Colon cancer stem cells: Controversies and perspectives', *World Journal of Gastroenterology*, 19, pp. 2997-3006.

Qin, J., Wen, B., Liang, Y., Yu, W. and Li, H. (2020) 'Histone Modifications and their Role in Colorectal Cancer (Review)', *Pathol Oncol Res*, 26(4), pp. 2023-2033.

Qin, M., Wei, G. and Sun, X. (2018) 'Circ-UBR5: An exonic circular RNA and novel small nuclear RNA involved in RNA splicing', *Biochem Biophys Res Commun*, 503(2), pp. 1027-1034.

Qiu, C., Zhang, Y. and Chen, L. (2020) 'Impaired Metabolic Pathways Related to Colorectal Cancer Progression and Therapeutic Implications', *Iran J Public Health*, 49(1), pp. 56-67.

Rassouli, F. B., Matin, M. M. and Saeinasab, M. (2016) 'Cancer stem cells in human digestive tract malignancies', *Tumour Biol*, 37(1), pp. 7-21.

Rawla, P., Sunkara, T. and Barsouk, A. (2019) 'Epidemiology of colorectal cancer: incidence, mortality, survival, and risk factors', *Prz Gastroenterol*, 14(2), pp. 89-103.

Ren, Y., Zhang, H. and Jiang, P. 2018. MicroRNA-382 inhibits cell growth and migration in colorectal cancer by targeting SP1. *Biological Research*. BioMed Central Ltd.

- Rengganaten, V. (2016) *Enrichment of Colorectal Cancer Stem Cells by Spheroidal Culture and Gene Expression Analysis of Selected ABC Transporters*. MSc, UTAR.
- Roche, K. C., Gracz, A. D., Liu, X. F., Newton, V., Akiyama, H. and Magness, S. T. (2015) 'SOX9 maintains reserve stem cells and preserves radioresistance in mouse small intestine', *Gastroenterology*, 149(6), pp. 1553-1563 e1510.
- Rossi, M., Jahanzaib Anwar, M., Usman, A., Keshavarzian, A. and Bishehsari, F. (2018) 'Colorectal Cancer and Alcohol Consumption-Populations to Molecules', *Cancers (Basel)*, 10(2), pp. 38.
- Sakaguchi, M., Hisamori, S., Oshima, N., Sato, F., Shimono, Y. and Sakai, Y. (2016) 'miR-137 Regulates the Tumorigenicity of Colon Cancer Stem Cells through the Inhibition of DCLK1', *Mol Cancer Res*, 14(4), pp. 354-362.
- Sakshi, S., Jayasuriya, R., Ganesan, K., Xu, B. and Ramkumar, K. M. (2021) 'Role of circRNA-miRNA-mRNA interaction network in diabetes and its associated complications', *Mol Ther Nucleic Acids*, 26, pp. 1291-1302.
- Sanger, H. L., Klotz, G., Riesner, D., Gross, H. J. and Kleinschmidt, A. K. (1976) 'Viroids are single-stranded covalently closed circular RNA molecules existing as highly base-paired rod-like structures', *Proc Natl Acad Sci U S A*, 73(11), pp. 3852-3856.
- Sangiorgi, E. and Capecchi, M. R. (2008) 'Bmi1 is expressed in vivo in intestinal stem cells', *Nat Genet*, 40(7), pp. 915-920.
- Sawicki, T., Ruszkowska, M., Danielewicz, A., Niedzwiedzka, E., Arlukowicz, T. and Przybylowicz, K. E. (2021) 'A Review of Colorectal Cancer in Terms of Epidemiology, Risk Factors, Development, Symptoms and Diagnosis', *Cancers (Basel)*, 13(9), pp. 2025.
- Scheel, C., Eaton, E. N., Li, S. H. J., Chaffer, C. L., Reinhardt, F., Kah, K. J., Bell, G., Guo, W., Rubin, J., Richardson, A. L. and Weinberg, R. A. 2011. Paracrine and autocrine signals induce and maintain mesenchymal and stem cell states in the breast. *Cell*.
- Schliemann, D., Paramasivam, D., Dahlui, M., Cardwell, C. R., Somasundaram, S., Ibrahim Tamin, N. S. B., Donnelly, C., Su, T. T. and Donnelly, M. (2020) 'Change in public awareness of colorectal cancer symptoms following the Be Cancer Alert Campaign in the multi-ethnic population of Malaysia', *BMC Cancer*, 20(1).

Schmoker, A. M., Ebert, A. M. and Ballif, B. A. (2019) 'The DCBLD receptor family: Emerging signaling roles in development, homeostasis and disease', *Biochemical Journal*, 476, pp. 931-950.

Sengupta, S., Jana, S., Biswas, S., Mandal, P. K. and Bhattacharyya, A. 2013. Cooperative involvement of NFAT and SnoN mediates transforming growth factor- β (TGF- β) induced EMT in metastatic breast cancer (MDA-MB 231) cells. *Clinical and Experimental Metastasis*.

Shao, T., Pan, Y. H. and Xiong, X. D. (2021) 'Circular RNA: an important player with multiple facets to regulate its parental gene expression', *Mol Ther Nucleic Acids*, 23, pp. 369-376.

Shi, Y., Qiu, M., Wu, Y. and Hai, L. 2015. MiR-548-3p functions as an anti-oncogenic regulator in breast cancer. *Biomedicine and Pharmacotherapy*. Elsevier Masson SAS.

Shilova, O. N., Shilov, E. S. and Deyev, S. M. (2017) 'The effect of trypan blue treatment on autofluorescence of fixed cells', *Cytometry A*, 91(9), pp. 917-925.

Shirmohamadi, M., Eghbali, E., Najjary, S., Mokhtarzadeh, A., Kojabad, A. B., Hajiasgharzadeh, K., Lotfinezhad, P. and Baradaran, B. (2020) 'Regulatory mechanisms of microRNAs in colorectal cancer and colorectal cancer stem cells', *J Cell Physiol*, 235(2), pp. 776-789.

Siegel, R. L., Miller, K. D., Goding Sauer, A., Fedewa, S. A., Butterly, L. F., Anderson, J. C., Cercek, A., Smith, R. A. and Jemal, A. (2020) 'Colorectal cancer statistics, 2020', *CA Cancer J Clin*, 70(3), pp. 145-164.

Slack, F. J. and Chinnaiyan, A. M. (2019) 'The Role of Non-coding RNAs in Oncology', *Cell*, 179(5), pp. 1033-1055.

Smoot, M. E., Ono, K., Ruscheinski, J., Wang, P. L. and Ideker, T. (2011) 'Cytoscape 2.8: new features for data integration and network visualization', *Bioinformatics*, 27(3), pp. 431-432.

Song, D., Diao, J., Yang, Y. and Chen, Y. 2017. MicroRNA-382 inhibits cell proliferation and invasion of retinoblastoma by targeting BDNF-mediated PI3K/AKT signalling pathway. *Molecular Medicine Reports*. Spandidos Publications.

Song, L., Li, Z. Y., Liu, W. P. and Zhao, M. R. (2015) 'Crosstalk between Wnt/beta-catenin and Hedgehog/Gli signaling pathways in colon cancer and implications for therapy', *Cancer Biol Ther*, 16(1), pp. 1-7.

Suwannakul, N., Ma, N., Midorikawa, K., Oikawa, S., Kobayashi, H., He, F., Kawanishi, S. and Murata, M. 2020. CD44v9 Induces Stem Cell-Like Phenotypes in Human Cholangiocarcinoma. *Frontiers in Cell and Developmental Biology*. Frontiers Media S.A.

Taborda, M. I., Ramírez, S. and Bernal, G. 2017. Circular RNAs in colorectal cancer: Possible roles in regulation of cancer cells. *World Journal of Gastrointestinal Oncology*.

Tang, W., Ji, M., He, G., Yang, L., Niu, Z., Jian, M., Wei, Y., Ren, L. and Xu, J. (2017) 'Silencing CDR1as inhibits colorectal cancer progression through regulating microRNA-7', *Onco Targets Ther*, 10, pp. 2045-2056.

Tang, X., Ren, H., Guo, M., Qian, J., Yang, Y. and Gu, C. (2021) 'Review on circular RNAs and new insights into their roles in cancer', *Comput Struct Biotechnol J*, 19, pp. 910-928.

Todaro, M., Alea, M. P., Di Stefano, A. B., Cammareri, P., Vermeulen, L., Iovino, F., Tripodo, C., Russo, A., Gulotta, G., Medema, J. P. and Stassi, G. (2007) 'Colon cancer stem cells dictate tumor growth and resist cell death by production of interleukin-4', *Cell Stem Cell*, 1(4), pp. 389-402.

Tsunekuni, K., Konno, M., Haraguchi, N., Koseki, J., Asai, A., Matsuoka, K., Kobunai, T., Takechi, T., Doki, Y., Mori, M. and Ishii, H. (2019) 'CD44/CD133-Positive Colorectal Cancer Stem Cells are Sensitive to Trifluridine Exposure', *Sci Rep*, 9(1), pp. 14861.

Tsuneyoshi, N., Tan, E. K., Sadasivam, A., Poobalan, Y., Sumi, T., Nakatsuji, N., Suemori, H. and Ray Dunn, N. 2012. The SMAD2/3 corepressor SNON maintains pluripotency through selective repression of mesendodermal genes in human ES cells. *Genes and Development*. Genes Dev.

Vales, S., Bacola, G., Biraud, M., Touvron, M., Bessard, A., Geraldo, F., Dougherty, K. A., Lashani, S., Bossard, C., Flamant, M., Duchalais, E., Marionneau-Lambot, S., Oullier, T., Oliver, L., Neunlist, M., Vallette, F. M. and Van Landeghem, L. (2019) 'Tumor cells hijack enteric glia to activate colon cancer stem cells and stimulate tumorigenesis', *EBioMedicine*, 49, pp. 172-188.

Van Der Heijden, M. and Vermeulen, L. (2019) 'Stem cells in homeostasis and cancer of the gut', *Mol Cancer*, 18(1), pp. 66.

Van Schaijik, B., Davis, P. F., Wickremesekera, A. C., Tan, S. T. and Itinteang, T. (2018) 'Subcellular localisation of the stem cell markers OCT4, SOX2, NANOG, KLF4 and c-MYC in cancer: a review', *J Clin Pathol*, 71(1), pp. 88-91.

Varnat, F., Duquet, A., Malerba, M., Zbinden, M., Mas, C., Gervaz, P. and Ruiz I Altaba, A. (2009) 'Human colon cancer epithelial cells harbour active HEDGEHOG-GLI signalling that is essential for tumour growth, recurrence, metastasis and stem cell survival and expansion', *EMBO Mol Med*, 1(6-7), pp. 338-351.

Velletri, T., Villa, C. E., Cilli, D., Barzaghi, B., Lo Riso, P., Lupia, M., Luongo, R., Lopez-Tobon, A., De Simone, M., Bonnal, R. J. P., Marelli, L., Piccolo, S., Colombo, N., Pagani, M., Cavallaro, U., Minucci, S. and Testa, G. (2022) 'Single cell-derived spheroids capture the self-renewing subpopulations of metastatic ovarian cancer', *Cell Death Differ*, 29(3), pp. 614-626.

Verduci, L., Tarcitano, E., Strano, S., Yarden, Y. and Blandino, G. (2021) 'CircRNAs: role in human diseases and potential use as biomarkers', *Cell Death Dis*, 12(5), pp. 468.

Vo, J. N., Cieslik, M., Zhang, Y., Shukla, S., Xiao, L., Zhang, Y., Wu, Y. M., Dhanasekaran, S. M., Engelke, C. G., Cao, X., Robinson, D. R., Nesvizhskii, A. I. and Chinnaiyan, A. M. (2019) 'The Landscape of Circular RNA in Cancer', *Cell*, 176(4), pp. 869-881 e813.

Vromman, M., Vandesompele, J. and Volders, P. J. (2021) 'Closing the circle: current state and perspectives of circular RNA databases', *Brief Bioinform*, 22(1), pp. 288-297.

Wahab, S. M. R., Islam, F., Gopalan, V. and Lam, A. K. (2017) 'The Identifications and Clinical Implications of Cancer Stem Cells in Colorectal Cancer', *Clin Colorectal Cancer*, 16(2), pp. 93-102.

Wang, D., Zhang, F. and Gao, G. (2020) 'CRISPR-Based Therapeutic Genome Editing: Strategies and In Vivo Delivery by AAV Vectors', *Cell*, 181(1), pp. 136-150.

Wang, X., Qu, H., Dong, Y., Wang, G., Zhen, Y. and Zhang, L. 2018. Targeting signal-transducer-and-activator-of-transcription 3 sensitizes human cutaneous melanoma cells to BRAF inhibitor. *Cancer Biomarkers*. IOS Press.

Wang, Z., Wu, X., Hou, X., Zhao, W., Yang, C., Wan, W. and Chen, L. (2019) 'miR-548b-3p functions as a tumor suppressor in lung cancer', *Lasers in Medical Science*.

Wang, Z., Wu, X., Hou, X., Zhao, W., Yang, C., Wan, W. and Chen, L. (2020) 'miR-548b-3p functions as a tumor suppressor in lung cancer', *Lasers Med Sci*, 35(4), pp. 833-839.

Wang, Z., Yang, J., Di, J., Cui, M., Xing, J., Wu, F., Wu, W., Yang, H., Zhang, C., Yao, Z., Zhang, N., Jiang, B. and Su, X. 2017. Downregulated USP3 mRNA functions as a competitive endogenous RNA of SMAD4 by sponging miR-224 and promotes metastasis in colorectal cancer. *Scientific Reports*. Nature Publishing Group.

Wells, D. J. (2017) 'Systemic AAV Gene Therapy Close to Clinical Trials for Several Neuromuscular Diseases', *Mol Ther*, 25(4), pp. 834-835.

Wong, M. C., Ding, H., Wang, J., Chan, P. S. and Huang, J. (2019) 'Prevalence and risk factors of colorectal cancer in Asia', *Intest Res*, 17(3), pp. 317-329.

Wu, C., Zhu, X., Liu, W., Ruan, T. and Tao, K. (2017) 'Hedgehog signaling pathway in colorectal cancer: function, mechanism, and therapy', *Onco Targets Ther*, 10, pp. 3249-3259.

Xi, Y. and Xu, P. (2021) 'Global colorectal cancer burden in 2020 and projections to 2040', *Transl Oncol*, 14(10), pp. 101174.

Xia, L., Wu, L., Bao, J., Li, Q., Chen, X., Xia, H. and Xia, R. 2018. Circular RNA circ-CBFB promotes proliferation and inhibits apoptosis in chronic lymphocytic leukemia through regulating miR-607/FZD3/Wnt/ β -catenin pathway. *Biochemical and Biophysical Research Communications*. Elsevier B.V.

Xie, Y. H., Chen, Y. X. and Fang, J. Y. (2020) 'Comprehensive review of targeted therapy for colorectal cancer', *Signal Transduct Target Ther*, 5(1), pp. 22.

Yan, N., Xu, H., Zhang, J., Xu, L., Zhang, Y., Zhang, L., Xu, Y. and Zhang, F. (2017) 'Circular RNA profile indicates circular RNA VRK1 is negatively related with breast cancer stem cells', *Oncotarget*, 8(56), pp. 95704-95718.

Yang, J., Yang, L., Li, S. and Hu, N. (2020) 'HGF/c-Met Promote Renal Carcinoma Cancer Stem Cells Enrichment Through Upregulation of Cir-CCDC66', *Technol Cancer Res Treat*, 19, pp. 1533033819901114.

Yao, H., Xia, D., Li, Z. L., Ren, L., Wang, M. M., Chen, W. S., Hu, Z. C., Yi, G. P. and Xu, L. 2019. MIR-382 functions as tumor suppressor and chemosensitizer in colorectal cancer. *Bioscience Reports*. Portland Press Ltd.

Ye, Y., Feng, W., Zhang, J., Zhu, K., Huang, X., Pan, L., Su, J., Zheng, Y., Li, R., Deng, S., Bai, R., Zhuang, L., Wei, L., Deng, J., Li, M., Chen, R., Lin, D., Zuo, Z. and Zheng, J. (2021) 'Genome-wide identification and characterization of circular RNA m6A modification in pancreatic cancer', *Genome Medicine*, 13(1).

Yu, C. Y., Li, T. C., Wu, Y. Y., Yeh, C. H., Chiang, W., Chuang, C. Y. and Kuo, H. C. (2017a) 'The circular RNA circBIRC6 participates in the molecular circuitry controlling human pluripotency', *Nat Commun*, 8(1), pp. 1149.

Yu, L., Lu, Y., Han, X., Zhao, W., Li, J., Mao, J., Wang, B., Shen, J., Fan, S., Wang, L., Wang, M., Li, L., Tang, J. and Song, B. 2016. microRNA -140-5p inhibits colorectal cancer invasion and metastasis by targeting ADAMTS5 and IGFBP5. *Stem Cell Research and Therapy*. BioMed Central Ltd.

Yu, T., Chen, X., Zhang, W., Colon, D., Shi, J., Napier, D., Rychahou, P., Lu, W., Lee, E. Y., Weiss, H. L., Evers, B. M. and Liu, C. (2012) 'Regulation of the potential marker for intestinal cells, Bmi1, by beta-catenin and the zinc finger protein KLF4: implications for colon cancer', *J Biol Chem*, 287(6), pp. 3760-3768.

Yu, Y., Gu, S., Li, W., Sun, C., Chen, F., Xiao, M., Wang, L., Xu, D., Li, Y., Ding, C., Xia, Z., Li, Y., Ye, S., Xu, P., Zhao, B., Qin, J., Chen, Y. G., Lin, X. and Feng, X. H. 2017b. Smad7 enables STAT3 activation and promotes pluripotency independent of TGF- β signaling. *Proceedings of the National Academy of Sciences of the United States of America*. National Academy of Sciences.

Zeng, K., Chen, X., Xu, M., Liu, X., Hu, X., Xu, T., Sun, H., Pan, Y., He, B. and Wang, S. (2018) 'CircHIPK3 promotes colorectal cancer growth and metastasis by sponging miR-7', *Cell Death Dis*, 9(4), pp. 417.

Zhang, C., Yang, Z., Dong, D. L., Jang, T. S., Knowles, J. C., Kim, H. W., Jin, G. Z. and Xuan, Y. (2020a) '3D culture technologies of cancer stem cells: promising ex vivo tumor models', *J Tissue Eng*, 11, pp. 2041731420933407.

Zhang, L. and Shay, J. W. (2017) 'Multiple Roles of APC and its Therapeutic Implications in Colorectal Cancer', *J Natl Cancer Inst*, 109(8).

Zhang, P. P., Sun, J. and Li, W. 2020. Genome-wide profiling reveals atrial fibrillation-related circular RNAs in atrial appendages. *Gene*. Elsevier B.V.

Zhang, Q., Han, Z., Zhu, Y., Chen, J. and Li, W. (2020b) 'The Role and Specific Mechanism of OCT4 in Cancer Stem Cells: A Review', *Int J Stem Cells*, 13(3), pp. 312-325.

Zhang, S., Sun, J., Gu, M., Wang, G. and Wang, X. (2021a) 'Circular RNA: A promising new star for the diagnosis and treatment of colorectal cancer', *Cancer Med*, 10(24), pp. 8725-8740.

Zhang, X., Wang, S., Wang, H., Cao, J., Huang, X., Chen, Z., Xu, P., Sun, G., Xu, J., Lv, J. and Xu, Z. (2019) 'Circular RNA circNRIP1 acts as a microRNA-149-5p sponge to promote gastric cancer progression via the AKT1/mTOR pathway', *Mol Cancer*, 18(1), pp. 20.

Zhang, Y., Nguyen, T. M., Zhang, X. O., Wang, L., Phan, T., Clohessy, J. G. and Pandolfi, P. P. (2021b) 'Optimized RNA-targeting CRISPR/Cas13d technology outperforms shRNA in identifying functional circRNAs', *Genome Biol*, 22(1), pp. 41.

Zhao, X., Zhong, Q., Cheng, X., Wang, S., Wu, R., Leng, X. and Shao, L. (2020a) 'miR-449c-5p availability is antagonized by circ-NOTCH1 for MYC-induced NOTCH1 upregulation as well as tumor metastasis and stemness in gastric cancer', *J Cell Biochem*, 121(10), pp. 4052-4063.

Zhao, X., Zhong, Q., Cheng, X., Wang, S., Wu, R., Leng, X. and Shao, L. (2020b) 'miR-449c-5p availability is antagonized by circ-NOTCH1 for MYC-induced NOTCH1 upregulation as well as tumor metastasis and stemness in gastric cancer', *Journal of Cellular Biochemistry*, 121(10), pp. 4052-4063.

Zhao, Y., Dong, Q., Li, J., Zhang, K., Qin, J., Zhao, J., Sun, Q., Wang, Z., Wartmann, T. and Jauch, K. W. 'Targeting cancer stem cells and their niche: perspectives for future therapeutic targets and strategies'. *Seminars in cancer biology*: Academic Press, 139-155.

Zhi, Y., Mou, Z., Chen, J., He, Y., Dong, H., Fu, X. and Wu, Y. (2015) 'B7H1 Expression and Epithelial-To-Mesenchymal Transition Phenotypes on Colorectal Cancer Stem-Like Cells', *PLoS One*, 10(8), pp. e0135528.

Zhong, M., Zhong, C., Cui, W., Wang, G., Zheng, G., Li, L., Zhang, J., Ren, R., Gao, H., Wang, T., Li, X., Che, J. and Gohda, E. 2019. Induction of tolerogenic dendritic cells by activated TGF- β /Akt/Smad2 signaling in RIG-I-deficient stemness-high human liver cancer cells. *BMC Cancer*. BioMed Central Ltd.

Zhou, B., Song, J., Han, T., Huang, M., Jiang, H., Qiao, H., Shi, J. and Wang, Y. (2016) 'MiR-382 inhibits cell growth and invasion by targeting NR2F2 in colorectal cancer', *Molecular Carcinogenesis*, 55, pp. 2260-2267.

Zhou, P., Zheng, G., Li, Y., Wu, D. and Chen, Y. (2020) 'Construction of a circRNA-miRNA-mRNA Network Related to Macrophage Infiltration in Hepatocellular Carcinoma', *Front Genet*, 11, pp. 1026.

Zhou, Y., Xia, L., Wang, H., Oyang, L., Su, M., Liu, Q., Lin, J., Tan, S., Tian, Y., Liao, Q. and Cao, D. (2018) 'Cancer stem cells in progression of colorectal cancer', *Oncotarget*, 9(70), pp. 33403-33415.

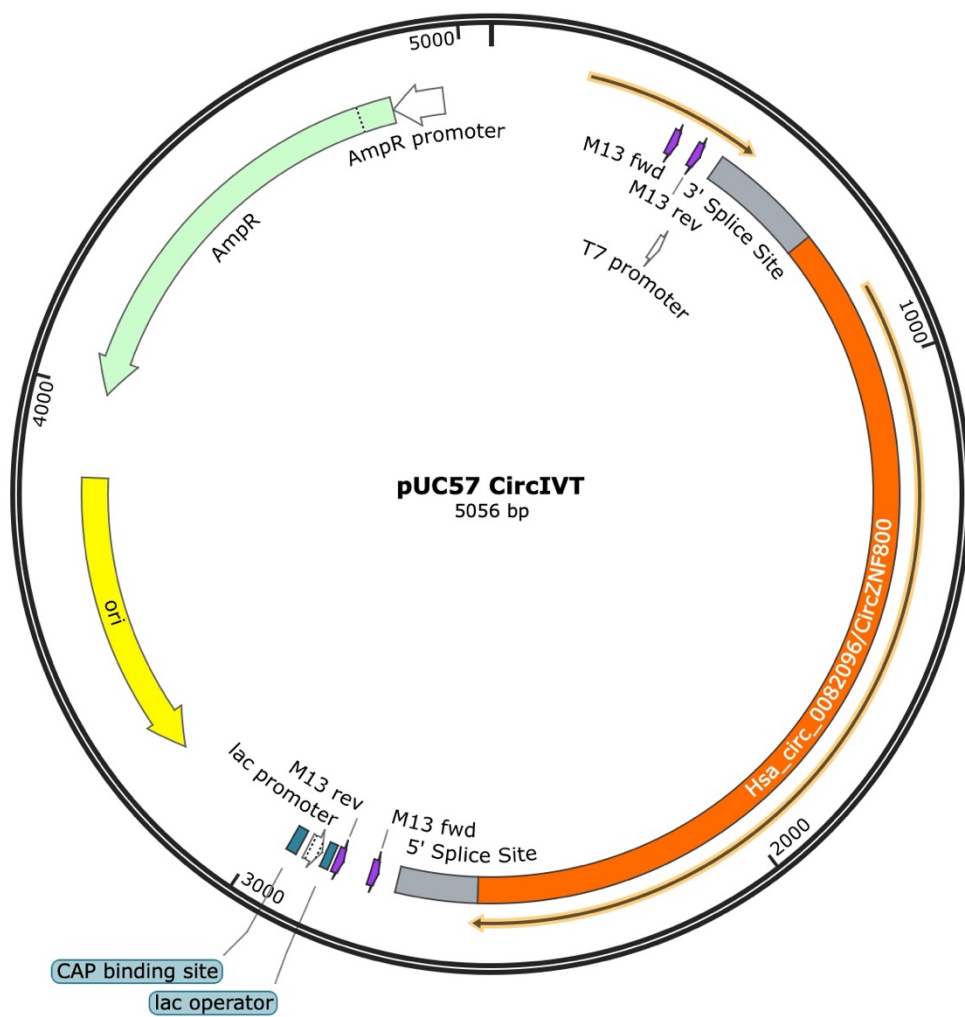
Zhu, Y., Kang, E., Wilson, M., Basso, T., Chen, E., Yu, Y. and Li, Y.-R. (2022) '3D Tumor Spheroid and Organoid to Model Tumor Microenvironment for Cancer Immunotherapy', *Organoids*, 1(2), pp. 149-167.

Zoratto, F., Rossi, L., Verrico, M., Papa, A., Basso, E., Zullo, A., Tomao, L., Romiti, A., Lo Russo, G. and Tomao, S. (2014) 'Focus on genetic and epigenetic events of colorectal cancer pathogenesis: implications for molecular diagnosis', *Tumour Biol*, 35(7), pp. 6195-6206.

APPENDICES

APPENDIX A

Full plasmid map of permuted group I self-catalytic of *td* gene intron plasmid with circZNF800 sequence used *in vitro* transcription for circZNF800 overexpression.



APPENDIX B

Full plasmid map of CRISPR Cas13d used for knockdown experiments.



Appendix C

Average tumour volume on circZNF800 overexpression.

Treatment Days	Average tumour volume (mm ³)		
	Vehicle	CircGFP	CircZNF800
0	597.1764937 ± 42.68734919	513.272608 ± 33.26167843	576.913368 ± 22.02193319
4	684.8212943 ± 26.89882564	600.2347633 ± 79.35676767	740.4737113 ± 40.64443146
8	931.111936 ± 182.2010573	779.025341 ± 53.87309166	1288.30316 ± 75.83514384
12	1319.208723 ± 115.3108357	916.8209877 ± 230.6335148	1536.784973 ± 56.91084653
16	1499.276637 ± 121.8329477	1105.533927 ± 237.6280303	1744.86964 ± 78.46191212
20	1805.33445 ± 83.71706433	1464.91877 ± 211.8727413	2268.13097 ± 149.0391605

Data obtained are average tumour volumes with standard error mean of three mice per group.

Appendix D

Average tumour volume on circZNF800 knockdown.

Days	Average tumour volume (mm ³)		
	CrSC	CrRNA 1	CrRNA 2
0	0	0	0
8	211.284929 ± 30.56139533	211.284929 ± 30.56139533	335.6908373 ± 26.50234336
11	306.143431 ± 33.92322536	306.143431 ± 33.92322536	621.214774 ± 49.84290424
14	472.8563637 ± 65.99397974	472.8563637 ± 65.99397974	643.762738 ± 148.1389931
17	514.9117317 ± 112.7851758	514.9117317 ± 112.7851758	768.4631463 ± 154.4074938
20	720.1857623 ± 71.13148754	720.1857623 ± 71.13148754	1030.773427 ± 279.0841258
23	909.4626617 ± 103.6872077	909.4626617 ± 103.6872077	1277.048676 ± 176.3665247
27	1280.765989 ± 183.9950736	1280.765989 ± 183.9950736	1584.548803 ± 203.788424
30	1330.179192 ± 201.0893661	1330.179192 ± 201.0893661	1841.221233 ± 183.7837087

Data obtained are average tumour volumes with standard error mean of three mice per group.